

**Genetic Microdissection of Insulin Action on
Neurocircuits in Control of Glucose and Energy
Homeostasis**

Inaugural-Dissertation

zur

Erlangung des Doktorgrades

der Mathematisch-Naturwissenschaftlichen Fakultät

der Universität zu Köln

vorgelegt von

Anne Christine Köner

aus Köln

Köln 2009

Berichterstatter: Prof. Dr. Jens C. Brüning
Prof. Dr. Wilhelm Krone
Prof. Dr. Tamas L. Horvath

Tag der mündlichen Prüfung: 23.10.2009

Wenn ein Tier oder Mensch seine ganze Aufmerksamkeit und seinen ganzen Willen auf eine bestimmte Sache richtet, dann erreicht er sie auch. Das ist alles.

Hermann Hesse, Demian

Figure Index.....	IV
Table Index	VI
Abbreviations.....	VII
1 Introduction.....	1
1.1 Obesity and Type 2 Diabetes Mellitus.....	1
1.2 Energy Homeostasis.....	2
1.3 Insulin.....	3
1.3.1 History, Structure and Biosynthesis	3
1.3.2 Metabolic Effects	3
1.4 The Insulin Receptor.....	5
1.4.1 Molecular Mechanisms of Insulin Receptor Signaling	5
1.5 Leptin.....	7
1.5.1 Mechanisms of Leptin Receptor Signaling.....	8
1.6 Central Regulation of Energy Homeostasis	10
1.6.1 The Hypothalamus	11
1.6.2 The Central Melanocortin System and Regulation by Peripheral Hormones.....	12
1.7 The Dopaminergic System of the Brain.....	16
1.7.1 Peripheral Hormonal Signals in Food Reward	18
1.8 Objectives.....	20
2 Materials and Methods	21
2.1 Chemicals and Biological Material.....	21
2.2 Molecular Biology	23
2.2.1 Isolation of Genomic DNA.....	23
2.2.2 Quantification of Nucleic Acids.....	24
2.2.3 Polymerase Chain Reaction (PCR)	24
2.2.4 RNA Extraction, RT PCR and Quantitative Realtime PCR.....	25
2.3 Cell Biology	26
2.3.1 Histological Analysis and Immunohistochemistry	26
2.3.1.1 Immunohistochemistry	26
2.3.1.2 Analysis of PIP3 formation <i>in situ</i>	28
2.3.2 Histomorphology.....	28
2.3.3 Electrophysiology.....	29

2.3.4	Electron Microscopy	29
2.4	Biochemistry.....	31
2.4.1	Enzyme-linked Immunosorbent Assay (ELISA)	31
2.4.2	Protein Extraction.....	31
2.4.3	Western Blot Analysis	32
2.5	Mouse Experiments	33
2.5.1	Animal Care	33
2.5.2	Mice	33
2.5.3	Collection of Blood Samples and Determination of Blood Glucose Levels	34
2.5.4	Food Intake and Indirect Calorimetry	34
2.5.5	Glucose and Insulin Tolerance Test	34
2.5.6	Insulin Signaling	35
2.5.7	Analysis of Body Composition	35
2.5.8	Fertility Assessment	35
2.5.9	Restraint Stress.....	35
2.5.10	Euglycemic-Hyperinsulinemic Clamp Studies in Awake Mice.....	36
2.5.10.1	Catheter Implantation	36
2.5.10.2	Radioactive Euglycemic-Hyperinsulinemic Clamp Experiment	36
2.5.10.2.1	Assays	37
2.5.10.2.2	Calculations	37
2.5.10.3	Long-term euglycemic-hyperinsulinemic clamp experiment	38
2.6	Computer Analysis	38
2.6.1	Densitometrical Analysis.....	38
2.6.2	Statistical Methods	38
3	Results.....	39
3.1	Generation of POMC and AgRP neuron-specific insulin receptor knockout mice.....	39
3.2	Insulin hyperpolarizes AgRP and POMC neurons via K_{ATP} channel activation.....	46
3.3	Normal body weight and energy homeostasis in $IR^{\Delta AgRP}$ and $IR^{\Delta POMC}$ mice	50
3.4	$IR^{\Delta AgRP}$ mice fail to fully suppress hepatic glucose production	55
3.5	Reduced hepatic IL-6 expression in $IR^{\Delta AgRP}$ mice	60
3.6	Inactivation of the <i>insulin receptor</i> gene in dopaminergic cells	64
3.7	Increased adiposity in $IR^{\Delta Th}$ mice	68
3.8	Unaltered glucose homeostasis in $IR^{\Delta Th}$ mice	70
3.9	Unaltered energy expenditure but increased food intake in $IR^{\Delta Th}$ mice	71

3.10	Increased expression of tyrosine hydroxylase and dopamine receptor 2 in the ventral tegmental area of IR ^{ΔTh} mice	73
3.11	Insulin action decreases excitatory inputs on dopaminergic neurons in the VTA	74
4	Discussion	77
4.1	Role of central insulin signaling in regulation of energy homeostasis and glucose metabolism.....	77
4.2	Inactivation of the <i>insulin receptor</i> gene specifically in POMC and AgRP neurons..	78
4.2.1	Role of insulin action on POMC and AgRP neurons in the regulation of energy homeostasis.....	79
4.2.2	Role of insulin action on POMC and AgRP neurons in the regulation of glucose metabolism	80
4.3	Inactivation of the <i>insulin receptor</i> gene specifically in dopaminergic cells.....	84
4.3.1	Role of insulin action on dopaminergic cells in the regulation of energy and glucose homeostasis.....	85
4.3.2	Role of insulin action on dopaminergic cells in the regulation of gene expression and synaptic plasticity	86
4.4	Perspectives	87
5	Summary.....	89
6	Zusammenfassung.....	90
7	References.....	91
8	Acknowledgements.....	108
9	Erklärung	109
10	Curriculum vitae	110

Figure Index

Figure 1: Insulin receptor signal transduction.	7
Figure 2: Leptin receptor signal transduction.	9
Figure 3: Schematic anatomical structure of the hypothalamus.	12
Figure 4: Central regulation of energy homeostasis.	15
Figure 5: POMC and AgRP neuron-restricted inactivation of the <i>insulin receptor</i> gene.	39
Figure 6: General scheme of mice with POMC (IR ^{ΔPOMC}) and AgRP (IR ^{ΔAgRP}) neuron-restricted inactivation of the <i>insulin receptor</i> gene.	40
Figure 7: Verification of Cre-mediated recombination in <i>PomcCre</i> and <i>AgRPCre</i> mice.	41
Figure 8: Western blot analysis of insulin receptor expression.	42
Figure 9: Insulin signaling in peripheral organs of control, IR ^{ΔPOMC} and IR ^{ΔAgRP} mice.	42
Figure 10: Regulation of the hypothalamic-pituitary-adrenal axis in IR ^{ΔPOMC} mice.	43
Figure 11: Fertility of IR ^{ΔPOMC} and IR ^{ΔAgRP} mice.	44
Figure 12: PIP3 formation in hypothalamic neurons of control, IR ^{ΔPOMC} and IR ^{ΔAgRP} reporter mice.	45
Figure 13: <i>Z/EG</i> expression construct.	47
Figure 14: Effects of insulin on electrical activity of control and IR ^{ΔPOMC} - <i>Z/EG</i> neurons.	48
Figure 15: Effects of insulin and tolbutamide on electrical activity of control and IR ^{ΔAgRP} - <i>Z/EG</i> neurons.	49
Figure 16: Body weight of IR ^{ΔPOMC} and IR ^{ΔAgRP} mice.	50
Figure 17: Serum leptin concentrations in IR ^{ΔPOMC} and IR ^{ΔAgRP} mice.	51
Figure 18: Daily food intake of IR ^{ΔPOMC} and IR ^{ΔAgRP} mice.	51
Figure 19: Body weight, leptin levels and food intake of IR ^{ΔPOMC} and IR ^{ΔAgRP} female mice.	52
Figure 20: Epigonadal fat pad weights of female and male IR ^{ΔPOMC} and IR ^{ΔAgRP} mice.	53
Figure 21: Hypothalamic neuropeptide expression in IR ^{ΔPOMC} and IR ^{ΔAgRP} male mice.	54
Figure 22: Body length of IR ^{ΔPOMC} and IR ^{ΔAgRP} male mice.	55
Figure 23: Fasting blood glucose levels and serum insulin concentrations in IR ^{ΔPOMC} and IR ^{ΔAgRP} male mice.	56
Figure 24: Glucose tolerance in IR ^{ΔPOMC} and IR ^{ΔAgRP} male mice.	57
Figure 25: General scheme of a euglycemic-hyperinsulinemic clamp.	58
Figure 26: Regulation of glucose homeostasis in IR ^{ΔPOMC} and IR ^{ΔAgRP} mice.	59

Figure 27: Insulin-stimulated tissue glucose uptake in euglycemic-hyperinsulinemic clamps.	60
Figure 28: Hepatic interleukin-6 expression under steady state and basal conditions in euglycemic-hyperinsulinemic clamps.....	61
Figure 29: Hepatic G6Pase-expression under steady state and basal conditions in euglycemic- hyperinsulinemic clamps.....	62
Figure 30: Hepatic cytokine and chemokine expression at the end of euglycemic- hyperinsulinemic clamps.....	63
Figure 31: Restricted inactivation of the <i>insulin receptor</i> gene in tyrosine hydroxylase- expressing cells.....	64
Figure 32: General scheme of mice with restricted inactivation of the <i>insulin receptor</i> gene in tyrosine hydroxylase-expressing cells ($IR^{\Delta Th}$).....	64
Figure 33: Verification of Cre-mediated recombination in <i>ThIRESCre</i> mice.....	65
Figure 34: PIP3 formation in neurons of control and $IR^{\Delta Th}$ reporter mice.....	66
Figure 35: Fertility of $IR^{\Delta Th}$ mice.....	67
Figure 36: Body weight, fat content and leptin levels of $IR^{\Delta Th}$ mice.....	69
Figure 37: Glucose tolerance and insulin sensitivity in $IR^{\Delta Th}$ mice.....	70
Figure 38: Serum insulin concentrations in $IR^{\Delta Th}$ mice.....	71
Figure 39: Food intake of $IR^{\Delta Th}$ mice.....	71
Figure 40: Basal metabolic rate and locomotor activity in $IR^{\Delta Th}$ mice.....	72
Figure 41: Expression levels of genes critically involved in dopamine signaling in the VTA, NAc, and CPu of $IR^{\Delta Th}$ mice.....	73
Figure 42: Long-term euglycemic-hyperinsulinemic clamps in C57BL/6 mice.....	75
Figure 43: Synaptic input on dopaminergic neurons in C57BL/6 mice after long-term euglycemic-hyperinsulinemic clamp studies.....	76
Figure 44: Model of hepatic-regulation via insulin action on AgRP neurons.....	83

Table Index

Table 1: Chemicals.....	21
Table 2: Enzymes.....	23
Table 3: Oligonucleotides used for genotyping.....	25
Table 4: Probes used for Realtime PCR.....	26
Table 5: Primary antibodies used for Western blot analysis.....	32

Abbreviations

°C	degrees Celsius
3'	three prime end of DNA sequences
5'	five prime end of DNA sequences
A	adenosine
a.m.	ante meridiem
AAAD (Ddc)	aromatic L-amino acid decarboxylase
ACTH	adrenocorticotrophin
AgRP	agouti-related peptide
Akt	proteinkinase B
ARC	arcuate nucleus
Avertin	tribromoethyl alcohol and <i>tert</i> -amyl alcohol
Ba(OH) ₂	barium hydroxide
BAT	brown adipose tissue
BMI	body mass index
bp	base pairs
C	cytosine
c	DNA concentration
CaCl ₂	calcium chloride
cAMP	cyclic adenosine monophosphate
Ccl	chemoligand (C-C motif)
cDNA	complementary DNA
Ci	Curie
CNS	central nervous system
COMT	catechol-O-methyl transferase
CPu	caudate putamen
Cre	site specific recombinase from phage P1 (causes <u>re</u> combination)
Cxcl	chemoligand (C-X-C motif)
d	deci
Da	Dalton
DAPI	4',6-diamidino-2-phenylindole
DAT	dopamine transporter

ddH ₂ O	double distilled water
DMH	dorsomedial hypothalamic nucleus
DMSO	dimethylsulfoxide
DNA	desoxyribonucleic acid
DNase	desoxyribonuclease
dNTP	desoxyribonucleotide-triphosphate
dpm	disintegrations per minute
DTT	1,4-Dithio-DL-threitol
e.g.	exempli gratia
ECL	enhanced chemiluminescence
EDTA	ethylenediamine tetraacetate
EGFP	enhanced green fluorescent protein
EGTA	ethylene glycol tetraacetic acid
ELISA	enzyme-linked immunosorbent assay
EtBr	ethidium bromide
EtOH	ethanol
floxed / lox	loxP flanked
FOXO1	forkhead-O transcription factor 1
g	gram
G	guanine
G6Pase α	glucose-6-phosphatase α
Gab	growth factor receptor binding protein associated binder
GABA	γ -aminobutyric acid
GFP	green fluorescent protein
GLUT-4	glucose transporter 4
Grb2	growth factor receptor binding protein 2
GTT	glucose tolerance test
Gusb	glucuronidase beta
h	hour
H&E	hematoxylin/eosin
H ₂ O ₂	hydrogen peroxide
HCl	hydrochloric acid
HEPES	N-2-hydroxyethylpiperazine-N'-2-ethansulfonic acid
HFD	high fat diet

HGP	hepatic glucose production
Hprt-1	hypoxanthine guanine phosphoribosyl transferase-1
Hz	Hertz
i.e.	id est
icv	intracerebroventricular
IGF-1	insulin-like growth factor-1
IL-6	interleukin-6
ip	intraperitoneal
IR	insulin receptor
IRES	internal ribosome entry site
IRS	insulin receptor substrate
ITT	insulin tolerance test
JAK	Janus kinase
k	kilo
kb	kilobase pairs
KCl	potassium chloride
kDa	kilodalton
KOH	potassium hydroxide
l	liter
<i>LacZ</i>	gene encoding the enzyme β -galactosidase
lepr	leptin receptor
LH	lateral hypothalamic area
loxP	recognition sequence for Cre (<u>l</u> ocus of <u>x</u> -ing over phage <u>P</u> 1)
m	milli
M	molar
MAOB	monoamine oxidase B
MAPK	mitogen-activated protein kinase
MCR	melanocortin receptor
ME	median eminence
MgCl ₂	magnesium chloride
min	minute
mRNA	messenger RNA
MSH	melanocyte-stimulating hormone
n	nano

n	counts
Na ₂ HPO ₄	disodium hydrogen phosphate
Na ₃ O ₄ V	sodium orthovanadate
NAc	nucleus accumbens
NaCl	sodium chloride
NaF	sodium fluoride
NaH ₂ PO ₄	monosodium phosphate
NaHCO ₃	sodium bicarbonate
NaOH	sodium hydroxide
ND	normal diet
NIRKO	neuron-restricted insulin receptor knockout mice
NMR	nuclear magnetic resonance
NPY	neuropeptide Y
ObRb	long isoform of the leptin receptor
OD	optical density
P	phospho
PAGE	polyacrylamid gel electrophoresis
PB	phosphate buffer
PBS	phosphate buffered saline
PCR	polymerase chain reaction
PDK1	phosphoinositide-dependent protein kinase 1
PFA	paraformaldehyde
PH	pleckstrin homology
PI3 kinase	phosphatidylinositol 3 kinase
PIP2	phosphatidylinositol (4,5) bisphosphate
PIP3	phosphatidylinositol (3,4,5) trisphosphate
POMC	proopiomelanocortin
PTB	phosphotyrosine binding
PTEN	phosphatase and tensin homolog
PVN	paraventricular nucleus
Raf	proto-oncogene serine/threonine protein kinase
Ras	Ras small GTPase
RNA	ribonucleic acid
RNAi	RNA interference

RNase	ribonuclease
RT	room temperature
SDS	sodiumdodecylsulfate
sec	second
SEM	standard error of the mean
SH	src homology
Shp-2	tyrosine phosphatase-2
SIM-1	single minded homolog-1
SN	substantia nigra
SOCS	suppressor of cytokine signaling
STAT	signal transducer and activator of transcription
TAE	Tris-acetic acid-EDTA buffer
TBS	Tris buffered saline
TE	Tris-EDTA buffer
Th	tyrosine hydroxylase
TNF- α	tumor necrosis factor- α
Tris	2-amino-2-(hydroxymethyl)-1,3-propanediol
Trp	tryptophan
TWEEN	polyoxethylene-sorbitan-monolaureate
Tyr	tyrosine
U	units
UV	ultraviolet
V	Volt
v/v	volume per volume
VMH	ventromedial nucleus of the hypothalamus
VO ₂	volume of consumed oxygen
VTA	ventral tegmental area
w/v	weight per volume
WAT	white adipose tissue
WHO	World Health Organization
ZnSO ₄	zinc sulfate
β -gal	β -galactosidase
β -me	β -mercaptoethanol
μ	micro

1 Introduction

1.1 Obesity and Type 2 Diabetes Mellitus

As the obesity epidemic shows no signs of abating, concern about this development has heightened during the last years. Obesity has been linked to numerous chronic conditions, including type 2 diabetes mellitus, hypertension, heart disease, stroke, and some forms of cancer. Therefore, increases in the prevalence of obesity carries potentially serious implications for the future health of populations and health care expenditures of countries (1, 2). Although initially most abundant in developed countries, principally in the United States, obesity and overweight are now dramatically on the rise in low- and middle-income countries. Latest projections from the World Health Organization (WHO) indicated that in 2005 approximately 1.6 billion adults were overweight and at least 400 million adults were obese (3). Furthermore, the WHO estimates that by 2015, approximately 2.3 billion adults will be overweight and more than 700 million will be obese. Moreover, childhood obesity is dramatically on the rise, as in 2005 at least 20 million children under the age of 5 years were considered overweight (3).

The Body Mass Index (BMI), a simple index of weight-for-height, is one of the most commonly recommended and widely used methods for classifying overweight and obesity in adults. It is defined as the weight in kilograms divided by the square of the height in meters (kg/m^2) (4). The WHO defines overweight as a BMI ≥ 25 , and obesity as a BMI ≥ 30 . However, while BMI classification provides a useful method for measurement of total adiposity, it needs adjustment for additional factors such as age, gender, and ethnicity. It is estimated that there are more than 300,000 obesity-attributable annual deaths and 80% of these occur among individuals with a BMI of more than $30 \text{ kg}/\text{m}^2$ (5). Compared to individuals with a normal BMI, there is substantial risk of developing type 2 diabetes mellitus in individuals with a BMI > 35 (6, 7).

A substantial portion of the health complications and costs attributed to obesity is related to type 2 diabetes mellitus; a progressive disease that is primarily defined by the level of hyperglycemia with concomitant hyperinsulinemia and leads to deterioration in multiple organs and systems. In particular, it increases the risk of microvascular damage (i.e. retinopathy, nephropathy and neuropathy) (8). Furthermore, it is associated with significant morbidity due to microvascular complications, increased risk of macrovascular complications (i.e. ischaemic heart disease, stroke and peripheral vascular disease), diminished quality of life and ultimately reduced life expectancy (1, 8). Estimations indicate that worldwide there

were 171 million people with type 2 diabetes mellitus in the year 2000 and this is estimated to increase to 366 million people by 2030 (9). Resistance to the biological effects of the peptide hormone insulin represents one of the hallmarks during the development of type 2 diabetes mellitus (10, 11) and obesity has been strongly associated with insulin resistance in normoglycemic persons and in individuals with type 2 diabetes mellitus (12, 13).

Many studies have indicated that genetic factors account for a substantial portion of variation in human adiposity. A genome-wide search for type 2 diabetes mellitus-susceptibility genes identified a common variant in the FTO (fat mass and obesity associated) gene that predisposes to type 2 diabetes mellitus through an effect on BMI (14). In addition, the importance of leptin, the leptin receptor and the melanocortin system in the control of human body weight has been demonstrated by identification of obese patients with mutations in leptin, the leptin receptor, proopiomelanocortin (POMC) or the melanocortin receptor 4 (15, 16). However, although rare obesity syndromes caused by mutations in single genes have been described, by far the greatest proportion of obesity in humans is not due to mutations in single genes. Thus, the most common forms of human obesity, that account for the obesity epidemic worldwide, are more likely to arise from the interactions of multiple genes, environmental factors and behavior (15, 16).

1.2 Energy Homeostasis

Body mass and composition are ultimately influenced by the long-term balance between energy intake and energy expenditure. With positive energy balance, body mass increases in order to restore energy balance. On the other hand, a state of negative energy balance leads to a decrease in body mass. Thus, understanding the regulation of energy balance is crucial in the development of therapeutical strategies in the treatment of obesity (for review see (17-20)).

Research over the last years suggested a key role for the central nervous system (CNS) in the control of energy homeostasis. Neuronal systems involved in regulation of energy intake, energy expenditure, and endogenous glucose production sense and integrate input from peripheral hormones and nutrient-related signals that convey information about body energy stores and energy availability (for review see (21)). In response, the brain activates anabolic pathways (inhibition of energy intake and endogenous glucose production) to restore energy balance. Conversely, a decreased neuronal input from these afferent signals activates catabolic responses that promote positive energy balance (increased energy intake and

endogenous glucose production). Afferent signals that convey information about body energy stores and energy availability include the pancreatic hormone insulin as well as the adipocyte-derived hormone leptin.

1.3 Insulin

1.3.1 History, Structure and Biosynthesis

In 1889, the physicians Oscar Minkowski and Joseph von Mering first noted that surgical removal of the pancreas led to the development of diabetes mellitus in dogs ((22), for review see (23)). Despite considerable effort, no significant progress was made in the isolation or characterization of the “antidiabetic factor” until 1921, when F. Banting, C. Best, J.J.R. Macleod and J. Collip finally identified a substance in extracts of the pancreas that had the remarkable ability to reduce blood glucose levels in diabetic animals; and by 1923 these pancreas extracts were being used to successfully treat diabetic patients (for review see (24, 25)). In 1923, Banting and Macleod were awarded the Nobel Prize in Medicine for their discovery of insulin.

Insulin, a 51 amino acid anabolic peptide hormone, is synthesized in the β -cells of the pancreatic islets of Langerhans, which are endocrine cells within the primarily exocrine pancreatic tissue. In the β -cells, insulin is cleaved from the inactive precursor proinsulin, which consists of two peptide chains linked by an intervening region called the C-peptide (26). Proinsulin is synthesized in the endoplasmic reticulum, and then transported to the Golgi apparatus where it is packed into secretory granules and converted to native insulin and the C-peptide by the action of two endopeptidases and one carboxypeptidase (27, 28). Removal of the C-peptide results in a conformational change of the protein, which enables the interaction with its receptor, the insulin receptor (29). After binding to and activating its receptor, insulin is either released back into the circulation or degraded by the cell via endocytosis of the insulin receptor complex followed by the action of the insulin degrading enzyme (for review see (30)).

1.3.2 Metabolic Effects

Insulin release from the pancreatic β -cells is rapidly triggered in response to increased blood glucose levels, although insulin release is also stimulated by amino acids from ingested proteins, acetylcholine, cholecystokinin, glucose-dependent insulinotropic peptide (GIP) and

glucagon-like peptide (GLP)-1 (31-35). Moreover, plasma insulin levels are also directly correlated with the degree of body adiposity (36-38). Upon release, binding of insulin to its receptor induces a cascade of intracellular signaling events that regulate key cellular functions, including glucose transport and oxidation, synthesis of glycogen, triglycerides and proteins, and regulation of gene expression. Insulin acts on peripheral tissues, particularly on muscle cells and adipocytes, via translocation of the glucose transporter GLUT-4 into the cell membrane, thereby increasing glucose uptake in these tissues (39-41). Moreover, insulin promotes anabolic processes such as stimulation of amino acid uptake and protein synthesis in muscle, glycogen synthesis in liver and muscle as well as lipogenesis in adipose tissue. Catabolic processes, on the other hand, such as glycogenolysis, lipolysis and proteolysis are inhibited by insulin (for review see (31)).

In addition, insulin controls hepatic glucose production through regulation of both glycogen metabolism and gluconeogenesis (for review see (42)). Prager *et al.* expanded the model of insulin's direct hepatic effects by demonstrating that suppression of hepatic glucose production in obese, nondiabetic humans could also occur after peripheral insulin infusion, even when portal vein insulin concentrations remained unchanged, suggesting that insulin is also able to suppress hepatic glucose production through indirect hepatic actions (43). Subsequent work in dogs confirmed this notion (44-46), and, in 2002, Obici *et al.* defined the mediobasal hypothalamus, a region known to be involved in regulation of energy balance, as one important extrahepatic site of insulin action to regulate hepatic glucose production (47). They demonstrated that hypothalamic insulin signaling is required for insulin's ability to suppress hepatic glucose production in euglycemic-hyperinsulinemic clamps of rats, a finding that was subsequently also described in mice (47, 48). Further recent work has indicated that hypothalamic insulin signaling is required for blood glucose lowering during insulin treatment of diabetes mellitus in rats (49).

The finding that insulin, when infused into the brain, decreases food intake and body weight led to the proposal by Woods and Porte that insulin serves as an adiposity signal in the brain, where it provides a signal related to the amount of body fat and causes a long-term, net catabolic response, decreasing food intake and increasing energy expenditure (50-53). Peripheral circulating insulin has access to the brain via a saturable transporter across the blood-brain barrier and insulin receptors are widely expressed in the brain, with the highest concentrations in the olfactory bulb, hypothalamus, cerebral cortex, cerebellum and the hippocampus (54-57). Importantly, mice with a neuron-specific insulin receptor deficiency

are obese and display impaired fertility, further supporting a role for insulin receptor signaling in the regulation of fuel metabolism and reproduction (58).

1.4 The Insulin Receptor

The insulin receptor is present in virtually all vertebrate tissues, including classic insulin responsive tissues such as skeletal muscle, liver and adipose tissue, as well as tissues previously thought to be unresponsive to insulin like the CNS, the pancreas, lymphatic cells, endothelial cells or gonadal cells (59-62). The receptor gene is located on the short arm of human chromosome 19, is more than 150 kb in length and contains 22 exons, which encode a 4.2 kb cDNA (63). The receptor, a typical ligand-activated receptor tyrosine kinase of which two different isoforms due to alternative splicing of exon 11 exist, is composed of two α -subunits that are each linked to a β -subunit and to each other by disulfide bonds (64, 65). Both insulin receptor isoforms (IR-A and IR-B) display differences in ligand binding affinity, kinase activity, receptor internalization, recycling as well as intracellular signaling capacity and tissue distribution (66-71). From the two isoforms, IR-B is predominantly expressed in insulin target tissues (64, 66) that are responsible for glucose homeostasis such as liver, skeletal muscle and adipose tissue (72).

Both subunits of the insulin receptor are products of a single gene and are derived from a polypeptide precursor by proteolytic processing (73). The α -subunits are located entirely outside of the cell and contain the insulin binding site(s), whereas the intracellular portion of the β -subunit contains the insulin-regulated tyrosine protein kinase (74). The family of ligand-activated receptor tyrosine kinases contains two other structurally related molecules, the insulin-like growth factor (IGF)-1 receptor and the insulin receptor-related receptor, an orphan receptor for which no ligand has been identified yet (75-77).

The complete amino acid sequences, structural details and framework for the functional domains were determined by the cloning of the human insulin receptor precursor cDNA (73, 78). Subsequent cloning of the mouse and rat insulin receptor revealed a highly conserved sequence to the human insulin receptor gene (79).

1.4.1 Molecular Mechanisms of Insulin Receptor Signaling

Insulin exerts its pleiotropic functions by binding to and activating its membrane-bound tyrosine kinase receptor. Binding of insulin to the α -subunit induces a conformational

change of the receptor, thereby activating the intrinsic tyrosine kinase activity of the β -subunits leading to autophosphorylation of multiple tyrosine residues (Figure 1) (80). Phosphorylation of these residues creates a binding site for intracellular signaling proteins that are recruited to the receptor via their phosphotyrosine-binding (PTB) domain and subsequently become tyrosine phosphorylated (81-83). In addition, intracellular substrates contain a N-terminal Pleckstrin homology (PH) domain which, through interaction with inositol phosphates in the cell membrane, allows for the localization of the substrate to the membrane (84-86). Intracellular signaling molecules of the insulin receptor are the four closely related insulin receptor substrate (IRS 1 - 4) proteins and the growth factor receptor binding (Grb)2 protein-associated binder (Gab) proteins (87-93). These insulin receptor substrates serve, when tyrosine phosphorylated, as a docking platform for Rous sarcoma virus (Src)-homology 2 (SH2) domain containing signaling proteins, such as the regulatory subunit of the phosphatidylinositol (PI) 3 kinase, Grb2 and the SH2 domain containing phosphatase (Shp)-2, among which the most important and best studied is the PI3 kinase (94-98). Binding to the insulin receptor substrates is then followed by activation of the PI3 kinase and the Ras/Raf Mitogen-activated protein (MAP)-kinase pathway (Figure 1) (for review see (32)).

The most common form of the widely expressed PI3 kinase consists of a 85 kDa regulatory subunit, p85, and a 110 kDa catalytic subunit, p110 (for review see (99)). Activation occurs when the SH2 domain of the regulatory subunit binds to the phosphorylated tyrosine residues of the activated IRS molecule. This relieves the inhibition of the catalytic subunit and serves to localize the catalytic subunit to the cell membrane, where the substrate of the PI3 kinase is located. PI3 kinase primarily catalyzes the phosphorylation of phosphatidylinositol (4,5) biphosphate (PIP₂) to phosphatidylinositol (3,4,5) trisphosphate (PIP₃) (Figure 1) (100, 101). PIP₃, in turn, recruits and activates numerous other downstream molecules containing PIP₃ binding domains (PH domains), including serine-threonine kinases, tyrosine kinases, and others. One of the key downstream targets is protein kinase B (PKB, also known as Akt), which upon binding to PIP₃ via its PH domain translocates to the cell membrane and co-localizes with phosphoinositide-dependent protein kinase 1 (PDK1) (for review see (102)). The subsequent conformational change enables PDK1 to phosphorylate Akt, and thereby activating the enzyme. Activation of the IRS-PI3 kinase cascade is crucial for most of insulin's well-known effects, including glucose transporter translocation, glycogen synthesis, protein synthesis and the regulation of gene transcription (Figure 1) (for review see (103)).

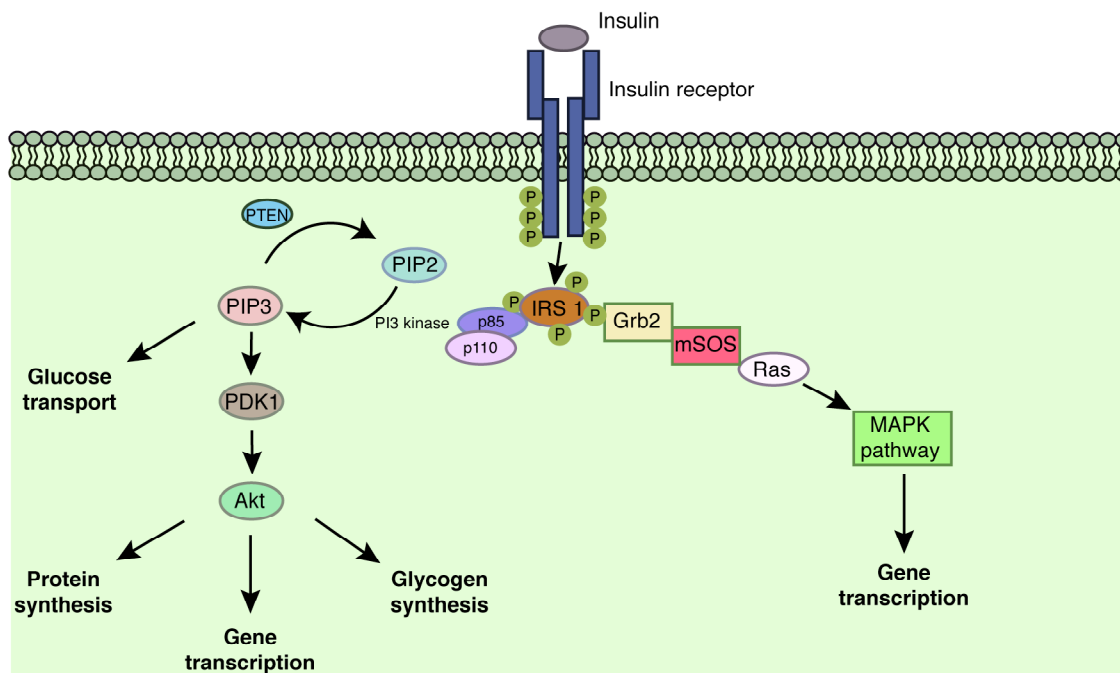


Figure 1: Insulin receptor signal transduction.

Binding of insulin to the insulin receptor results in activation of the membrane-bound insulin receptor tyrosine kinase, which consists of two α -subunits and two β -subunits forming a $\alpha_2\beta_2$ heterotetramer. Upon insulin binding to the extracellular α -subunits, the receptor undergoes a conformational change, activating the tyrosine kinase activity of the β -subunits, resulting in receptor autophosphorylation and subsequently in the phosphorylation of intracellular insulin receptor substrate (IRS) 1 proteins on tyrosine residues. These phosphorylation sites are located in domains that characterize them as binding sites for src-homology 2 (SH2) domain-containing proteins such as the p85-regulatory subunit of phosphatidylinositol 3 kinase (PI3 kinase) and the growth factor receptor binding protein (Grb) 2. Binding of these proteins to tyrosine-phosphorylated IRS 1 proteins results in their activation, initiating downstream signals such as the activation of the Ras-Raf-MAPK cascade or activation of serine/threonine kinases downstream of PIP3. These signals finally result in the diverse biological effects of insulin signaling. Abbreviations: Akt, protein kinase B; MAPK, mitogen-activated protein kinase; mSOS, son of sevenless; PDK1, protein-dependent kinase 1; p110, catalytic subunit of PI3 kinase; PIP2, phosphatidylinositol (4,5) bisphosphate; PIP3, phosphatidylinositol (3,4,5) trisphosphate; PTEN, phosphatase and tensin homolog; Raf, proto-oncogene serine/threonine protein kinase; Ras, Ras small GTPase.

1.5 Leptin

In 1994, another prototypic adiposity signal was discovered as the *ob* (obese) gene product, which encodes the leptin protein (104). Mice carrying a mutation in the *ob* gene exhibit dramatic weight gain (*ob/ob*) (104), and a naturally occurring loss-of-function mutation of the leptin receptor in both CNS and periphery underlies the phenotype of obese and diabetic mice (*db/db*) (105). Leptin (leptos (Greek): thin) is primarily expressed in the

adipose tissue and, at lower levels, in gastric epithelium, placenta and testis (104, 106-108). The 16 kDa protein circulates in rodent and human plasma (109), and plasma leptin levels are highly correlated with adipose tissue mass and decrease in mice and humans after weight loss (110). In particular, the amount of *ob* gene expression per cell directly correlates with the lipid content and the size of individual adipocytes (111). Thus, plasma leptin levels have been found to be increased in obese humans as well as in multiple genetically induced forms of rodent obesity (110). Peripheral administration of leptin results in a dose-dependent decrease in body weight by reducing food intake and increasing energy expenditure in *ob/ob* and wild type mice, with weight loss restricted to adipose tissue but not lean mass (109, 112, 113).

As shown by Cohen *et al.*, the neuron-specific deletion of the leptin receptor resembles the phenotype of the *db/db* mouse (114), indicating that the major role of leptin action to control energy homeostasis is accounted for by its signaling in the CNS. Along this line, administration of leptin in the CNS decreases food intake and body weight in various species, underlining the pivotal role of leptin in the regulation of energy homeostasis in the CNS (for review see (21, 115, 116)). Circulating leptin is transported to the brain across the blood-brain barrier via a saturable process (117).

In humans, rarely occurring loss-of-function mutations of the leptin gene result in morbid obesity, that can be rescued by leptin treatment (118, 119). However, the majority of obese patients develop overweight in the presence of elevated plasma leptin concentrations, indicative of leptin resistance (110, 118). Consistent with this, rats fed a high fat diet as a model of diet-induced obesity developed resistance to leptin's anorectic effect in the presence of hyperleptinemia (120). However, studies indicate that leptin responsiveness may be restored if applied in combination with other drugs (121).

1.5.1 Mechanisms of Leptin Receptor Signaling

The leptin receptor is a cytokine receptor of which different isoforms exist, all arising from alternative mRNA splicing and/or proteolytic processing of the single *lepr* gene (122-124). Among the different isoforms only the Lepr-B (ObRb) has been shown to activate intracellular signaling (123). ObRb is highly conserved among species and is critical for leptin action as observed in *db/db* mice, which indeed lack only the ObRb (122, 123, 125). Many effects of leptin on energy homeostasis are attributable to its action in the CNS, especially in the mediobasal hypothalamus, where ObRb is highest expressed (126).

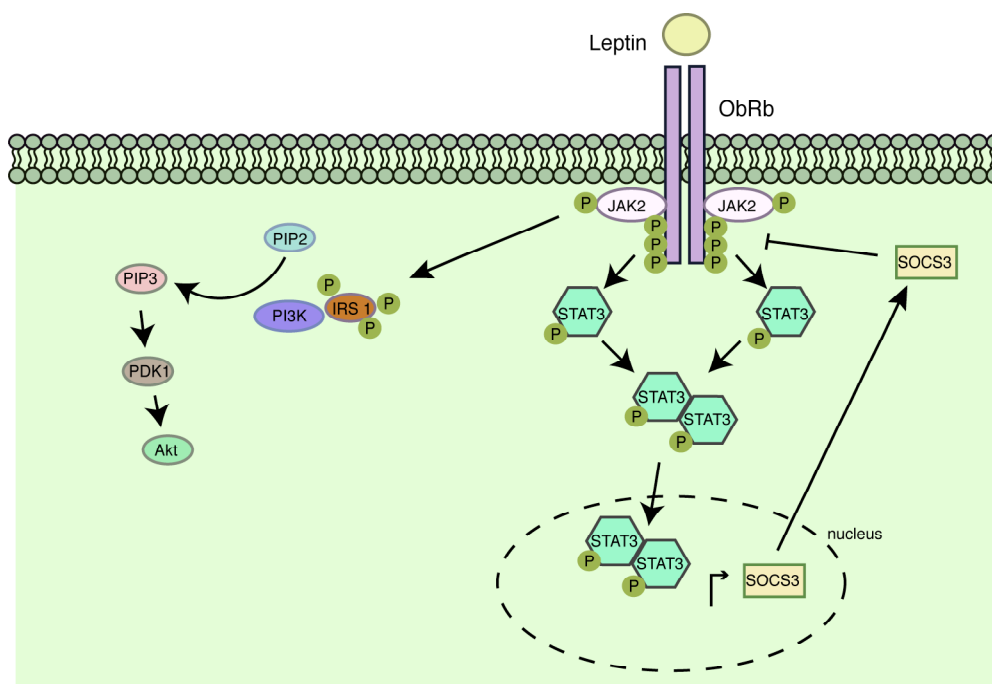


Figure 2: Leptin receptor signal transduction.

Binding of leptin to the long form of the leptin receptor (ObRb) leads to activation of janus kinase (JAK) 2 and subsequently to JAK2-mediated phosphorylation of three different intracellular tyrosine residues of the receptor. This results in the phosphorylation and activation of signal transducer and activator of transcription (STAT)3 molecules. Activated STAT3 molecules form dimers, which translocate to the nucleus and activate target genes including suppressor of cytokine signaling (SOCS)3, resulting in inhibition of leptin signaling via a negative feedback loop. Additionally, phosphorylated JAK2 directly activates the IRS 1/PI3K signaling pathway, initiating downstream signals such as activation of serine/threonine kinases downstream of PIP3. Abbreviations: Akt, protein kinase B; IRS 1, insulin receptor substrate 1; PDK 1, protein-dependent kinase 1, PI3K, phosphatidyl inositol 3 kinase, PIP2, phosphatidylinositol (4,5) bisphosphate; PIP3, phosphatidylinositol (3,4,5) trisphosphate.

ObRb consists of a single membrane-spanning domain and hormone binding to the receptor triggers the activation of a member of the janus kinase (JAK) family, JAK2 (127). Activation of the JAK2 associated tyrosine kinases leads to autophosphorylation of JAK2 on multiple tyrosine residues and phosphorylation of three tyrosine residues on the intracellular domain of ObRb to create a binding site for signal transducers and activators of transcription (STAT) molecules (Figure 2) (123, 127, 128). Activated phosphorylated STAT molecules dimerize and translocate to the nucleus where they act as a transcription factor to regulate gene expression via STAT-responsive elements (Figure 1) (127, 129, 130). Here, STAT3 activates expression of the suppressor of cytokine signaling (SOCS)3 (131), thereby providing an intracellular negative feedback loop to leptin signaling. SOCS3 directly binds to JAK2,

thereby reducing phosphorylation of downstream molecules by JAK2 and attenuating leptin-induced tyrosine phosphorylation of JAK2 (Figure 2) (132-135).

Binding of leptin to the leptin receptor not only activates the JAK/STAT-pathway, but also PI3 kinase signaling via tyrosine-phosphorylation of IRS proteins and direct activation of the PI3 kinase by JAK2 (127, 136), thus providing a potential point of convergence and synergism with insulin-stimulated signals (Figure 2) (137). The importance of leptin-mediated activation of the PI3 kinase signaling pathway has been demonstrated in IRS 2 deficient mice which develop hyperphagia and decreased energy expenditure in the presence of increased adiposity and circulating leptin concentrations, indicating leptin resistance (138).

1.6 Central Regulation of Energy Homeostasis

Already in the 1940s and 1950s, classic lesion experiments in the rodent hypothalamus could identify the brain as a critical organ in the regulation of body weight and energy homeostasis. In 1940, Hetherington demonstrated that destruction of the ventromedial hypothalamus (VMH) caused hyperphagia, obesity, and diabetes mellitus in rats (139), while lesions of the lateral hypothalamus (LH) carried out by Anand *et al.* resulted in a failure to eat and drink (140). It was thus concluded that the “satiety center” was located in the VMH and the “feeding center” in the LH. In 1953, Kennedy first proposed that hormonal signals are released into the blood stream in proportion to the body’s energy stores and are able to regulate body weight by influencing energy intake and expenditure (141). Parabiosis studies, in which the circulation of animals was surgically joined, demonstrated that food intake and body weight were drastically decreased in normal rats joined to obese VMH-lesioned rats. In contrast, VMH-lesioned rats continued to overeat and gain weight when parabiosed with VMH-lesioned or non-lesioned rats. These experiments provided direct evidence that an intact hypothalamus is required for the regulating action of hormonal satiety signals produced in obesity and created the link between circulating satiety signals and their hypothalamic target regions (142).

Besides the brain’s ability to integrate peripheral hormonal signals in order to regulate energy intake and energy expenditure, it has long been suggested that the CNS plays an essential role in the control of peripheral blood glucose levels. The French physiologist Claude Bernard demonstrated more than 150 years ago that pricking of the floor of the fourth ventricle of the brain in rabbits results in glucosuria, and concluded that the CNS plays an essential role in the control of peripheral blood glucose levels (143).

1.6.1 The Hypothalamus

In vertebrates, the hypothalamus is a part of the diencephalon that lies below the thalamus, building up the floor of the third cerebral ventricle. The mammalian hypothalamus consists of more than 40 histologically distinct nuclei and areas, which often can be further divided into subnuclei (144). Lesion and electrical stimulation studies identified distinct hypothalamic nuclei in control of feeding and satiety. Here, the arcuate nucleus (ARC), the paraventricular nucleus (PVN), the VMH, the dorsomedial hypothalamic nucleus (DMH) and LH are the nuclei, which have been shown to be involved in regulation of feeding behavior (Figure 3). Importantly, the hypothalamus is involved in many other behaviors than food intake, such as regulation of drinking behavior, body temperature, stress response, reproduction and the autonomous nervous system (for review see (145)).

The ARC is located in the mediobasal hypothalamus adjacent to the third cerebral ventricle and the median eminence. Of the circumventricular organs, i.e. areas that lack a blood-brain barrier, the median eminence and its close relationship with the hypothalamic ARC plays an important role in controlling the entry of peripheral substances to neurons of the mediobasal hypothalamus (Figure 3) (146, 147). The PVN is located at the dorsal end of the third ventricle and represents a point of convergence for neuronal pathways implied in the regulation of energy balance, including projections from the ARC (144). Lesions of the PVN as well as the VMH, which is located directly above the ARC, results in hyperphagia and weight gain (Figure 3). The DMH is located dorsal of the VMH and major projections to this nucleus are provided by most other hypothalamic nuclei, including the ARC, the VMH, the PVN and the LH, indicating an integrative role for the DMH (148). The LH, a very large and heterogenous area, is the most extensively interconnected area of the hypothalamus, thereby allowing it to modulate different functions, including cognitive and autonomic functions (for review see (145)).

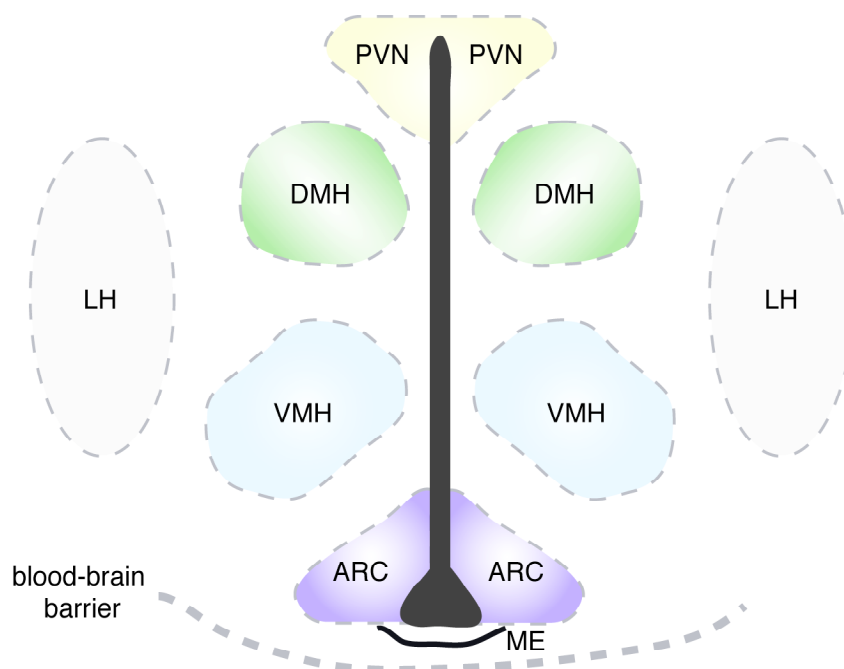


Figure 3: Schematic anatomical structure of the hypothalamus.

Diagram of the mediobasal hypothalamus, showing major hypothalamic regions implicated in regulation of food intake and energy expenditure. Abbreviations: 3V, third ventricle; ARC, arcuate nucleus, DMH, dorsomedial hypothalamic nucleus; LH, lateral hypothalamus; ME, median eminence; VMH, ventromedial nucleus of the hypothalamus; PVN, paraventricular nucleus.

1.6.2 The Central Melanocortin System and Regulation by Peripheral Hormones

The melanocortin system has been considered as the most promising model to explain neuronal control in regulation of long-term energy balance (Figure 4) (for review see (21, 149)). The ARC of the mediobasal hypothalamus is critical in this model. Here, two functionally opposing neuronal populations have been studied in great detail: the anorexigenic proopiomelanocortin (POMC)-expressing and the orexigenic agouti related peptide / neuropeptide Y (AgRP/NPY)-expressing neurons (Figure 4). AgRP and NPY are anabolic neuropeptides that stimulate feeding and reduce energy expenditure, while the catabolic neuropeptide POMC suppresses feeding and increases energy expenditure (150-152).

The anorectic POMC neurons express POMC as a precursor protein which, dependent on the cell type-specific expression pattern of prohormone convertases, is processed to different bioactive products, including melanocyte-stimulating hormones (α -, β -, and γ -MSH), adrenocorticotrophin (ACTH) and β -endorphin (153). Besides from the ARC, POMC is expressed in the pituitary, the nucleus tractus solitarius and in several peripheral tissues (154-156). Upon fasting, POMC mRNA levels are significantly reduced in the ARC, and expression is restored with refeeding (157).

Among the melanocyte-stimulating hormones, α -MSH reduces food intake and increases energy expenditure both in animals and humans (158-160). α - and β -MSH act on melanocortin receptor (MCR) type 3 and 4, which are G-protein coupled receptors that activate the adenylate cyclase and are expressed in the ARC, PVN, LH, VMH, and DMH (161-163). Recent elegant cell type-specific reconstitution experiments of MC4R on a null background in mice have defined single-minded homolog (SIM)-1-positive PVN neurons as the critical mediators of α -MSH stimulated anorexia (164). However, since energy expenditure remained unaltered in PVN/SIM1-reconstituted MC4R null mice, the nature and location of the energy expenditure controlling α -MSH target neurons remains elusive (164).

The second principal neuronal population in the ARC are the orexigenic AgRP/NPY neurons. The orexigenic neuropeptide NPY is one of the most abundant neurotransmitters that is widely expressed throughout the brain with highest concentration in the ARC (165-167). NPY is a potent stimulator of food intake, reduces energy expenditure (168, 169), and central NPY administration promotes a state of positive energy balance and increased fat storage (170).

AgRP acts as an inverse agonist of the MC3/4R and prevents the anorectic effect of α -MSH. Accordingly, overexpression of the Agouti protein, an AgRP-like peptide results in the obese, hyperphagic phenotype of the Agouti (A^y) mouse (171). The only peripheral tissue with detectable AgRP expression is the adrenal gland (171).

AgRP mRNA levels in the ARC are increased upon fasting (157), and reduction of hypothalamic AgRP mRNA results in an increased metabolic rate and reduction of body weight without affecting food intake (172). The pivotal role of these cells in the acute regulation of feeding in adult mammals has been further substantiated by toxin-mediated AgRP neuron ablation: ablation of these neurons in adult mice led to a hypophagic phenotype (173, 174). However, this phenotype of AgRP neuron-ablated mice conflicts that of NPY/AgRP single or double knockout mice (175), indicating that either developmental compensation accounts for the lack of a phenotype in the latter mice, or alternative neuropeptides or transmitters are released from these cells. Indeed, AgRP neurons are GABAergic and thereby account to a large extent for the GABAergic innervation on neighbouring POMC cells (Figure 4) (176). Strikingly, acute ablation of AgRP neurons in adult mice causes disinhibition of neurons, as assessed by cFos immunoreactivity, in numerous brain sites including the ARC, PVN, DMH, medial preoptic area, lateral septum, and nucleus of the solitary tract (177). Consistent with a role for GABA-signaling in AgRP neurons, AgRP cell-restricted inactivation of the vesicular GABA transporter results in

leanness (178). Very recent studies have demonstrated that GABAergic AgRP neuron projections into the parabrachial nucleus are critical for the maintenance of feeding (179).

Both, POMC and AgRP/NPY neuronal populations express insulin and leptin receptors and are targeted by the respective hormones (57, 58, 115), and large body of evidence has revealed an important role for leptin-activated STAT3 signaling in the CNS and POMC/AgRP neurons specifically in control of energy homeostasis. Neuron-specific disruption of STAT3 results in hyperphagia, obesity, diabetes and infertility (180). Along this line, mice with disruption of STAT3 specifically in leptin receptor-expressing neurons develop profound obesity (181). Further substantiating a role for STAT3 signaling in POMC/AgRP neurons for maintaining normal energy homeostasis, lack of leptin receptor signaling or inactivation of STAT3 specifically in POMC neurons results in obesity and other elements of the metabolic syndrome in rodents (182, 183), and deletion of STAT3 in AgRP/NPY neurons results in modest weight gain accompanied by mild hyperphagia (184). Interestingly, mice with a constitutive activation of STAT3 signaling specifically in AgRP neurons are lean due to increased locomotor activity (185), assigning AgRP neurons and specifically STAT3 signaling a role in control of locomotor activity. Administration of leptin to the ARC stimulates expression of POMC (115, 186) and inhibits expression of AgRP and NPY (187, 188). Moreover, administration of a MC4R antagonist attenuates the anorexigenic response to leptin (189).

Insulin fails to activate STAT3 signaling and thus alternative intracellular signaling pathways mediating insulin-evoked anorexia via control of the melanocortin system should exist. Since intracellular signaling pathways of both insulin and leptin converge at the level of the PI3 kinase (190), this pathway provided an excellent candidate for convergence of insulin and leptin action. Indeed, blockade of PI3 kinase activation inhibits both insulin's and leptin's acute anorexigenic effect in rats, indicating an important role for PI3 kinase activation in mediating the intracellular effects of both hormones (136, 191). Subsequently, it was demonstrated that insulin and leptin evoked PI3 kinase activation results in Akt-mediated phosphorylation of the transcription factor forkhead-O transcription factor (FOXO)1, thus leading to disinhibition of POMC transcription (186, 192). Central administration of insulin results in increased POMC and decreased NPY expression, without affecting AgRP expression (187, 193, 194). Besides regulating gene expression, PI3 kinase signaling and especially its product PIP3 has been shown to regulate cell excitability by binding to the regulatory subunit of ATP-dependent potassium channels (K_{ATP} channels) (195).

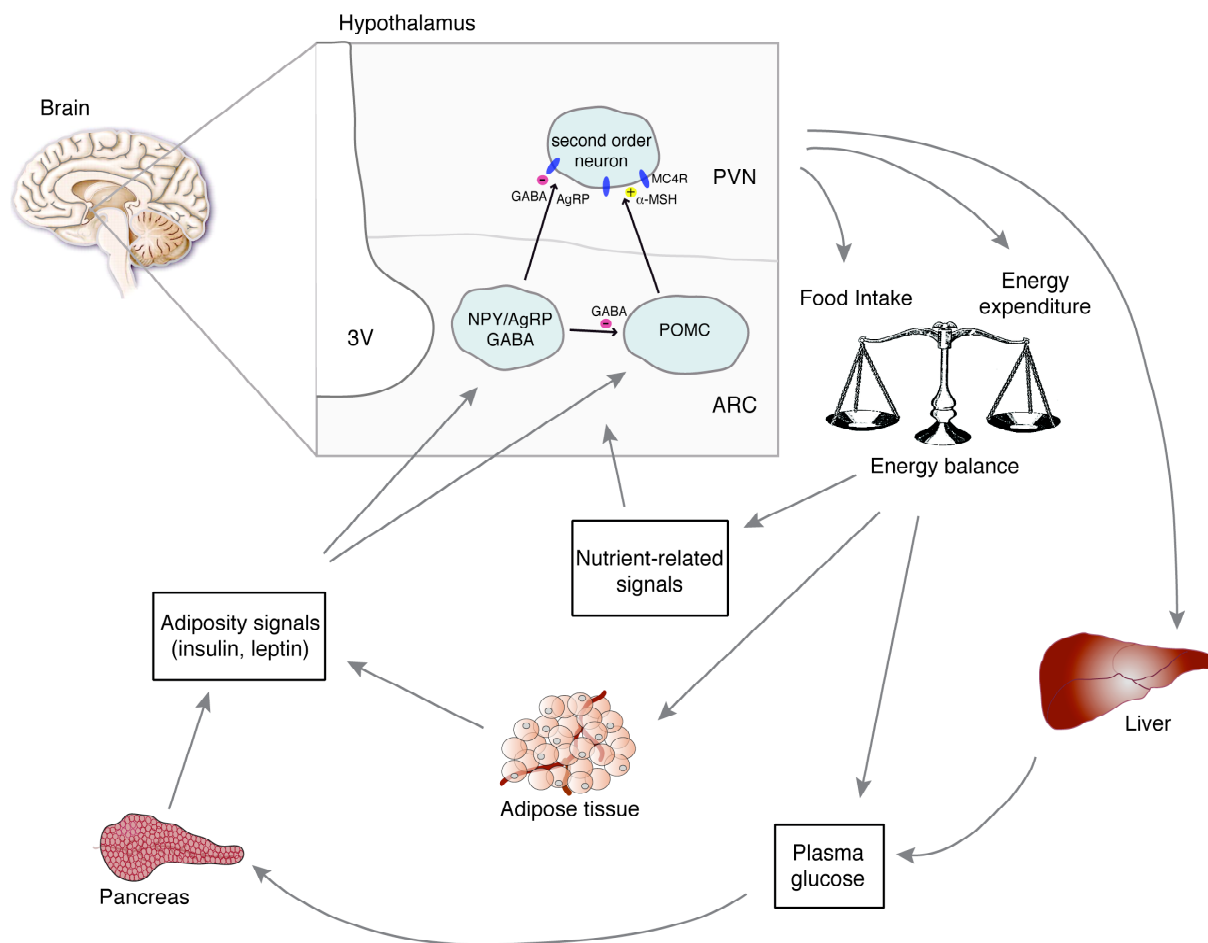


Figure 4: Central regulation of energy homeostasis.

The arcuate nucleus (ARC) contains both NPY/AgRP and POMC neurons, which are located close to the blood-brain barrier, where they have preferential access to peripheral humoral signals such as the pancreas-derived hormone insulin and the adipocyte-secreted hormone leptin as well as nutritional signals such as glucose and free fatty acids. Both neuronal populations exert potent effects on energy balance mediated by their characteristic neuropeptides, which allow modulation of second order neurons. POMC neurons project predominantly to second order neurons in the paraventricular nucleus (PVN) of the hypothalamus, where the POMC cleavage product α -MSH acts on melanocortin (MC) 4 receptors to suppress food intake. AgRP serves as an inverse agonist for the MC4 receptor, thus counteracting the function of α -MSH. In the ARC AgRP/NPY neurons provide inhibitory input onto POMC neurons via synaptic release of the transmitter GABA (γ -aminobutyric acid). AgRP/NPY and POMC neurons sense and integrate peripheral signals related to the amount of body fat such as insulin and leptin to cause a long-term, net catabolic response, decreasing food intake, increasing energy expenditure and regulating hepatic glucose production. Abbreviations: AgRP, agouti-related peptide; NPY, neuropeptide Y; POMC, proopiomelanocortin, α -MSH, α -melanocyte-stimulating hormone. [Adapted from Schwartz MW, Porte D; Diabetes, obesity, and the brain; 2005; (19)]

K_{ATP} channels were initially identified as metabolic sensors in the pancreas, where they sense elevated glucose levels through changes in ATP concentrations as a result of glucose metabolism in the cytoplasm. Elevated ATP concentrations lead to the closure of K_{ATP} channels, thereby opening voltage-dependent calcium channels, increasing intracellular calcium concentration, and thus triggering vesicle release (196).

K_{ATP} channels are widely expressed in different cell types of the brain: glia cells and neurons of the hippocampus and the hypothalamus (197-199), including POMC- and AgRP/NPY-expressing neurons. PIP3 modulates K_{ATP} channel activity via three different proposed mechanisms: (a) PIP3 increases the probability that K_{ATP} channels are open, which indirectly lowers the ability of ATP to inhibit the channels; (b) PIP3 directly decreases ATP binding to the channel (195, 200, 201); and (c) PIP 3 modulates K_{ATP} channel activity by degradation of local actin filaments around K_{ATP} channels (137).

Recent studies have addressed the role of PIP3 mediated K_{ATP} channel modulation in hypothalamic neurons with regard to energy and glucose metabolism. Constitutive activation of PIP3 formation in POMC cells by conditional ablation of the phospholipid phosphatase and tensin homolog (PTEN), a negative regulator of PI3 kinase signaling, results in hyperphagia, diet-sensitive obesity, and leptin resistance (202). Moreover, transgenic expression of a mutant subunit that prevents ATP-mediated closure of K_{ATP} channels resulted in impaired whole-body response to a systemic glucose load although with no obvious effect on body weight (203).

However, insulin and leptin receptors are expressed not only in the ARC, but also in the VMH, the LH and other hypothalamic sites, as well as in neurons of the midbrain (ventral tegmental area and substantia nigra) (56, 126, 204). Here, expression of the insulin and the leptin receptor and their functional signaling in dopaminergic neurons of the ventral tegmental area provides an interesting link between the hormonal control of food intake and the reward system (205-208).

1.7 The Dopaminergic System of the Brain

Regarding the functional components and brain substrates of reward, Berridge *et al.* proposed a model where they distinct between the components ‘wanting’ (appetite/incentive behavior) and ‘liking’ (pleasure/palatability) of food (209). Mediation of ‘wanting’ in terms of food reward involves in part the mesolimbic dopamine system, the nucleus accumbens and the amygdala (209).

Dopamine is a highly conserved catecholaminergic neurotransmitter involved in movement, goal-directed behavior, cognition, attention, and reward (for review see (210, 211)). It is utilized predominantly in the brain, where it controls the function of the basal nuclei and their associated projections. In the peripheral nervous system, it is used as a neurotransmitter in a few peripheral neuronal groups, but primarily serves as the substrate for the synthesis of norepinephrine and epinephrine in sympathetic neurons and the adrenal medulla (211, 212).

Dopamine is synthesized by hydroxylation of the amino acid L-tyrosine to L-dihydroxyphenylalanine (L-DOPA) via the enzyme tyrosine hydroxylase, the rate-limiting enzyme in catecholamine biosynthesis, and subsequent decarboxylation of L-DOPA by aromatic L-amino acid decarboxylase (dopa decarboxylase) (for review see (213)). In neurons, dopamine is stored in vesicles at the presynaptic nerve terminals, and is released into the synapse in response to a presynaptic action potential. Released dopamine activates its postsynaptic receptors, as well as presynaptic dopamine (D) 2 receptors to inhibit further release of the neurotransmitter. Extracellular dopamine is cleared from the synapses via the dopamine transporter (DAT) and inactivated by monoamine oxidase (MAO) and catechol-O-methyl-transferase (COMT) (213, 214).

The first dopamine receptors were identified by their ability to regulate cyclic adenosine monophosphate (cAMP) production and were shown to be the targets of neuroleptic agents (215). This defined two classes of dopamine receptors, D1 and D2, which respectively stimulate and inhibit cAMP production and can be differentiated pharmacologically, biologically, physiologically and by their anatomical distribution (for review see (216)). Subsequent cloning of these receptors demonstrated two D1-like receptors (D1 and D5) and three D2-like receptors (D2, D3, and D4). D1 and D2 are most abundant in the neostriatum, which comprises the caudate nucleus, putamen and nucleus accumbens. Here, they are enriched in distinct populations of striatal neurons, although there is a certain level of co-expression. All dopamine receptor subtypes are members of a large guanosine triphosphate-binding (G) protein-coupled receptor family, which is characterized by seven transmembrane hydrophobic domains, an extracellular N- and an intracellular C-terminus. Downstream effects are either inhibitory or stimulatory, depending on the types of G protein linked to the receptor – dopamine D1 and D5 receptors are linked to inhibitory G proteins, whereas dopamine receptor D2, D3 and D4 are linked to stimulatory G proteins (for review see (216)).

Dopamine neurons innervating the dorsal striatum (caudate nucleus and putamen (CPu)) are located in the substantia nigra (SN), while those innervating the ventral striatum (nucleus accumbens (NAc)) and the prefrontal cortex are located in the ventral tegmental area (VTA) (217).

The dopamine reward system, especially the projections from the VTA to the NAc, are well known for its link to drug addiction, and the rewarding aspects of food and sex (218, 219). In contrast, bradykinesia and impairment in movements, the characteristic symptoms of Parkinson's Disease, are caused by impaired dopamine signaling to the CPu, which is based on the degeneration of dopaminergic neurons in the SN (for review see (220)).

Midbrain dopaminergic neurons fire in bursts – a repetitive occurrence of groups of action potentials with short interspike intervals –, which is associated with the presentation of rewarding stimuli (221-223). Such burst firing results in an efficient release of dopamine from the nerve terminals and soma / dendrites (224), which helps an animal to highlight important environmental signals while suppressing irrelevant ones. Importantly, mice with selective inactivation of the *tyrosine hydroxylase* gene, the rate-limiting enzyme in dopamine biosynthesis, become hypophagic, hypoactive and die of starvation by 3 to 4 weeks of age (225).

1.7.1 Peripheral Hormonal Signals in Food Reward

Neuronal mechanisms underlying food reward may be closely related or similar to mechanisms of drug reward. Food and water are naturally rewarding and motivating stimuli, which promote burst firing of dopamine neurons, thereby facilitating goal-directed behavior towards the acquisition of food or water (222, 223, 226, 227). The brain regions activated by a food reward stimulus (e.g. highly palatable food) are the same regions responsive to drugs of abuse and involved in the development of drug addiction (for review see (228, 229)). There is also evidence that dysregulation of those drug reward circuits is involved in the development of obesity. Imaging studies in humans demonstrated that D2 receptor availability is decreased in obese individuals in proportion to their BMI (230), and treatment of *ob/ob* mice with dopamine D1/D2 receptor agonists normalizes hyperphagia, body weight gain, hyperglycemia, and hyperlipidemia (231). Notably, chronic food restriction and maintenance of low body weight increase the self-administration and motor-activating effects of abused drugs (232-234). By using a lateral hypothalamic self-stimulation rate frequency method, Carr *et al.* could demonstrate that food restriction augments the rewarding effect of diverse drugs of abuse (235). Electrical self-stimulation of a subset of neurons in the LH results in an

induced food intake in rats and this effect is augmented with food restriction (236). Furthermore, self-administration of food, and the ability of food to condition an animal to a place preference are increased with food deprivation (237-240).

Both insulin and leptin, when administered locally to the brain, are able to reverse the shifted threshold of LH self-stimulation after food restriction (241, 242). Moreover, intracerebroventricular (icv) administered leptin attenuates the acute food deprivation-induced relapse to heroin self-administration in rats (243). Furthermore, peripheral applied leptin reverses sucrose-conditioned place preference in food-restricted rats (244). Finally, studies have implicated the IRS 2-Akt signaling pathway as an important regulator of dopamine cell morphology and opiate reward (245). Taken together, insulin and leptin may play a role in modulating the reward system in the CNS.

Activity of the dopaminergic midbrain system is known to be involved in motivational driven behaviors, and the aspect of reward or motivation can be tested in different behavioral paradigms. Figlewicz *et al.* analyzed the ability of icv-administered insulin and leptin at physiological doses, which do not cause a change in body weight or food intake, to modify performance of an animal in such food reward tasks in *ad libitum* fed rats. To evaluate whether insulin is able to alter performance of a sucrose lick task, which is known to be dependent on intact dopaminergic signaling, the authors tested the effect of icv insulin and the selective D2 receptor antagonist raclopride. Although ineffective on its own, icv insulin combined with raclopride significantly suppressed sucrose lick rate in a five-minute task (246), indicating that insulin indeed could decrease the reward value of a sucrose solution. The conditioned place preference (CPP) task, which also depends on intact dopaminergic signaling in the CNS (238, 244), evaluates the preferences for environmental stimuli that have been associated with a reward (food or drug). CPP to a high fat diet is blocked in *ad libitum* fed rats given icv insulin or leptin (247), again indicating that insulin and leptin can influence the reward value of food. Finally, in a sucrose self-administration task, in which the motivation to work for a sucrose reward is measured by pressing a lever, both insulin and leptin icv decreased the number of presses on the lever (248). These results indicate that both insulin and leptin are involved in multiple aspects of food reward: hedonics, place preference, and the motivation to work for a reward (for review see (249)).

Consistent with a modulatory role of these hormones on the reward system, insulin and leptin receptors are co-expressed with tyrosine hydroxylase - a marker for dopamine neurons - in the VTA and SN (204). Furthermore, insulin or leptin administration into the VTA results in an increased formation of PIP3 as compared to control injections (249). Here,

PIP3, the product of the PI3 kinase, serves as an indicator for a functional signaling pathway. Furthermore, it has been shown that leptin receptor mRNA is expressed in the VTA and in response to peripheral, icv or direct VTA leptin injection the intracellular JAK-STAT pathway becomes activated (205, 242). This evidence suggests that the insulin and leptin receptors are functional, and that the respective signaling pathways are indeed activated in these dopaminergic cells. Moreover, activation of the JAK-STAT pathway has been shown to be critical for the effect of leptin in the VTA to decrease food intake (205). Finally, electrophysiology studies revealed that leptin significantly reduces the firing rate of dopaminergic neurons in the VTA (205).

1.8 Objectives

Obesity and type 2 diabetes mellitus are intimately connected diseases and their incidences are steadily increasing worldwide. Therefore, there is an urgent need for the development of therapeutical approaches to treat the obesity epidemic. The central nervous system serves as a central regulator of energy homeostasis by integrating hormonal signals from the periphery of the organism such as insulin and leptin to adapt food intake, energy expenditure and glucose metabolism to the degree of peripheral energy sources. Receptors for both insulin and leptin are expressed in various regions of the brain and extensive research over the last 30 years has identified the mediobasal hypothalamus, a region mainly involved in the regulation of energy homeostasis, as a major target for insulin and leptin. To precisely define the hypothalamic neuronal populations mediating insulin's central effects on energy and glucose homeostasis *in vivo*, the insulin receptor was genetically deleted in POMC- and AgRP-expressing neurons of mice, and physiological parameters in terms of energy homeostasis and glucose metabolism were analyzed in these animals. Furthermore, food palatability and reward are thought to be major factors involved in the regulation of food intake and energy homeostasis, and insulin has been shown to modulate the reward system of the brain. To analyze the role of insulin signaling in the dopaminergic system of the brain *in vivo*, the insulin receptor was genetically ablated in dopaminergic cells, and mice were analyzed in terms of energy homeostasis.

2 Materials and Methods

2.1 Chemicals and Biological Material

Size markers for agarose gel electrophoresis (Gene Ruler™ DNA Ladder Mix) and for SDS-PAGE (Page Ruler™ Prestained Protein Ladder Mix) were obtained from MBI Fermentas, St. Leon-Rot, Germany. RedTaq® DNA Polymerase and 10x RedTaq® buffer were purchased from Sigma-Aldrich, Seelze, Germany. All chemicals used in this work are listed in table 1 and all enzymes used in this work are listed in table 2. Solutions were prepared with double distilled water.

Table 1: Chemicals

Chemical	Supplier
β-Mercaptoethanol (β-ME)	AppliChem, Darmstadt, Germany
ε-aminocaproic acid	Sigma-Aldrich, Seelze, Germany
0.9% saline (sterile)	Delta Select, Pfullingen, Germany
2,2,2-Tribromoethanol (Avertin®)	Sigma-Aldrich, Seelze, Germany
2-Deoxy-D-[1- ¹⁴ C]-Glucose	Amersham, Freiburg, Germany
2-Methyl-2-Butanol	Sigma-Aldrich, Seelze, Germany
Acetic acid	Merck, Darmstadt, Germany
Acetone	KMF Laborchemie, Lohmar, Germany
Acrylamide	Roth, Karlsruhe, Germany
Agarose	Peqlab, Erlangen, Germany
Agarose (Ultra Pure)	Invitrogen, Karlsruhe, Germany
Ammonium Acetate	Merck, Darmstadt, Germany
Ammoniumpersulfat (APS)	Sigma-Aldrich, Seelze, Germany
Aprotinin	Sigma-Aldrich, Seelze, Germany
Avidin Biotin Complex-Vectastain Elite	Vector, Burlingame, USA
Bacillo®	Bode Chemie, Hamburg, Germany
Barium hydroxide	Fluka, Sigma-Aldrich, Seelze, Germany
Benzamidine	Sigma-Aldrich, Seelze, Germany
Bovine serum albumin (BSA)	Sigma-Aldrich, Seelze, Germany
Bromphenol blue	Merck, Darmstadt, Germany
Calcium chloride	Merck, Darmstadt, Germany
Chloroform	Merck, Darmstadt, Germany

Count off™	NEN® Research Products, Boston, USA
D-[3- ³ H]-Glucose	Amersham, Freiburg, Germany
Desoxy-Ribonucleotid-Triphosphates (dNTPs)	Amersham, Freiburg, Germany
Diaminobenzidin (DAB)	Dako, Denmark
Dimethylsulfoxide (DMSO)	Merck, Darmstadt, Germany
di-Natriumhydrogenphosphat	Merck, Darmstadt
Enhanced chemiluminescence (ECL) Kit	Perbio Science, Bonn, Germany
Ethanol, absolute	AppliChem, Darmstadt, Germany
Ethidium bromide	Sigma-Aldrich, Seelze, Germany
Ethylendiamine tetraacetate (EDTA)	AppliChem, Darmstadt, Germany
Forene® (isoflurane)	Abbot GmbH, Wiesbaden, Germany
Glucose 20%	DeltaSelect, Pfullingen, Germany
Glycerol	Serva, Heidelberg, Germany
Glycine	Applichem, Darmstadt, Germany
HEPES	Applichem, Darmstadt, Germany
Hydrochloric acid (37 %)	KMF Laborchemie, Lohmar, Germany
Hydrogen peroxide	Sigma-Aldrich, Seelze, Germany
Insulin	Novo Nordisk, Bagsværd, Denmark
Isopropanol (2-propanol)	Roth, Karlsruhe, Germany
Kaisers Glycerin Gelatine	Merck, Darmstadt, Germany
Magnesium chloride	Merck, Darmstadt, Germany
Methanol	Roth, Karlsruhe, Germany
Nitrogen (liquid)	Linde, Pullach, Germany
Octenisept®	Schülke & Mayr, Norderstedt, Germany
Paraformaldehyde (PFA)	Fluka, Sigma-Aldrich, Seelze, Germany
Phenylmethylsulfonylfluoride (PMSF)	Sigma-Aldrich, Seelze, Germany
Phosphate buffered saline (PBS)	Gibco BRL, Eggenstein, Germany
Potassium chloride	Merck, Darmstadt, Germany
Potassium hydroxide	Merck, Darmstadt, Germany
Ready Safe™, Liquid Scintillation Cocktail	Beckman Coulter, Fullerton, USA
Sodium acetate	AppliChem, Darmstadt, Germany
Sodium chloride	AppliChem, Darmstadt, Germany
Sodium citrate	Merck, Darmstadt, Germany
Sodium dodecyl sulfate	AppliChem, Darmstadt, Germany
Sodium fluoride	Merck, Darmstadt, Germany

Sodium heparin (Liquemin [®])	Roche, Grenzach-Wyhlen, Switzerland
Sodium hydroxide	AppliChem, Darmstadt, Germany
Sodium orthovanadate	Sigma-Aldrich, Seelze, Germany
Somatostatin	Sigma-Aldrich, Seelze, Germany
Sucrose	AppliChem, Darmstadt, Germany
Tetramethylethylenediamine (TEMED)	Sigma-Aldrich, Seelze, Germany
Tissue Freezing Medium	Jung, Heidelberg, Germany
Tramadolhydrochlorid (Tramal [®])	Grünenthal, Aachen, Germany
Trishydroxymethylaminomethane (Tris)	AppliChem, Darmstadt, Germany
Triton X-100	Appllichem, Darmstadt, Germany
Tween 20	Appllichem, Darmstadt, Germany
Vectashield [®] Mountin Medium with DAPI	Vector, Burlingame, USA
Western Blocking Reagent	Roche, Mannheim, Germany
Zinc sulfate	Fluka, Sigma-Aldrich, Seelze, Germany

Table 2: Enzymes

Enzymes	Supplier
DNase, RNase-free	Promega, Madison, WI, USA
EuroScript Reverse Transcriptase	Eurogentec, Seraing, Belgium
Proteinase K	Roche, Basel, Switzerland
Red Taq [®] DNA Polymerase	Sigma-Aldrich, Seelze, Germany
RNase Inhibitor	Eurogentec, Seraing, Belgium

2.2 Molecular Biology

Standard methods of molecular biology were performed according to protocols described by J. Sambrook (250), unless stated otherwise.

2.2.1 Isolation of Genomic DNA

Mouse tail biopsies were incubated 1 h in lysis buffer (100 mM Tris-HCl [pH 8.5], 5 mM EDTA, 0.2% (w/v) SDS, 0.2 M NaCl, 500 mg/ml proteinase K) in a thermomixer (Eppendorf, Hamburg, Germany) at 56°C. DNA was then precipitated from the solution by adding an equivalent of isopropanol. After washing with 70 % (v/v) EtOH and centrifugation, the DNA pellet was dried at 60°C for 10 min and resuspended in double distilled water (ddH₂O).

2.2.2 Quantification of Nucleic Acids

DNA and RNA concentrations were assessed by measuring the sample absorption at 260 nm with a NanoDrop® ND-1000 UV-Vis Spectrophotometer (Peqlab, Erlangen, Germany). An optical density of 1 corresponds to approximately 50 µg/ml of double stranded DNA and to 38 µg/ml of RNA. To assess purity of nucleic acids, the ratio of absorptions at 260 nm versus 280 nm was calculated, as proteins absorb maximum at 280 nm. An OD₂₆₀/OD₂₈₀ ratio of 2 refers to pure nucleic acids, lower values display protein contaminations.

2.2.3 Polymerase Chain Reaction (PCR)

The PCR method (251, 252) was used to genotype mice for the presence of floxed alleles or transgenes with customized primers listed in Table 3. Reactions were performed in a Thermocycler iCycler PCR machine (Bio-Rad, München, Germany) or in a Peltier Thermal Cycler PTC-200 (MJ Research, Waltham, USA). All amplifications were performed in a total reaction volume of 25 µl, containing a minimum of 50 ng template DNA, 25 pmol of each primer (listed in table 3), 25 µM dNTP Mix, 10 x RedTaq® reaction buffer and 1 unit of RedTaq® DNA Polymerase. Standard PCR programs started with 4 min of denaturation at 95°C, followed by 30 cycles consisting of denaturation at 95°C for 45 seconds (sec), annealing at oligonucleotide-specific temperatures for 30 sec and elongation at 72°C for 30 sec, and a final elongation step at 72°C for 7 min.

Table 3: Oligonucleotides used for genotyping.

All primer sequences are displayed in 5'-3' order. Primer orientation is designated "sense" when coinciding with transcriptional direction. All primers were purchased from Eurogentec, Cologne, Germany.

Primer	Sequence (5'-3')	T_{Annealing} [°C]	Orientation
<i>AgRPCre5'</i>	CCCTAAGGATGAGGAGAGAC	54	sense
<i>Cre-intern-rev-3</i>	ATGTTTAGCTGGCCCAAATGT	50	antisense
<i>AgRP-3</i>	CCAACCTGACCATACTCACC	54	antisense
<i>PomcCre N16R</i>	TGGCTCAATGTCCTTCCTGG	54	sense
<i>PomcCre N57R</i>	CACATAAGCTGCATCGTTAAG	50	antisense
<i>PomcCre AA03</i>	GAGATATCTTTAACCCCTGATC	49	antisense
<i>IR-5</i>	GATGTGCACCCCATGTCTG	53	sense
<i>IR-3</i>	CTGAATAGCTGAGACCACAG	52	antisense
<i>IR-delta-5</i>	GGGTAGGAAACAGGATGG	50	sense
<i>Th-5</i>	CACCCTGACCCAAGCACT	53	sense
<i>Th-3</i>	CTTTCCTTCCTTTATTGAGAT	47	antisense
<i>CreUD</i>	GATACCTGGCCTGGTCTG	53	antisense
<i>GFP-5</i>	CTGGTCGAGCTGGACGGCGACG	64	sense
<i>GFP-3</i>	CAGGAACTCCAGCAGGACCATG	59	antisense
<i>LacZ-5</i>	ATGGATGAGCAGACGATGGT	52	sense
<i>LacZ-3</i>	TTTGATCCAGCGATACAGCG	52	antisense

PCR-amplified DNA fragments were applied to 1% - 2% (w/v) agarose gels (1 x TAE, 0.5 mg/ml ethidium bromide) and electrophoresed at 100 V.

2.2.4 RNA Extraction, RT PCR and Quantitative Realtime PCR

Mouse tissues were dissected and homogenized using an Ultra Turrax homogenizer (IKA, Staufen, Germany). Total RNA was extracted using the Qiagen RNeasy Kit (Qiagen, Hilden, Germany). After treatment with RNase-free DNase, 200 ng of each RNA sample were reversely transcribed using the Eurogentec RT Kit (Eurogentec, Cologne, Germany) according to manufacturer's protocols. The cDNA was subsequently amplified using TaqMan® Universal PCR-Master Mix, NO AmpErase® UNG with TaqMan® Assay on demand kits (Applied Biosystems, Foster City, USA) with the exception of the detection of POMC mRNA (see Table 4). Customized primers were used for the detection of POMC

mRNA: POMC sense 5'-GACACGTGGAAGATGCCGAG-3'; anti-sense, 5'-CAGCGAGAGGTCGAGTTTGC-3'; probe sequence, 5'-FAM-CAACCTGCTGGCTTGCATCCGG-TAMRA-3'. Relative expression of samples was adjusted for total RNA content by glucuronidase beta (Gusb) and hypoxanthine guanine phosphoribosyl transferase (Hprt)-1 RNA quantitative Realtime PCR. Calculations were performed by a comparative method ($2^{-\Delta\Delta CT}$). Quantitative PCR was performed on an ABI-PRISM 7700 Sequence Detector (Applied Biosystems, Foster City, CA, USA). Assays were linear over 4 orders of magnitude.

Table 4: Probes used for Realtime PCR.

All probes were purchased from Applied Biosystems, Foster City, USA.

Probe	Catalogue N°	Probe	Catalogue N°
AgRP	Mm00475829_g1	DAT	Mm00438388_m1
Ccl2	Mm00441242_m1	Ddc	Mm00516688_m1
Ccl3	Mm00441258_m1	Gusb	Mm00446953_m1
Ccl5	Mm01302428_m1	Hprt-1	Mm00446968_m1
COMT	Mm00514377_m1	IL-6	Mm00446190_m1
Cxcl2	Mm00436450_m1	MAOB	Mm00558004_m1
D1R	Mm01353211_m1	NPY	Mm00445771_m1
D2R	Mm00438541_m1	TH	Mm00447557_m1
D3R	Mm00432887_m1	TNF- α	Mm00443258_m1

2.3 Cell Biology

2.3.1 Histological Analysis and Immunohistochemistry

2.3.1.1 Immunohistochemistry

IR^{ΔPOMC} and IR^{ΔAgRP} mice were mated with *LacZ* reporter mice (253). IR^{ΔPOMC/LacZ}, IR^{ΔAgRP/LacZ} and wildtype reporter (*PomcCre-*, *AgRPCre-LacZ*) mice were anesthetized and transcardially perfused with physiologic saline solution followed by 4% paraformaldehyde (PFA) in 0.1 M phosphate buffered saline (PBS; pH 7.4). The brains were dissected, post-fixed in 4% PFA at 4°C, transferred to 20% sucrose for 6 h and frozen in tissue freezing medium. Then, 25 μ m thick free-floating coronal sections were cut through the ARC using a freezing microtome (Leica). The sections were collected in PBS/azide (pH 7.4) and washed

extensively to remove cryoprotectant. Subsequently, the sections were treated with 0.3% H₂O₂ in PBS for 20 min to quench endogenous peroxidase activity. Following pretreatments, the sections were processed using the Renaissance[®] TSA[™] Fluorescence Systems Tyramide Signal Amplification Kit (PerkinElmer[™]) according to manufacturer's guidelines (primary antibody: rabbit anti-lacZ, # 55976; Cappel; secondary antibody: goat anti-rabbit peroxidase labeled, Vector Laboratories).

For visualization of GFP expression after Cre-recombination, *ThIRESCre* mice were mated with *Z/EG* reporter mice (254). Double heterozygous *ThIRESCre-Z/EG* reporter mice were anesthetized and transcardially perfused with physiologic saline solution followed by 4% paraformaldehyde. Brains were dissected and post-fixed in 4% PFA at 4°C, transferred to 20% sucrose for 6 h and frozen in tissue freezing medium. Then, 25 µm thick free-floating coronal sections were cut through the ventral tegmental area using a freezing microtome (Leica). The sections were washed, pretreated with 0.3% H₂O₂, blocked with PBT/azide containing 3% donkey serum, and incubated overnight with primary antibody (anti-GFP rabbit serum, 1:10.000 in blocking solution; A6455 from Invitrogen/Molecular Probes). Incubation with secondary antibody (anti-rabbit IgG biotin, 1:500; 711-065-152 from Jackson ImmunoResearch) was followed by an additional incubation with the VECTASTAIN Elite ABC kit (Vector Laboratories) for 1 h and visualization with 0.4% DAB/0.01% H₂O₂. Afterwards the sections were mounted onto gelatin-coated slides and covered with glycerin and processed as previously described (255).

For determination of the functional effects of neuron-restricted insulin receptor deficiency IR^{ΔPOMC}, IR^{ΔAgRP} as well as IR^{ΔTh} mice were mated with *LacZ* reporter mice (253). IR^{ΔPOMC/LacZ}, IR^{ΔAgRP/LacZ}, IR^{ΔTh/LacZ} and wildtype reporter (*PomcCre-*, *AgRPCre-*, *ThIRESCre-LacZ*) mice were starved over night, anesthetized, and intravenously injected with either saline or 5U of human regular insulin (NovoNordisc) for 10 min. Mice were then perfused transcardially with physiologic saline solution; brains were dissected, frozen in tissue freezing medium (Jung Tissue Freezing Medium[™]) and sectioned on a cryostat (7 µm). Tissues were stained with galactosidase (# 55976; Cappel) and PIP3 (# Z-G345; Echelon, FITC) and double fluorescence immunostaining was performed as previously described (202).

Slides were viewed through a Zeiss Axioskop equipped with a Zeiss AxioCam for acquisition of digital images using Spot Advanced 3.0.3 software.

2.3.1.2 Analysis of PIP3 formation *in situ*

For quantitative analysis of PIP3 levels in POMC neurons, a total of 1812 LacZ-positive neurons was counted in ARC slices of control mice injected with NaCl, (n = 3; 365 POMC neurons), insulin-stimulated control mice (n = 4, 532 POMC neurons), IR^{ΔPOMC} mice injected with NaCl (n = 3; 423 POMC neurons) and insulin-stimulated IR^{ΔPOMC} mice (n = 3, 492 POMC-neurons). For quantitative analysis of PIP3 levels in AgRP neurons, a total of 673 LacZ-positive neurons was counted in ARC slices of control mice injected with NaCl, (n = 2; 75 AgRP neurons), insulin-stimulated control mice (n = 2, 57 AgRP neurons), IR^{ΔAgRP} mice injected with NaCl (n = 1; 95 AgRP-neurons) and insulin-stimulated IR^{ΔAgRP} mice (n = 4, 446 AgRP-neurons). For quantitative analysis of PIP3 levels in Th-expressing neurons, a total of 531 LacZ-positive neurons was counted in VTA/SN slices of control mice injected with NaCl, (n = 2; 128 Th-expressing neurons), insulin-stimulated control mice (n = 3, 179 Th-expressing neurons), IR^{ΔTh} mice injected with NaCl (n = 2; 64 Th-expressing neurons) and insulin-stimulated IR^{ΔTh} mice (n = 4, 160 Th-expressing neurons).

The amount of PIP3 was classified either as low (immunoreactive cytoplasmatic dots/sprinkles in the proximity of the nucleus at background levels, i.e., 6 or fewer dots, no cloudy aspect, no confluent areas), moderate (dots/sprinkles at levels above background, i.e., more than 6 dots, cloudy aspect), or high (numerous dots/sprinkles, cloudy with confluent areas). Slides were viewed through a Zeiss Axioskop equipped with a Zeiss AxioCam for acquisition of digital images. Neurons positive for β-gal were counted and marked digitally to prevent multiple counts, and PIP3 immunoreactivity was rated as previously described (202) using Zeiss AxioVision version 4.2 imaging software. Results were expressed as percentage of POMC, AgRP or Th-expressing neurons, which show the respective PIP3 levels.

2.3.2 Histomorphology

Dissected samples (ovaries, testes) were incubated in fixation solution containing 4% (w/v) PFA at 4 °C overnight and embedded in paraffin according to a standard protocol. 7 μm sections were mounted onto gelatin-coated slides and hematoxylin/eosin-stained (H&E) (Sigma, St. Louis, MO, USA) after deparaffinization. Stained sections were viewed under a Zeiss Axiophot and pictures were taken with a digital color camera (Spot Diagnostic Instruments, Inc., MI, USA) using Spot Advanced 3.0.3 software.

2.3.3 Electrophysiology

Coronal brain slices (250 - 300 μm) containing the ARC were prepared from 6-week-old *AgRPCre-Z/EG* and *IR^{ΔAgRP}-Z/EG* mice. After at least 15 min recovery at 35°C in artificial cerebrospinal fluid (aCSF) gassed with 95% O₂ and 5% CO₂, brain slices were transferred to a recording chamber and continuously perfused at 2 - 4 ml/min with gassed aCSF. aCSF contained (in mM): 125 NaCl, 21 NaHCO₃, 2.5 KCl, 1.2 NaH₂PO₄, 2 CaCl₂, 2 MgCl₂, 10 HEPES (pH 7.4), and 5 glucose. Brain slices were viewed with a Zeiss Axioskop fitted with fluorescence and infrared differential interference contrast (IR-DIC) videomicroscopy. Fluorescent AgRP-EGFP neurons were identified by epifluorescence and patched under IR-DIC optics. Whole-cell current-clamp and voltage-clamp recordings were made using an EPC-9 patch-clamp amplifier, as previously described (202, 256). Patch pipettes had resistances of 3-5 M Ω when filled with internal solution. For most experiments, patch pipettes were filled with internal solution containing (in mM): 128 K-gluconate, 10 KCl, 10 HEPES (pH 7.3, adjusted with KOH), 0.1 EGTA, 2 MgCl₂, 0.3 Na-GTP, and 3 K₂-ATP. The external solution was aCSF in all experiments. Experiments were carried out at 22 - 25°C. Data were filtered, sampled with Pulse/Pulsefit and software (Heka, Elektronik, Germany, version 8.67) and analyzed with Pulsefit and Origin (Microcal, Northampton, MA) software (version 6.0).

Responses to insulin (200 nM; Sigma) in fluorescently labeled POMC neurons in brain slices from 10 week old transgenic mice (*PomcCre-Z/EG* and *IR^{ΔPOMC}-Z/EG*) were assessed using standard whole cell patch clamp in the current clamp mode, using Axopatch 200B (Molecular Devices, Sunnyvale CA), as previously described (176). Baseline membrane potential and action potential firing frequency were determined using Mini Analysis (Synaptosoft, Decatur GA).

2.3.4 Electron Microscopy

After a long-term euglycemic-hyperinsulinemic clamp, 11-week-old C57BL/6 male mice from the control group (somatostatin) and the treatment group (somatostatin + insulin) were perfused for electron microscopy. Mice were anesthetized and perfused transcardially with saline followed by Somogyi-Takagi fixative containing 4% paraformaldehyde and 0.8% glutaraldehyde in 0.1 M phosphate buffer. A tissue block containing the ventral tegmental area was dissected from each brain. 50 μm thick vibratome sections were cut and thoroughly washed in 0.1 M phosphate buffer (PB). To eliminate unbound aldehydes, sections were

incubated in 1% sodiumborohydride for 15 min, and then rinsed in PB. Next, sections were incubated in rabbit anti-GFP (Molecular Probes Inc., Eugene, OR) (dilution 1:1000 in PB) for 24 h at room temperature. Subsequently, sections were incubated in biotinylated goat anti-rabbit immunoglobulin (dilution 1: 250; Vector Laboratories, Burlingame, CA, USA) at room temperature. After a thorough wash in PB, sections were placed in avidin-biotin-complex (ABC Elite Kit, Vector Labs) for 2 h at room temperature. The tissue-bound peroxidase was visualized by a diaminobenzidine reaction. After the immunostaining, the sections were osmicated (15 min in 1% osmic acid in PB), and dehydrated in increasing ethanol concentrations. During the dehydration, 1% uranyl-acetate was added to the 70% ethanol to enhance ultrastructural membrane contrast. Dehydration was followed by flatembedding in Araldite. Ultrathin sections were cut on a microtome, collected on Formvar-coated single-slot grids and analyzed with a Tecnai 12 Biotwin (FEI Company) electron microscope. The quantitative analysis of synapse numbers was performed in a double-blind fashion on electron micrographs from mice of different experimental groups. To obtain a complementary measure of axo-somatic synaptic number, unbiased for possible changes in synaptic size, the disector technique was used (S4). On consecutive 90-nm-thick sections, the average projected height of the synapses was determined and about 30% of this value was used as the distance between the disectors. On the basis of this calculation, the number of axo-somatic synapses was counted from 7 perikaryal profiles in two consecutive serial sections roughly 270 nm apart (the "reference" and "look-up" sections) from each tissue block. In order to increase the sampling size, the procedure was repeated in such a way that the reference and look-up sections were reversed. The numbers of symmetrical, asymmetrical and total contacts were collected independently from serial sections. Synapse characterization was performed at 20,000 magnification, while all quantitative measurements were performed on electron micrographs at a magnification of 11,000. Symmetric and asymmetric synapses were counted on all selected neurons only if the pre- and/or postsynaptic membrane specializations were clearly seen and synaptic vesicles were present in the presynaptic bouton. Asymmetric synapses are formed by axons that contain large vesicles and excitatory neurotransmitters (i.e. primarily glutamate; excitatory synapses). In contrast, symmetric synapses have presynaptic axons with small synaptic vesicles that contain the inhibitory transmitter γ -aminobutyric acid (GABA). The presynaptic and postsynaptic densities of these synapses are approximately of equal thickness (inhibitory synapses). Synapses with neither clearly symmetric nor asymmetric membrane specializations were excluded from the assessment. The plasma membranes of selected cells were outlined on photomicrographs and their length was

measured with the help of a chartographic wheel. Plasma membrane length values measured in the individual animals were added and the total length was corrected to the magnification applied. Synaptic densities were evaluated according to the formula $NV=Q-/V_{dis}$ where Q- represents the number of synapses present in the "reference" section that disappeared in the "look-up" section. V_{dis} is the disector volume (volume of reference) which is the area of the perikaryal profile multiplied by the distance between the upper faces of the reference and look-up sections, i.e. the data are expressed as numbers of synaptic contacts per unit volume of perikaryon. Section thickness was determined by using the Small's minimal fold method. The synaptic counts were expressed as numbers of synapses on a membrane length unit of 100 μm . Since an F-test analysis of synaptic counts in the ARC of the mice has revealed a significant nonhomogeneity of variances between groups, the Kruskal-Wallis one-way non-parametric analysis of variance test was selected for multiple statistical comparisons. The Mann-Whitney U-test was used to determine significance of differences between the groups. A level of confidence of $P < 0.05$ was employed for statistical significance.

2.4 Biochemistry

2.4.1 Enzyme-linked Immunosorbent Assay (ELISA)

Serum insulin and leptin, as well as plasma corticosterone concentrations were measured by ELISA according to manufacturer's guidelines (Mouse Leptin ELISA, Mouse/Rat Insulin ELISA, Crystal Chem, Downers Grove, IL, USA; Insulin Mouse Ultrasensitive ELISA, DRG Instruments GmbH; Mouse Leptin Immunoassay, Quantikine; Corticosterone Enzyme Immunoassay Kit, Assay Designs Inc.). For evaluation of steady state clamped insulin serum levels, an ultrasensitive Insulin ELISA for determination of human insulin was performed according to manufacturer's guidelines (Ultrasensitive Insulin ELISA, #EIA-2337, DRG Instruments).

2.4.2 Protein Extraction

Snap-frozen tissues were thawed and homogenized in lysis buffer (50 mM HEPES (pH 7.4), 1% Triton X-100, 0.1 M NaF, 10 mM EDTA, 50 mM NaCl, 10 mM $\text{Na}_3\text{O}_4\text{V}$, 0.1% SDS, 10 $\mu\text{g}/\text{ml}$ Aprotinin, 2 mM Benzamidine, 2 mM PMSF) using a polytron homogenizer (IKA Werke, Staufen, Germany). Particulate matter was removed by centrifugation for 1 h at 4°C. The supernatant was transferred to a new vial and protein concentrations were

determined by measuring the sample absorption at 280 nm with a NanoDrop® ND-1000 UV-Vis Spectrophotometer (Peqlab, Erlangen, Germany). Proteins that contain Trp, Tyr residues or Cys-Cys disulphide bonds absorb in the UV range of 280 nm. Subsequently, protein extracts were diluted to 10 mg/ml with lysis buffer and 4 x SDS sample buffer (125 mM Tris-HCl (pH 6.8), 5% SDS, 43.5% glycerol, 100 mM DTT, and 0.02% bromophenol blue), incubated at 95°C for 5 min and stored at -80°C.

2.4.3 Western Blot Analysis

Frozen protein extracts were thawed at 95°C for 5 min, then separated on 8 - 10% (v/v) SDS polyacrylamide gels and blotted onto PVDF membranes (Bio-Rad, München, Germany). Membranes were then incubated with 1% blocking reagent (Roche, Mannheim, Germany) for 1 h at RT or overnight at 4°C. Subsequently, primary antibodies (Table 5) diluted in 0.5% blocking solution were applied for 1 h at RT or overnight at 4°C. PVDF membranes were then washed twice for 10 min with 1 x TBS/Tween and incubated twice for 10 min with 0.5% blocking solution. After 1 h incubation at RT with the respective secondary antibodies, membranes were washed 4 times for 5 min with 1 x TBS/Tween, incubated for 1 min in Pierce ECL Western Blotting Substrate (Perbio Science, Bonn, Germany), sealed in a plastic bag and exposed to chemiluminescence films (Amersham, Braunschweig, Germany). Films were developed in an automatic developer.

Table 5: Primary antibodies used for Western blot analysis.

Antibody	Catalogue N°	Distributor	Dilution
β-Actin	#A5441	Sigma Aldrich, Seelze, Germany	1:5000
α-Tubulin	#T6074	Sigma Aldrich, Seelze, Germany	1:5000
Akt	#4685	Cell Signaling, Danvers, MA, USA	1:1000
G6Pase-α	sc-25840	Santa Cruz, Heidelberg, Germany	1:200
IRβ (C-19)	sc-711	Santa Cruz, Heidelberg, Germany	1:200
pAkt	#4056	Cell Signaling, Danvers, MA, USA	1:1000

2.5 Mouse Experiments

General animal handling was performed as described by Hogan (257) and Silver (258).

2.5.1 Animal Care

All animal procedures and euthanasia were reviewed by the animal care committee of the University of Cologne, approved by local government authorities (Bezirksregierung Köln) and were in accordance with National Institutes of Health guidelines. Mice were housed in groups of 3 to 5 or individually if required for an experiment as indicated. Mice were housed in a virus-free facility at 22 - 24°C on a 12 h light / 12 h dark cycle with the light on at 7 a.m. and were either fed a normal chow diet (Teklad Global Rodent # T.2018.R12; Harlan, Borchon, Germany) containing 53.5 % of carbohydrates, 18.5 % of protein, and 5.5 % of fat (12 % of calories from fat) or a high fat containing diet (# C1057; Altromin, Lage, Germany) containing 32.7 %, 20 % and 35.5 % of carbohydrates, protein and fat (55.2 % of calories from fat), respectively. All animals had access to water *ad libitum*. Food was only withdrawn if required for an experiment. At the end of the study period, animals were sacrificed by CO₂ anesthesia or cervical dislocation. Body weight was measured once a week.

2.5.2 Mice

AgRPCre (259, 260) and *PomcCre* mice (182) were mated with $IR^{lox/lox}$ mice (58), and breeding colonies were maintained by mating $IR^{lox/lox}$ with *AgRPCre-IR^{lox/lox}* ($IR^{\Delta AgRP}$) and *PomcCre-IR^{lox/lox}* ($IR^{\Delta POMC}$) mice, respectively. $IR^{lox/lox}$ mice had been backcrossed for at least 5 generations on a C57BL/6 background, and *AgRPCre* and *PomcCre* mice – initially established on a FVB background – had been backcrossed for 2 generations on a C57BL/6 background before intercrossing them with $IR^{lox/lox}$ mice. *ThIRESCre* mice (261) were mated with $IR^{lox/lox}$ mice, and breeding colonies were maintained by mating $IR^{lox/lox}$ with *ThIRESCre-IR^{lox/lox}* ($IR^{\Delta Th}$). Only animals from the same mixed background strain generation were compared to each other. Mice were genotyped by PCR using genomic DNA isolated from tail tips. Germline deletion was excluded within the $IR^{lox/lox}$ PCR using three primers, one binding upstream the first loxP site and the others flanking the second loxP site.

2.5.3 Collection of Blood Samples and Determination of Blood Glucose Levels

Tail bleeding of mice was performed according to Hogan (257) and Silver (258). Blood glucose values were determined from whole venous blood using an automatic glucose monitor (GlucoMen® *GlycÓ*; A. Menarini Diagnostics, Florence, Italy). Determination of blood glucose levels and collection of blood samples were performed in the morning to avoid deviations due to circadian variations.

2.5.4 Food Intake and Indirect Calorimetry

Food intake was measured over a two-week period, during which mice were housed individually in regular cages using food racks. To minimize handling of the animals, food racks were weighed every second day and daily food intake was calculated as the average daily intake of chow within the time stated. Indirect calorimetry was measured in a Calorimetry Module (CaloSys V2.1, TSE Systems, Bad Homburg, Germany and CLAMS, Oximax Windows 4.00, Columbus Instruments, Columbus, OH, USA). After two hours of acclimatization, parameters of indirect calorimetry were measured for at least 48 h. For the measurement of physical activity, transmitters (PDT-4000 E-Mitter, VitalView Data Acquisition System 4.1; Mini Mitter, Bend, OR, USA) were implanted into the peritoneal cavity of Avertin-anesthetized mice. After 7 days mice that reached at least 90 % of their preoperative body weight were placed into 3.0 l chambers of a Comprehensive Laboratory Animal Monitoring System (CLAMS, Oximax Windows 4.00, Columbus Instruments, Columbus, OH, USA). Food and water were provided *ad libitum* for the measurement of basal locomotor activity. Mice were allowed to acclimatize in the chambers for 2 h. Physical activity was measured for at least the following 48 h.

2.5.5 Glucose and Insulin Tolerance Test

Glucose tolerance tests (GTT) were performed on animals that had been fasted overnight for 16 hours. Insulin tolerance tests (ITT) were performed on random fed mice. Animals were injected with 2 g/kg body weight of glucose or 0.75 U/kg body weight of human regular insulin into the peritoneal cavity, respectively. Glucose levels were determined in blood collected from the tail tip immediately before and 15, 30 and 60 minutes after the injection, with an additional value determined after 120 minutes for the GTT.

2.5.6 Insulin Signaling

Mice were anesthetized by intraperitoneal (ip) injection of avertin and adequacy of the anesthesia was ensured by loss of pedal reflexes. The abdominal cavity of the mice was opened and 125 μ l samples containing 5U regular human insulin diluted in 0.9% saline were injected into the *Vena cava inferior*. Sham injections were performed with 125 μ l of 0.9% saline. Samples of liver tissue and skeletal muscle tissue were harvested two and five minutes after injection, respectively, and proteins were extracted from tissues for Western blot analysis.

2.5.7 Analysis of Body Composition

Nuclear magnetic resonance (NMR) was employed to determine whole body composition of live animals using the NMR Analyzer minispec mq7.5 (Bruker Optik, Ettlingen, Germany). Radiofrequency (RF) pulse sequences are transmitted into the tissue. In response, RF signals are generated by the hydrogen in the tissues, which are detected by the minispec. The amplitude and duration of these signals are related to properties of the material.

2.5.8 Fertility Assessment

IR^{lox/lox} (control), IR ^{Δ POMC}, IR ^{Δ AgRP} and IR ^{Δ Th} females were bred with IR ^{Δ POMC}, IR ^{Δ AgRP}, IR ^{Δ Th} or IR^{lox/lox} (control) males, respectively. Mean litter size and litter intervals were assessed over a period of at least three litters. For histological examination, ovaries and testes of 15 weeks old animals were dissected, fixed overnight in 4% formaldehyde and then embedded for paraffin sections. Subsequently, 7 μ m thick sections were deparaffinized and stained using haematoxylin and eosin (H&E) for general histology.

2.5.9 Restraint Stress

Mice were familiarized with gentle handling for approximately 8 weeks prior to the experiment. For determination of basal serum corticosterone levels, blood was drawn from the tail vein during the first 3 h of the light phase. The following day, mice were subjected to 1 h of restraint stress at the same time of the light phase. Restraint stress was achieved by enclosing the animals in a plastic tube with a diameter of 3 cm and openings at both ends for tail and nose. The length of the tube was adjusted to the size of the animal to ensure complete

immobilization. At the end of the experiment, blood samples were collected from the tail vein.

2.5.10 Euglycemic-Hyperinsulinemic Clamp Studies in Awake Mice

2.5.10.1 Catheter Implantation

At the age of 14 weeks, male mice were anesthetized by ip injection of avertin (240 mg/kg) (2,2,2-tribromoethanol) and adequacy of the anesthesia was ensured by the loss of pedal reflexes. A Micro-Renathane catheter (MRE 025; Braintree Scientific Inc.) was inserted into the right internal jugular vein, advanced to the level of the superior *vena cava*, and secured in its position in the proximal part of the vein with 4-0 silk; the distal part of the vein was occluded with 4-0 silk. After irrigation with physiological saline solution, the catheter was filled with heparin solution and sealed at its distal end. The catheter was subcutaneously tunneled, thereby forming a subcutaneous loop, and exteriorized at the back of the neck. Cutaneous incisions were closed with a 4-0 silk suture and the free end of the catheter was attached to the suture in the neck as to permit the retrieval of the catheter on the day of the experiment. Mice were intraperitoneally injected with 1 ml of saline containing 15 μ g/g body weight of tramadol and placed on a heating pad in order to facilitate recovery.

2.5.10.2 Radioactive Euglycemic-Hyperinsulinemic Clamp Experiment

Only mice that had regained at least 90% of their preoperative body weight after 6 days of recovery were included in the experimental groups. After starvation for 16 h, awake animals were placed in restrainers for the duration of the clamp experiment. After a D-[3-³H] Glucose tracer solution bolus infusion (5 μ Ci), the tracer was infused continuously (0.05 μ Ci/min) for the duration of the experiment. At the end of the 40-minute basal period, a blood sample (50 μ l) was collected for determination of the basal parameters. To minimize blood loss, red blood cells were collected by centrifugation and reinfused after being resuspended in saline. Insulin solution containing 0.1% BSA was infused at a fixed rate (4 μ U/g/min) following a bolus infusion (40 μ U/g). Blood glucose levels were determined every 10 minutes (B-Glucose Analyzer; Hemocue) and physiological blood glucose levels (between 120 and 145 mg/dl) were maintained by adjusting a 20% glucose infusion to prevent a counterregulatory response to hypoglycemia. Approximately 120 minutes before steady state was achieved, a bolus of 2-Deoxy-D-[1-¹⁴C] Glucose (10 μ Ci) was infused. Steady state

was ascertained when glucose measurements were constant for at least 30 min at a fixed glucose infusion rate. During the clamp experiment, blood samples (5 μ l) were collected after the infusion of the 2-Deoxy-D-[1-¹⁴C] Glucose at time points 0, 5, 15, 25, 35 min etc. until reaching the steady state. During the steady state, blood samples (50 μ l) for the measurement of steady state parameters were collected. At the end of the experiment, mice were sacrificed by cervical dislocation, and brain, liver, white adipose tissue and skeletal muscle were dissected and stored at -80°C.

2.5.10.2.1 Assays

Plasma [3-³H] Glucose radioactivity of basal and steady state control-, IR^{ΔAgRP}- and IR^{ΔPomc} samples was determined directly after deproteinization with 0.3M Ba(OH)₂ and 0.3M ZnSO₄ and after removal of ³H₂O by evaporation, using a liquid scintillation counter (Beckmann). Plasma Deoxy-[1-¹⁴C] Glucose radioactivity was directly measured in the liquid scintillation counter. White adipose tissue, skeletal muscle and brain lysates were processed by using Ion exchange chromatography columns (Poly-Prep[®] Prefilled Chromatography Columns, AG[®]1-X8 formate resin, 200-400 mesh dry; Bio Rad Laboratories) to separate 2-Deoxy-D-[1-¹⁴C] Glucose (2DG) from 2-Deoxy-D-[1-¹⁴C] Glucose-6-Phosphate (2DG6P).

For determination of basal G6Pase- α protein and IL-6 mRNA expression, 16 h fasted animals were dissected and livers were stored at -80°C until further preparation. Basal and steady state liver samples were processed for Western blot analysis as well as for Realtime PCR. 200 ng of each total RNA sample was reverse-transcribed, then PCR-amplified using TaqMan[®] Principles ABI Prism 7700 Sequence Detection System.

2.5.10.2.2 Calculations

Glucose turnover rate ($\text{mg} \times \text{kg}^{-1} \times \text{min}^{-1}$) was calculated as the rate of tracer infusion (dpm/min) divided by the plasma glucose-specific activity (dpm/mg) corrected for body weight. Hepatic glucose production ($\text{mg} \times \text{kg}^{-1} \times \text{min}^{-1}$) was calculated as the difference between the rate of glucose appearance and glucose infusion rate. *In vivo* glucose uptake for white adipose tissue, brain, and skeletal muscle ($\text{nmol} \times \text{g}^{-1} \times \text{min}^{-1}$) was calculated based on the accumulation of 2DG6P in the respective tissue and the disappearance rate of 2DG from plasma as described previously (262).

2.5.10.3 Long-term euglycemic-hyperinsulinemic clamp experiment

Only 11-week-old C57BL/6 male mice that had regained at least 90% of their preoperative body weight after 6 days of recovery were included in the experimental groups. After starvation for 18 h, awake animals were placed in restrainers for the duration of the clamp experiment. After collection of a blood sample (100 μ l) for determination of basal parameters, mice received a continuous intravenous infusion of somatostatin (3 μ g/kg/min) (control group) to inhibit endogenous insulin and glucagon release or continuous intravenous infusion of somatostatin (3 μ g/kg/min) and insulin (4 μ U/g/min) (treatment group). Blood glucose levels were determined every 20 minutes (B-Glucose Analyzer; Hemocue) and physiological blood glucose levels (between 100 and 145 mg/dl) were maintained by adjusting a 20% glucose infusion in both groups. At the end of the experiment (after 6 h) and collection of a blood sample, mice were perfused for electron microscopy.

2.6 Computer Analysis

2.6.1 Densitometrical Analysis

Protein expression was assessed by Western blot analysis and bands were measured in intensity per mm² using the Quantity One Software (Bio-Rad, München, Germany). After background subtraction, each sample was normalized to an internal loading control. Average protein expression of control mice was set to 100% and compared to protein expression of knockout animals unless stated otherwise.

2.6.2 Statistical Methods

Data sets were analyzed for statistical significance using a two-tailed unpaired student's t test. All *p* values below 0.05 were considered significant. All displayed values are means \pm SEM. * *p* \leq 0.05 ; ** *p* \leq 0.01 ; *** *p* \leq 0.001 versus controls.

3 Results

3.1 Generation of POMC and AgRP neuron-specific insulin receptor knockout mice

To investigate the role of insulin signaling in POMC- and/or AgRP-expressing neurons, the *insulin receptor* gene was inactivated specifically in each of these cells. To this end, mice expressing a Cre recombinase under control of either the *Pomc*- or the *AgRP*-promoter (182, 259, 260) were crossed with mice carrying a loxP-flanked *insulin receptor* gene ($IR^{lox/lox}$) (Figure 5) (58).

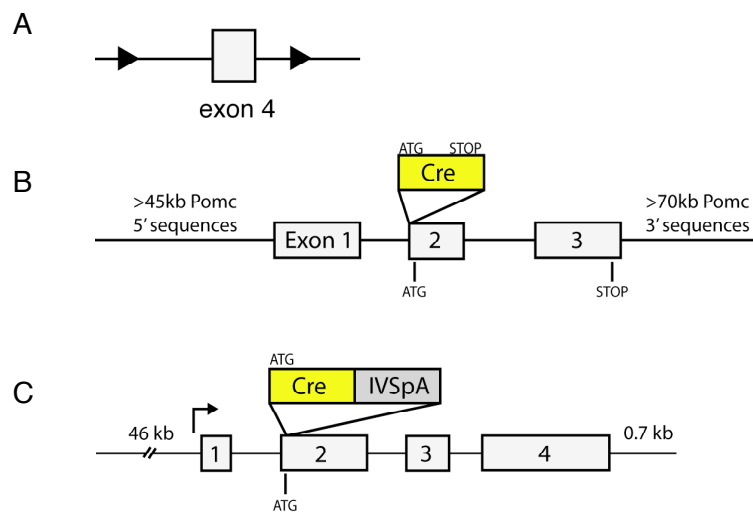


Figure 5: POMC and AgRP neuron-restricted inactivation of the *insulin receptor* gene.

(A) Map of the loxP-flanked *insulin receptor* gene exon 4. LoxP sites were introduced 2 kb upstream and 80 bp downstream of exon 4. Cre mediated recombination of this allele will lead to deletion of exon 4 and splicing of exon 3 and 5, and is predicted to cause a frameshift mutation resulting in a stop of translation. Each loxP site is here and hereafter depicted as a triangle. (B) Map of the *PomcCre* transgene. Mice expressing Cre recombinase (Cre) under *Pomc* promoter control were generated by engineering a *Pomc* bacterial artificial chromosome. The Cre translational initiation site (ATG) was inserted into the *Pomc* ATG and deleted the first 30 bp of the *Pomc* gene. (C) Map of the *AgRPCre* transgene. Mice expressing Cre recombinase (Cre) under *AgRP* promoter control were generated by engineering an *AgRP* bacterial artificial chromosome. The Cre/IVSpA cassette is targeted precisely upstream of the normal *AgRP* translational initiation site (ATG) in exon 2.

In $IR^{lox/lox}$ mice, harboring the *Pomc*Cre or the *AgRPCre* recombinase transgene, the loxP-flanked *insulin receptor* gene is selectively removed upon Cre-mediated recombination, leading to the inactivation of the insulin receptor selectively in POMC or AgRP neurons, respectively (Figure 6).

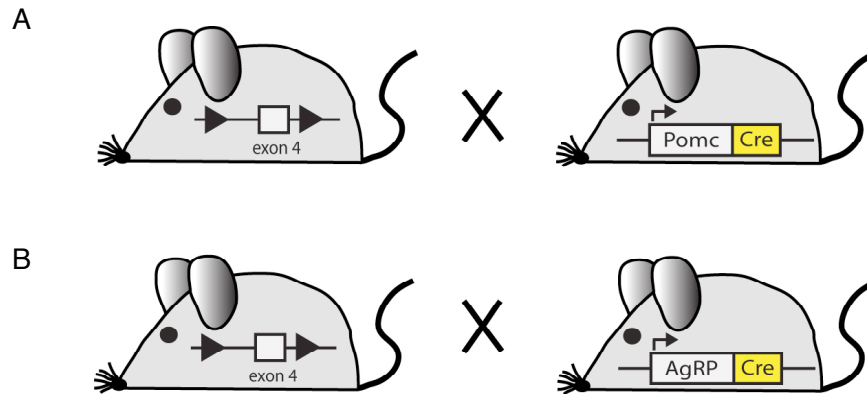


Figure 6: General scheme of mice with POMC ($IR^{\Delta POMC}$) and AgRP ($IR^{\Delta AgRP}$) neuron-restricted inactivation of the *insulin receptor* gene.

(A) Mice, homozygous for a loxP-flanked exon 4 of the insulin receptor allele ($IR^{lox/lox}$) were crossed with mice expressing the Cre protein under the control of the *Pomc* promoter. Only one loxP-flanked allele is depicted here. (B) Mice, homozygous for a loxP-flanked exon 4 of the insulin receptor allele ($IR^{lox/lox}$) were crossed with mice expressing the Cre protein under the control of the *AgRP* promoter. Only one loxP-flanked allele is depicted here.

To analyze cell type-specific inactivation of the insulin receptor, Cre-mediated recombination was visualized by crossing *Pomc*Cre as well as *AgRPCre* mice to a reporter mouse strain in which transcription of the β -galactosidase gene (*LacZ*) under control of the ubiquitously expressed *Rosa26* promoter is prevented by a floxed *hygromycin resistance* gene (*LacZ* reporter mice), thus leading to β -galactosidase expression only in cells expressing the Cre recombinase (Figure 7 A) (253). These mice showed a pattern of LacZ immunoreactivity in the ARC of the hypothalamus reflecting the described expression pattern of endogenously expressed POMC and AgRP (Figure 7 B, C), consistent with the previously demonstrated colocalization of endogenous POMC/AgRP expression and Cre recombinase activity (182, 259, 260).

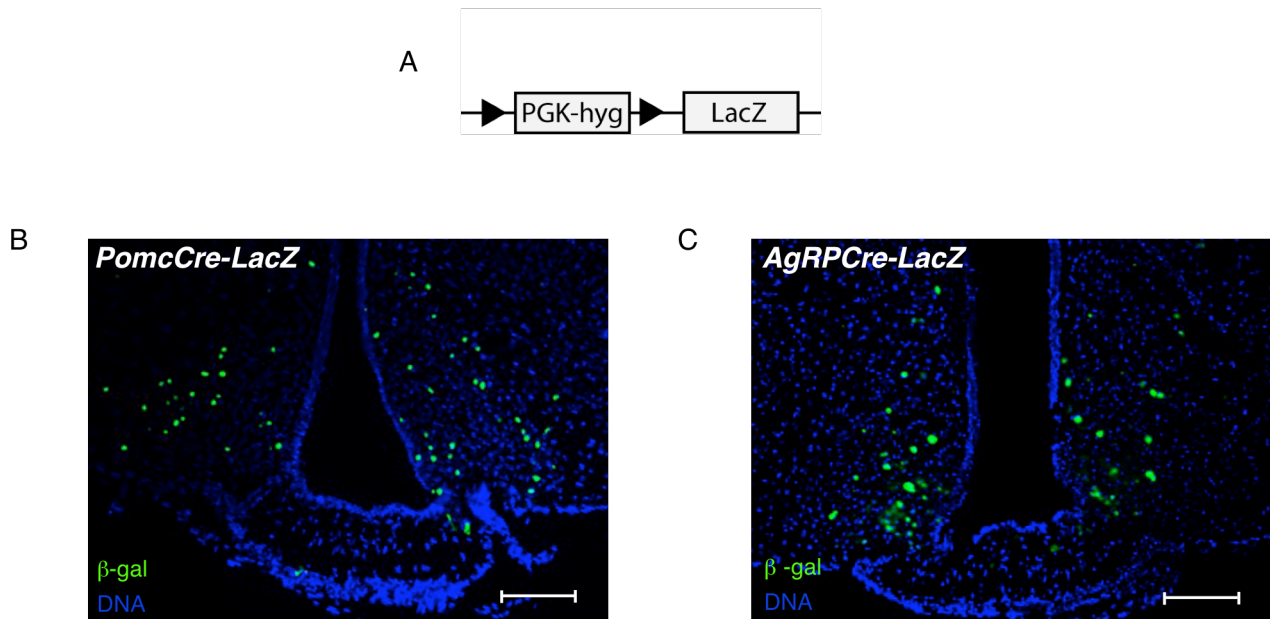


Figure 7: Verification of Cre-mediated recombination in *PomcCre* and *AgRPCre* mice.

(A) Map of the *LacZ* transgene for Cre-mediated expression from the *Rosa26* locus. pGK-hyg: *hygromycin resistance* gene driven by the pGK (*phosphoglycerate kinase*) promoter. In this configuration Cre-mediated recombination removes the loxP-flanked *hygromycin resistance* gene only in cell types expressing Cre recombinase, resulting in transcription of β -galactosidase (β -gal). (B) Immunohistochemistry for β -gal in brains of double heterozygous reporter mice (*LacZ*^{+/+} *PomcCre*) at the age of ten weeks. Blue (DAPI), DNA; green, β -gal (POMC neurons). Scale bar 100 μ m. (C) Immunohistochemistry for β -gal in brains of double heterozygous reporter mice (*LacZ*^{+/+} *AgRPCre*) at the age of ten weeks. Blue (DAPI), DNA; green, β -gal (AgRP neurons). Scale bar 100 μ m.

To confirm the specificity of insulin receptor inactivation, Western blot analyses were performed on tissue lysates obtained from mice with specific insulin receptor inactivation in POMC (IR ^{Δ POMC}) and AgRP (IR ^{Δ AgRP}) neurons. Consistent with restricted inactivation of the insulin receptor in defined subpopulations of hypothalamic neurons, Western blot analysis revealed no alterations in overall brain and hypothalamic insulin receptor protein expression (Figure 8). Similarly, insulin receptor expression in peripheral tissues, including liver, skeletal muscle and pancreas remained unchanged in IR ^{Δ POMC} and IR ^{Δ AgRP} mice (Figure 8).

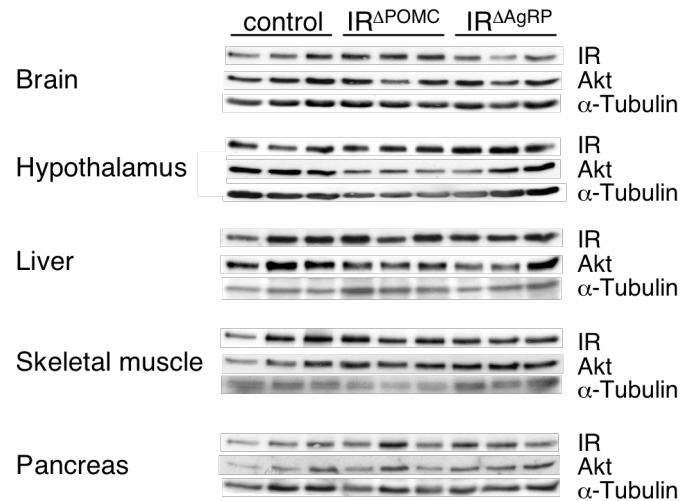


Figure 8: Western blot analysis of insulin receptor expression.

Western blot analysis of insulin receptor β subunit (IR), protein kinase B (Akt) (loading control) and α -Tubulin (loading control). Proteins were extracted from whole brain, hypothalamus, liver, skeletal muscle and pancreas of control, IR ^{Δ POMC} and IR ^{Δ AgRP} mice.

Next, insulin's ability to activate signaling in skeletal muscle and liver of control, IR ^{Δ POMC} and IR ^{Δ AgRP} mice was assessed. Consistent with restricted inactivation of the insulin receptor, insulin-stimulated Akt-phosphorylation occurred normally in liver and skeletal muscle of IR ^{Δ POMC} and IR ^{Δ AgRP} mice as compared to controls (Figure 9).

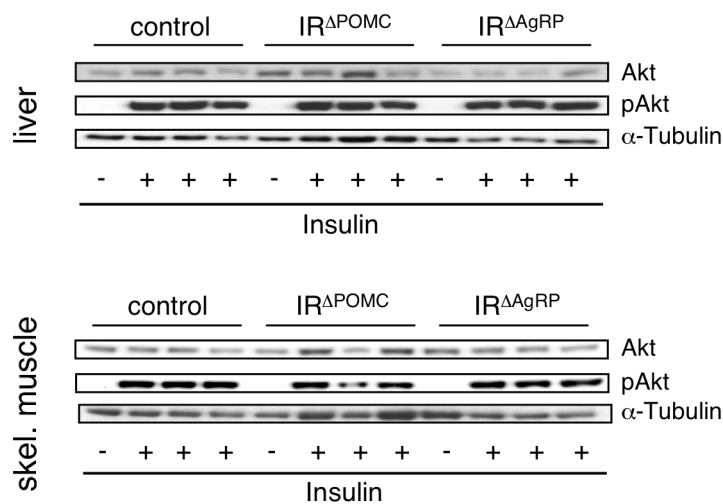


Figure 9: Insulin signaling in peripheral organs of control, IR ^{Δ POMC} and IR ^{Δ AgRP} mice.

Western blot analysis of protein kinase B (Akt), phosphorylated Akt and α -Tubulin (loading control) in liver and skeletal muscle (skel. muscle) of control, IR ^{Δ POMC} and IR ^{Δ AgRP} mice after injection of either saline (-) or insulin (+) into the *Vena cava inferior*.

Consistent with the expression pattern of endogenously expressed POMC, the only non-hypothalamic site of recombination detectable in *PomcCre* transgenic mice was the pituitary (255). However, this did not have any effect on the response to stress of $IR^{\Delta POMC}$ mice assessed by measurement of stress-induced plasma corticosterone levels (Figure 10). Restraint-stress induced increases in plasma corticosterone concentrations were similar in control and $IR^{\Delta POMC}$ mice (Figure 10), indicating that insulin receptor expression is not required for the development, maintenance or normal function of anterior pituitary corticotrope cells.

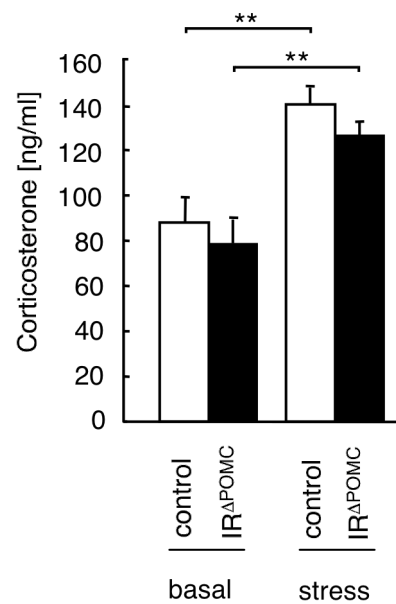


Figure 10: Regulation of the hypothalamic-pituitary-adrenal axis in $IR^{\Delta POMC}$ mice.

Basal and stress-induced plasma corticosterone levels in 12-week-old male control ($n = 7$) and $IR^{\Delta POMC}$ ($n = 10$) mice. Displayed values are means \pm S.E.M.; **, $p \leq 0.01$.

Since mice with a neuron-specific insulin receptor knockout (NIRKO) exhibit hypogonadism (58), parameters of fertility were assessed in $IR^{\Delta POMC}$ and $IR^{\Delta AgRP}$ mice. This revealed no significant differences concerning litter-to-litter intervals, litter size and morphology of reproductive organs between control, $IR^{\Delta POMC}$ and $IR^{\Delta AgRP}$ mice, indicating that insulin signaling in these neurons is not required for control of fertility (Figure 11).

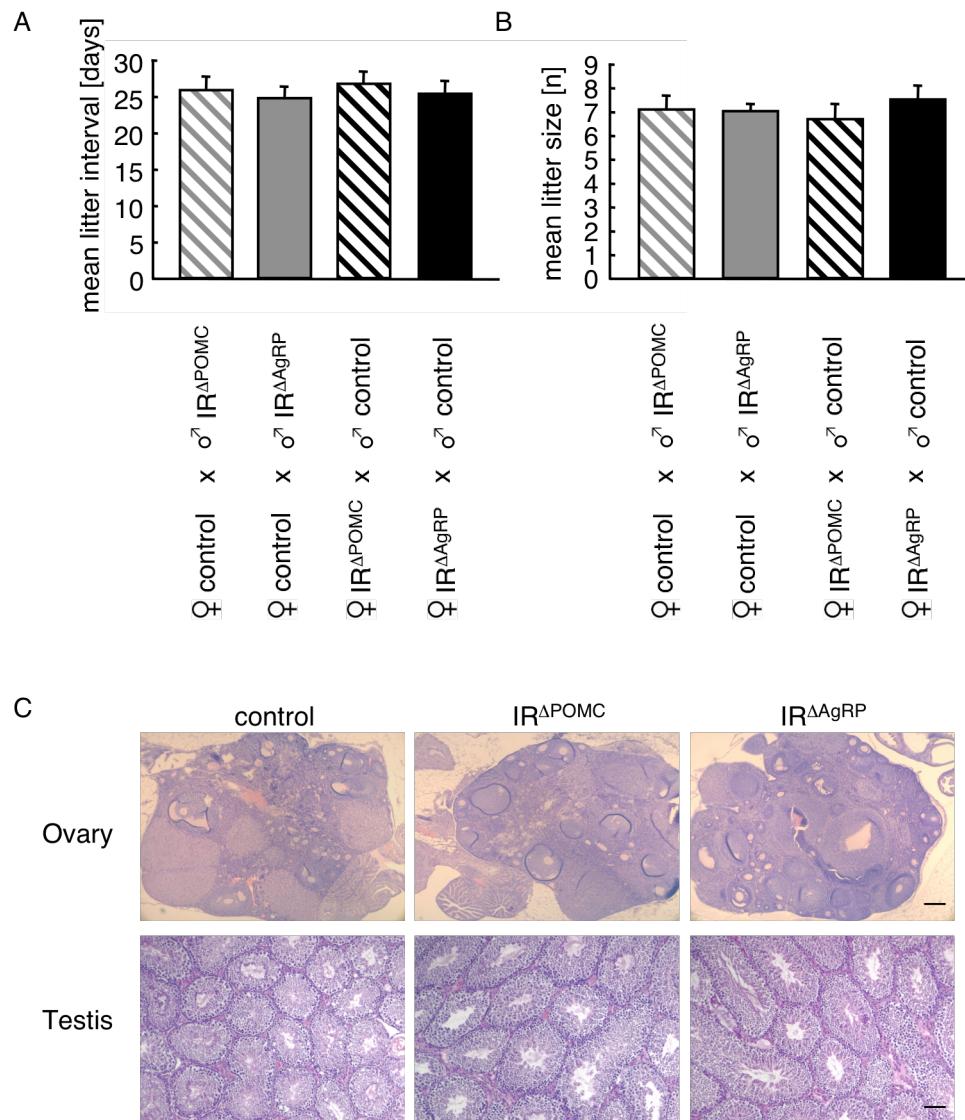


Figure 11: Fertility of IR^{ΔPOMC} and IR^{ΔAgRP} mice.

(A) Mean litter intervals for control, IR^{ΔPOMC} and IR^{ΔAgRP} mice assessed over a period of at least three litters (n = 3 breedings). (B) Mean litter size for control, IR^{ΔPOMC} and IR^{ΔAgRP} mice assessed over a period of at least three litters (n = 3 breedings). (C) Representative hematoxylin/eosin staining of ovaries and testes from control, IR^{ΔPOMC} and IR^{ΔAgRP} mice. Scale bar 100μm. Displayed values are means ± S.E.M..

Next, functional effects of POMC and AgRP neuron-restricted insulin receptor deficiency on insulin's ability to activate the PI3 kinase pathway in control, IR^{ΔPOMC} and IR^{ΔAgRP} *LacZ* reporter mice were determined. To this end, overnight fasted mice were intravenously injected with either saline or insulin and sacrificed 10 min afterwards. Following, phosphatidylinositol (3,4,5) trisphosphate (PIP3) formation was analyzed by immunohistochemistry in hypothalamic slices (Figure 12).

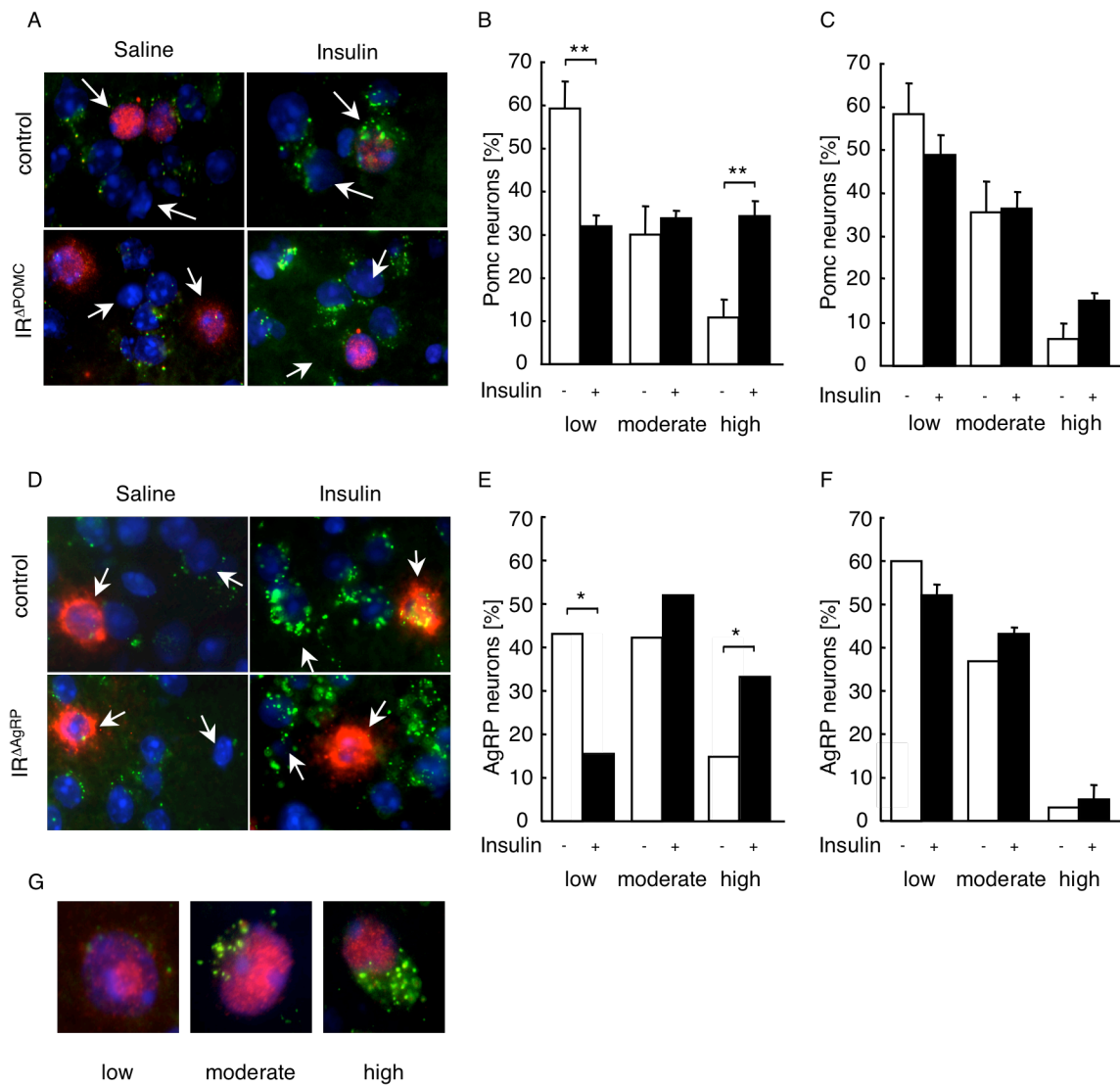


Figure 12: PIP3 formation in hypothalamic neurons of control, IR^{ΔPOMC} and IR^{ΔAgRP} reporter mice.

(A) Double immunohistochemistry of ARC neurons of control and IR^{ΔPOMC} reporter mice was performed in overnight fasted mice, which were intravenously injected with either saline or insulin and sacrificed 10 min afterwards. Arrows indicate 1 POMC and 1 non-POMC neuron in each panel. (B) Quantification of PIP3 levels in control reporter mice in the basal state (-) and after insulin (+) stimulation. Values are means \pm S.E.M. of sections obtained from 3 unstimulated and 4 insulin-stimulated control mice. **, $p \leq 0.01$. (C) Quantification of PIP3 levels in IR^{ΔPOMC} reporter mice in the basal state (-) and after insulin (+) stimulation. Values are means \pm S.E.M. of sections obtained from 3 unstimulated and 3 insulin-stimulated IR^{ΔPOMC} mice. (D) Double immunohistochemistry of ARC neurons of control and IR^{ΔAgRP} reporter mice was performed in overnight fasted mice, which were intravenously injected with either saline or insulin and sacrificed 10 min afterwards. Arrows indicate 1 AgRP and 1 non-AgRP neuron in each panel. (E) Quantification of PIP3 levels in control reporter mice in the basal state (-) and after insulin (+) stimulation. Values are means \pm S.E.M. of sections obtained from 2 unstimulated and 2 insulin-stimulated control mice. *, $p \leq 0.05$. (F) Quantification of PIP3 levels in IR^{ΔAgRP} reporter mice in the basal state (-) and after insulin (+) stimulation. Values are means \pm S.E.M. of sections obtained from 1 unstimulated and 4 insulin-stimulated IR^{ΔAgRP} mice. (G) Examples of different magnitudes of PIP3 immunoreactivity as described in the Materials & Methods section. Blue (DAPI), DNA; red, β -gal (AgRP or POMC neurons); green, PIP3.

In the basal state, little immunoreactive PIP3 was detectable in POMC, AgRP and adjacent neurons of control, IR^{ΔPOMC} and IR^{ΔAgRP} reporter mice (Figure 12). In control mice, insulin treatment resulted in profound activation of PIP3 formation in POMC-, AgRP- and non-POMC- or non-AgRP-expressing neurons of the ARC (Figure 12). In contrast, in IR^{ΔPOMC} and IR^{ΔAgRP} mice insulin stimulation resulted in PIP3 formation in non-POMC or non-AgRP cells, but it failed to activate PIP3 formation in POMC and AgRP neurons (Figure 12). These data indicate efficient and specific insulin receptor inactivation in POMC cells of IR^{ΔPOMC} mice and AgRP cells of IR^{ΔAgRP} mice.

Taken together, these data demonstrate an efficient inactivation of the *insulin receptor* gene in POMC and AgRP neurons of the hypothalamus, while functional signaling in the periphery, fertility, and regulation of the hypothalamic-pituitary-adrenal axis are unaltered in these mice.

3.2 Insulin hyperpolarizes AgRP and POMC neurons via K_{ATP} channel activation

Insulin has previously been shown to reduce the electrical activity of unidentified hypothalamic neurons (263) as well as identified POMC neurons (202), via activation of K_{ATP} channels; whereas blockade of central K_{ATP} channels abrogates insulin's ability to inhibit hepatic glucose production (47, 264). Therefore, insulin's ability to modulate membrane potential and action potential frequency in POMC and AgRP neurons of control, IR^{ΔPOMC} and IR^{ΔAgRP} mice was examined using the reporter mouse strain *LacZ/EGFP (Z/EG)*, which carries a transgene comprising a loxP-flanked *β-galactosidase/neomycin-resistance (βgeo)* fusion gene followed by the coding sequence of the enhanced green fluorescent protein (EGFP) (254). In this configuration, EGFP (herein after referred to as GFP) is expressed only in cells expressing Cre recombinase (Figure 13).

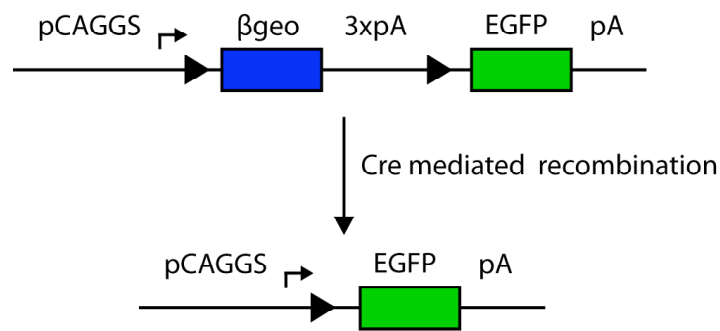


Figure 13: Z/EG expression construct.

Map of the *Z/EG* expression construct: The *Z/EG* transgene consists of the strong *pCAGGS* (chicken β actin promoter with upstream CMV enhancer) promoter, directing expression of a loxP-flanked β geo (*lacZ*/neomycin-resistance) fusion gene and three SV40 polyadenylation sequences (3xpA). Following that is the coding sequence of the enhanced green fluorescent protein (EGFP) and a rabbit β globin polyadenylation sequence (pA). In this configuration, β geo is expressed before Cre excision and EGFP is expressed after Cre excision.

Consistent with previous reports (202), insulin caused membrane hyperpolarization and reduced the firing frequency of identified POMC neurons in control mice (Figure 14). In contrast, insulin had no effect on POMC neurons of $IR^{\Delta POMC}$ mice, while basal firing rate appeared to be lower in these cells.

Taken together, these data demonstrate the efficiency of insulin receptor inactivation in $IR^{\Delta POMC}$ mice and show that insulin stimulates POMC neuron hyperpolarization by direct interaction with insulin receptors on POMC neurons.

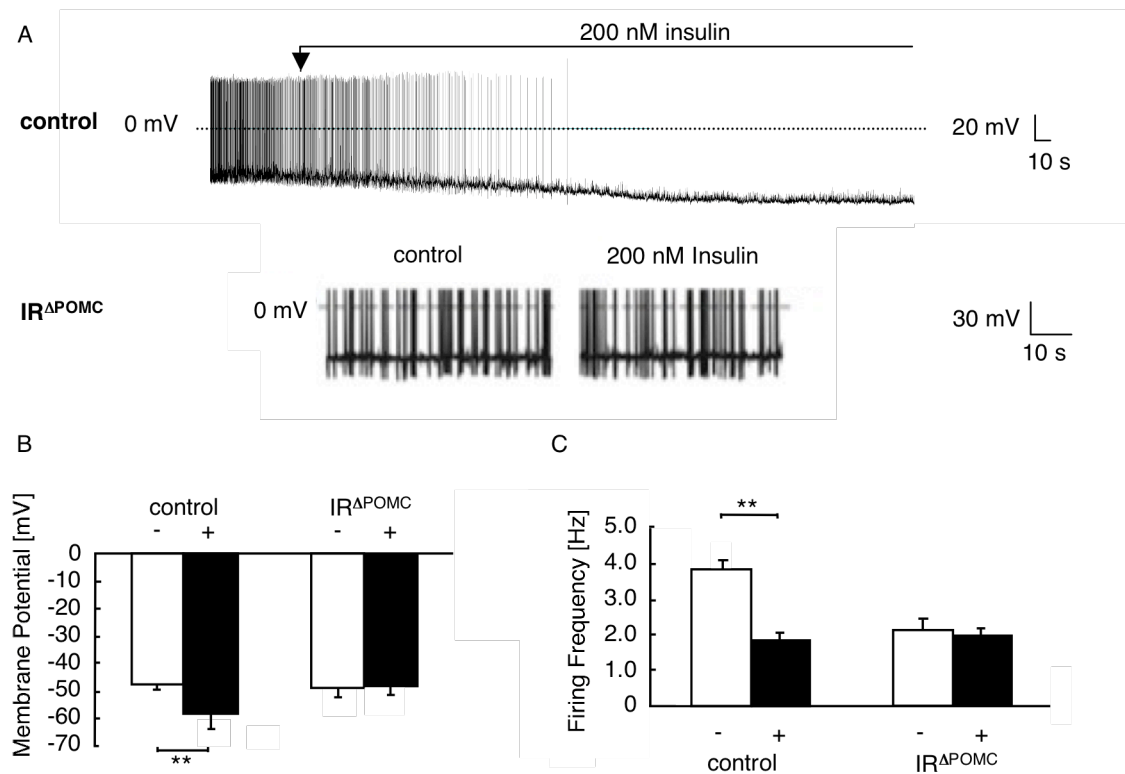


Figure 14: Effects of insulin on electrical activity of control and IR^{ΔPOMC}-Z/EG neurons.

(A) Representative membrane potential recordings of identified POMC neurons in ARC slices from *PomcCre-Z/EG* (control) and IR^{ΔPOMC}-Z/EG mice before and after addition of 200 nM insulin. (B) Mean membrane potential of identified POMC neurons in ARC slices from *PomcCre-Z/EG* (n = 4) and IR^{ΔPOMC}-Z/EG (n = 6) mice before (-) and after (+) addition of 200 nM insulin. (C) Mean firing frequency of *PomcCre-Z/EG* (n = 4) and IR^{ΔPOMC}-Z/EG (n = 6) neurons before (-) and after (+) addition of 200 nM insulin. Displayed values are means ± S.E.M.; **, p ≤ 0.01.

Next, similar experiments were performed in identified AgRP neurons of control and IR^{ΔAgRP} mice. Insulin hyperpolarized AgRP cells of control mice and reduced their action potential frequency (Figure 15), which is consistent with the finding that AgRP cells also express K_{ATP} channels (265). In contrast, insulin failed to alter either membrane potential or action potential frequency in all AgRP neurons tested from IR^{ΔAgRP} mice (Figure 15), indicating that the insulin-induced hyperpolarization and changes in action potential frequency of AgRP neurons are directly mediated by the insulin receptors on these cells. Thus, abrogation of insulin signaling had been successfully achieved in AgRP cells of IR^{ΔAgRP} mice. Additionally, the effect of the K_{ATP} channel blocker tolbutamide was analyzed in these cells. Application of tolbutamide reversed the insulin-induced hyperpolarization in identified AgRP cells of control mice; consistent with the finding that inactivation of POMC neurons by

insulin occurs via K_{ATP} channel activation (202) (Figure 15). Thus, these findings indicate that the same mechanism reported for POMC neurons also holds true for AgRP neurons.

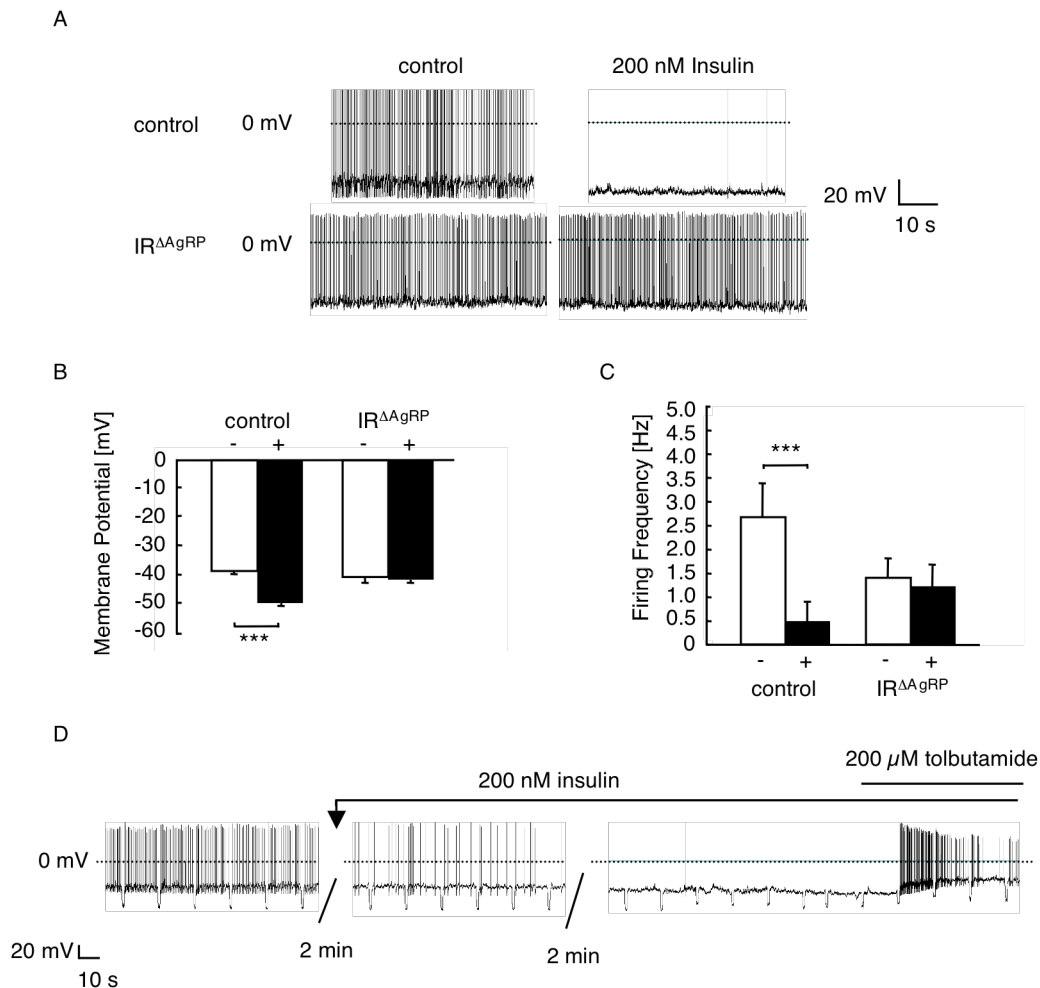


Figure 15: Effects of insulin and tolbutamide on electrical activity of control and IR Δ AgRP-Z/EG neurons.

(A) Representative membrane potential recordings of identified AgRP neurons in ARC slices from *AgRPCre-Z/EG* (control) and IR Δ AgRP-Z/EG mice before and after addition of 200 nM insulin. (B) Mean membrane potential of identified AgRP neurons in ARC slices from *AgRPCre-Z/EG* ($n = 6$) and IR Δ AgRP-Z/EG ($n = 6$) mice before (-) and after (+) addition of 200 nM insulin. (C) Mean firing frequency of *AgRPCre-Z/EG* ($n = 6$) and IR Δ AgRP-Z/EG ($n = 6$) neurons before (-) and after (+) addition of 200 nM insulin (control vs. IR Δ AgRP before addition of insulin $p = 0.11$). (D) Representative membrane potential recording of an identified AgRP neuron in an ARC slice from an *AgRPCre-Z/EG* (control) mouse before and after addition of 200 nM insulin, and addition of 200 μ M tolbutamide. Displayed values are means \pm S.E.M. ***, $p \leq 0.001$.

3.3 Normal body weight and energy homeostasis in $IR^{\Delta AgRP}$ and $IR^{\Delta POMC}$ mice

To determine the importance of insulin receptor signaling in POMC and AgRP cells on the regulation of energy homeostasis, body weight of control ($IR^{lox/lox}$), $IR^{\Delta POMC}$ and $IR^{\Delta AgRP}$ mice was monitored from weaning until 4 months of age. This revealed no differences in body weight between the three types of male mice on normal diet (Figure 16 A, B) and all three genotypes responded to high fat diet with similar increases in body weight (Figure 16 C, D).

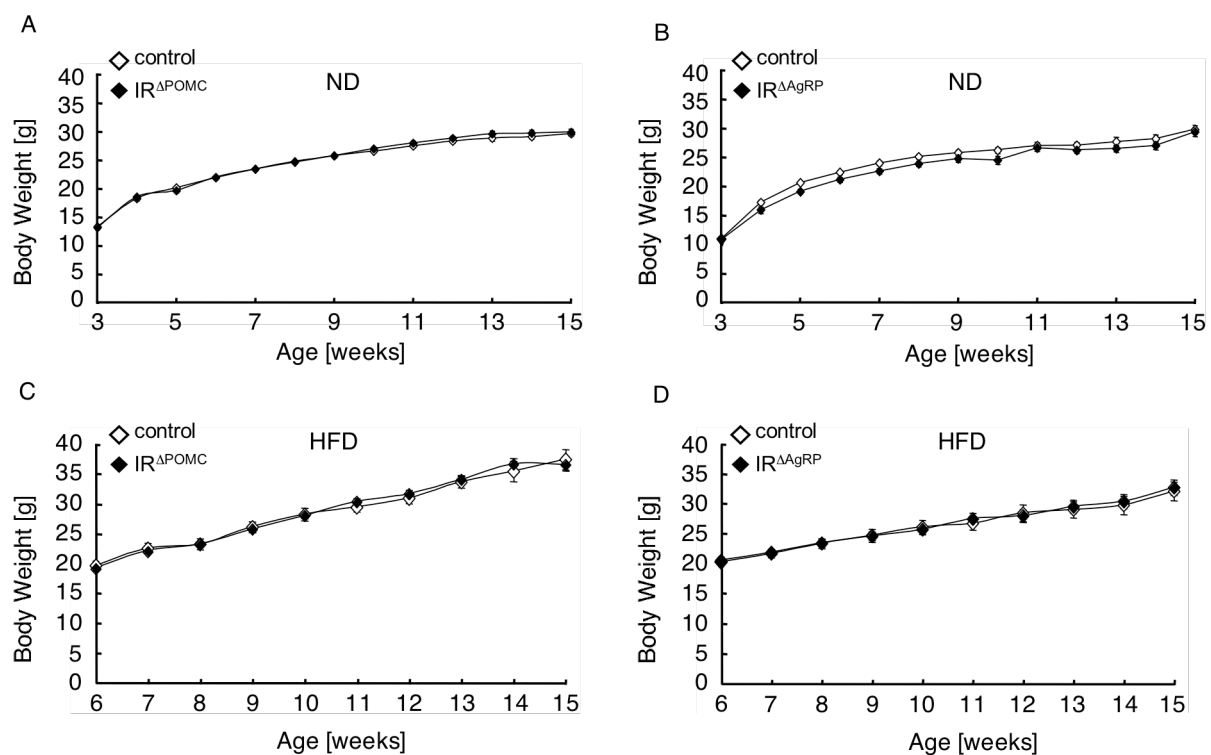


Figure 16: Body weight of $IR^{\Delta POMC}$ and $IR^{\Delta AgRP}$ mice.

(A) Average body weight of male control (◇) and $IR^{\Delta POMC}$ (◆) mice on normal diet (ND) (n = 26 - 31). (B) Average body weight of male control (◇) and $IR^{\Delta AgRP}$ (◆) mice on normal diet (ND) (n = 18 - 25). (C) Average body weight of male control (◇) and $IR^{\Delta POMC}$ (◆) mice on high fat diet (HFD) (n = 7 - 12). (D) Average body weight of male control (◇) and $IR^{\Delta AgRP}$ (◆) mice on high fat diet (HFD) (n = 16 - 22). Displayed values are means \pm S.E.M..

Consistent with these findings, circulating serum leptin concentrations were indistinguishable between control, $IR^{\Delta POMC}$ and $IR^{\Delta AgRP}$ mice on normal diet and all increased to the same extent under high fat diet conditions (Figure 17).

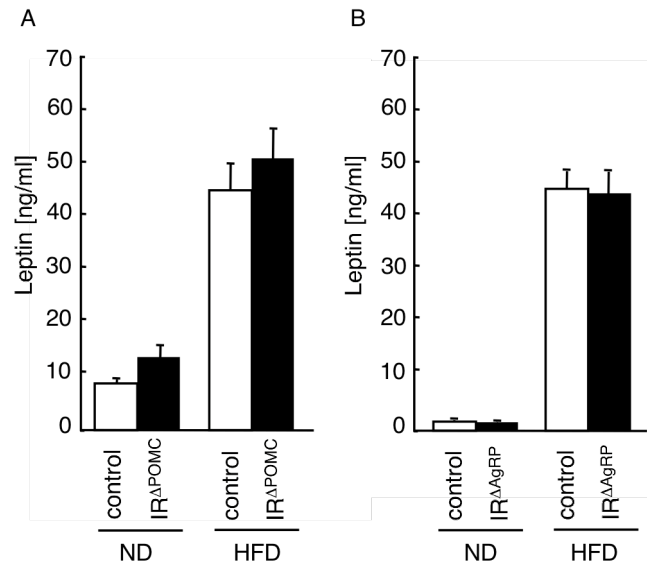


Figure 17: Serum leptin concentrations in IR^{ΔPOMC} and IR^{ΔAgRP} mice.

(A) Serum leptin levels of male control (n = 10) and IR^{ΔPOMC} (n = 10) mice on normal (ND) and high fat diet (HFD) at the age of 15 weeks. (B) Serum leptin levels of male control (n = 11 - 15) and IR^{ΔAgRP} (n = 8 - 15) mice on normal (ND) and high fat diet (HFD) at the age of 15 weeks. Displayed values are means ± S.E.M..

Furthermore, daily food intake was measured and compared between control, IR^{ΔPOMC} and IR^{ΔAgRP} mice. Consistent with unaltered body weight in these mice, both IR^{ΔPOMC} and IR^{ΔAgRP} showed a food intake comparable to control mice (Figure 18).

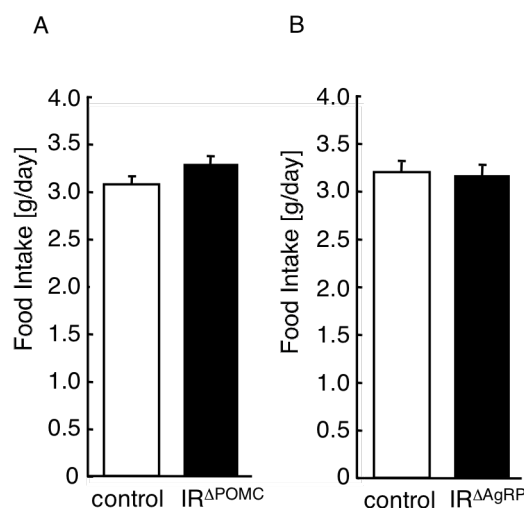


Figure 18: Daily food intake of IR^{ΔPOMC} and IR^{ΔAgRP} mice.

(A) Daily food intake of male control (n = 15) and IR^{ΔPOMC} (n = 20) mice on normal diet at the age of 11 - 13 weeks. (B) Daily food intake of male control (n = 11) and IR^{ΔAgRP} (n = 11) mice on normal diet at the age of 11 - 13 weeks. Displayed values are means ± S.E.M..

Next, parameters of energy homeostasis were investigated in female control, $IR^{\Delta POMC}$ and $IR^{\Delta AgRP}$ mice. Body weight, serum leptin concentrations and food intake were also unaltered in female mice both on normal and high fat diet (Figure 19).

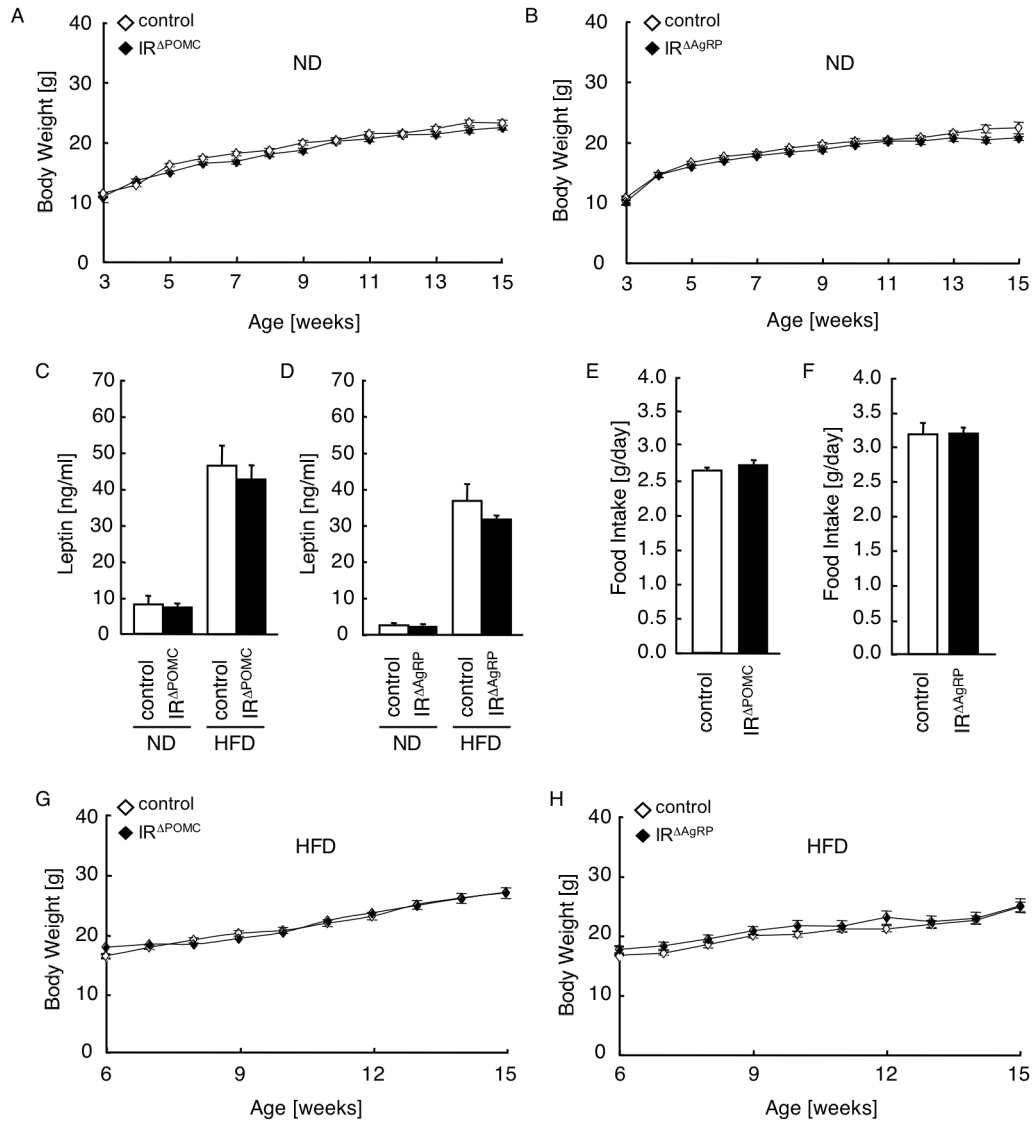


Figure 19: Body weight, leptin levels and food intake of $IR^{\Delta POMC}$ and $IR^{\Delta AgRP}$ female mice.

(A) Average body weight of female control (\diamond) and $IR^{\Delta POMC}$ (\blacklozenge) mice on normal diet (ND) (n = 10 - 16). (B) Average body weight of female control (\diamond) and $IR^{\Delta AgRP}$ (\blacklozenge) mice on normal diet (ND) (n = 16 - 25). (C) Serum leptin levels of female control (n = 7 - 10) and $IR^{\Delta POMC}$ (n = 10) mice on normal diet (ND) and high fat diet (HFD) at the age of 15 weeks. (D) Serum leptin levels of female control (n = 5 - 15) and $IR^{\Delta AgRP}$ (n = 10 - 15) mice on normal diet (ND) and high fat diet (HFD) at the age of 15 weeks. (E) Daily food intake of female control (n = 11) and $IR^{\Delta POMC}$ (n = 10) mice on normal diet at the age of 11-13 weeks. (F) Daily food intake of female control (n = 15) and $IR^{\Delta AgRP}$ (n = 12) mice on normal diet at the age of 11 - 13 weeks. (G) Average body weight of female control (\diamond) and $IR^{\Delta POMC}$ (\blacklozenge) mice on high fat diet (n = 6 - 17). (H) Average body weight of female control (\diamond) and $IR^{\Delta AgRP}$ (\blacklozenge) mice on high fat diet (n = 9 - 20). Displayed values are means \pm S.E.M..

Furthermore, male and female $IR^{\Delta POMC}$ and $IR^{\Delta AgRP}$ mice showed unaltered relative (corrected for body weight) fat pad weights both on normal and high fat diet as compared to controls (Figure 20).

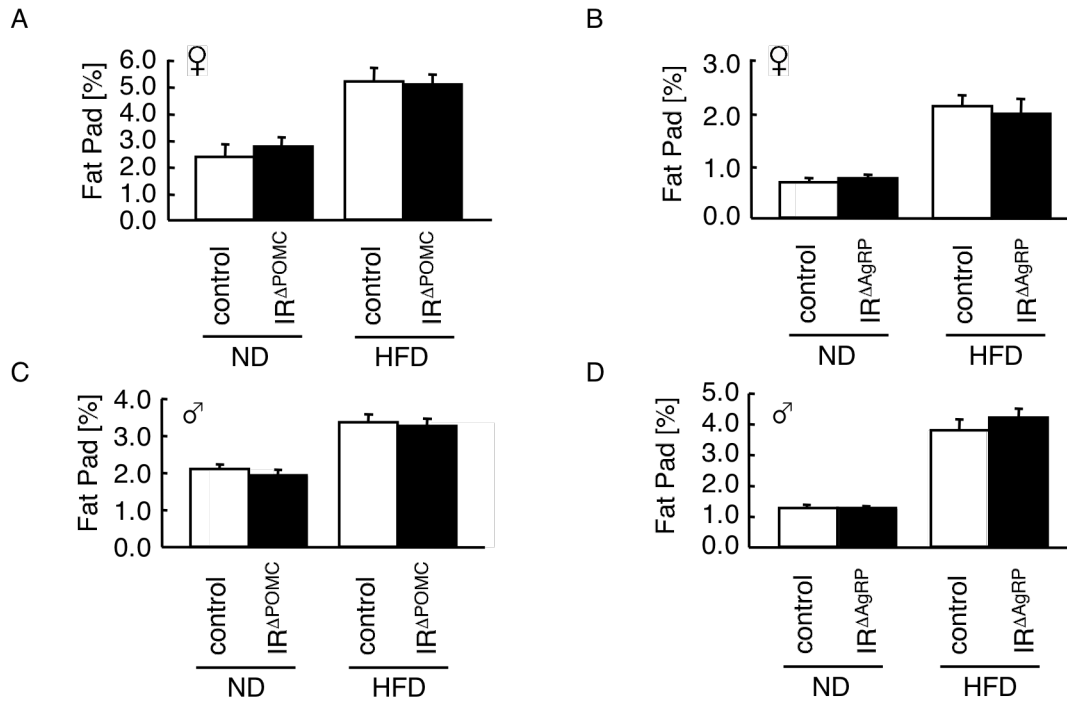


Figure 20: Epigonadal fat pad weights of female and male $IR^{\Delta POMC}$ and $IR^{\Delta AgRP}$ mice.

(A) Relative parametrial fat pad weights of female control and $IR^{\Delta POMC}$ mice on normal diet (ND) and high fat diet (HFD) (n = 10 - 16) at the age of 20 weeks. (B) Relative parametrial fat pad weights of female control and $IR^{\Delta AgRP}$ mice on normal diet (ND) and high fat diet (HFD) (n = 10 - 14) at the age of 15 weeks. (C) Relative epididymal fat pad weights of male control and $IR^{\Delta POMC}$ mice on normal diet (ND) and high fat diet (HFD) (n = 11 - 18) at the age of 20 weeks. (D) Relative epididymal fat pad weights of male control and $IR^{\Delta AgRP}$ mice on normal diet (ND) and high fat diet (HFD) (n = 8 - 15) at the age of 15 weeks. Displayed values are means \pm S.E.M..

Taken together, these data indicate that energy homeostasis in mice is unaffected by selective, targeted disruption of the *insulin receptor* gene in POMC or AgRP neurons of the ARC.

Next, the expression of different neuropeptides critically involved in the regulation of energy homeostasis was determined. Expression of anorexigenic neuropeptides (e.g. POMC) and orexigenic neuropeptides (such as NPY and AgRP) did not differ between $IR^{\Delta POMC}$ and control mice (Figure 21 A). $IR^{\Delta AgRP}$ mice did exhibit a slight increase in AgRP expression (Figure 21 B), which is expected since insulin suppresses NPY and AgRP expression (186, 266, 267).

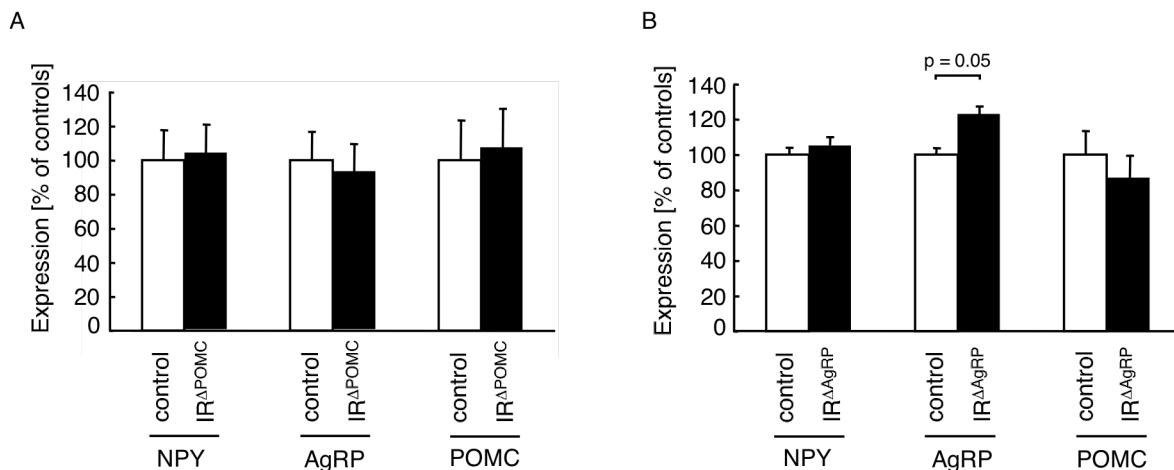


Figure 21: Hypothalamic neuropeptide expression in $IR^{\Delta POMC}$ and $IR^{\Delta AgRP}$ male mice.

(A) Neuropeptide expression in male control (n = 8) and $IR^{\Delta POMC}$ (n = 12) mice at the age of 12 weeks. (B) Neuropeptide expression in male control (n = 8) and $IR^{\Delta AgRP}$ (n = 8) mice at the age of 12 weeks. Displayed values are means \pm S.E.M..

Since mice with mutations in the melanocortin system develop an increased body length (268), body length was measured in control and insulin receptor knockout mice (Figure 22). This analysis revealed no alterations in body length in these animals, a further indication of the intact function of the melanocortin pathway despite the absence of insulin receptor signaling in either POMC or AgRP neurons.

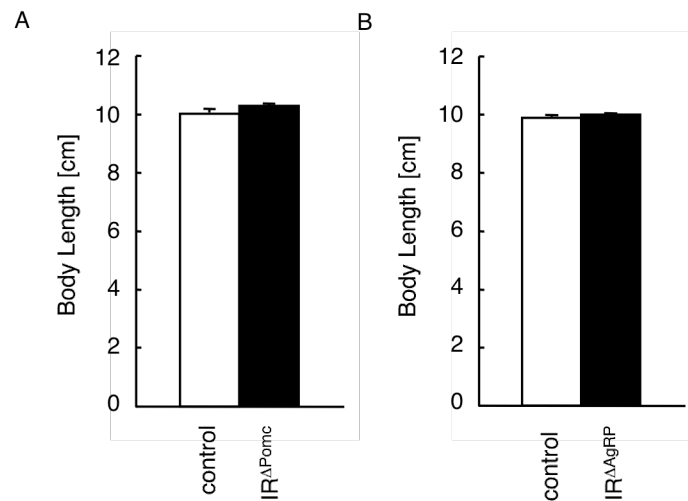


Figure 22: Body length of $IR^{\Delta POMC}$ and $IR^{\Delta AgRP}$ male mice.

(A) Naso-anal body length of male control (n = 10) and $IR^{\Delta POMC}$ (n = 9) mice at the age of 15 weeks. (B) Naso-anal body length of female control (n = 10) and $IR^{\Delta AgRP}$ (n = 11) mice at the age of 15 weeks. Displayed values are means \pm S.E.M..

3.4 $IR^{\Delta AgRP}$ mice fail to fully suppress hepatic glucose production

Since global knockout of the insulin receptor in brain and pharmacological studies using infusion of insulin or a small-molecule insulin mimetic had shown effects on glucose homeostasis and hepatic glucose production (47, 58), these parameters were assessed in control, $IR^{\Delta POMC}$ and $IR^{\Delta AgRP}$ mice. Fasted blood glucose and serum insulin concentrations were comparable between male $IR^{\Delta POMC}$ and $IR^{\Delta AgRP}$ mice as compared to controls (Figure 23). Moreover, glucose tolerance tests revealed no major disturbance of glucose homeostasis in either of the knockout mice both on normal diet or high fat diet (Figure 24).

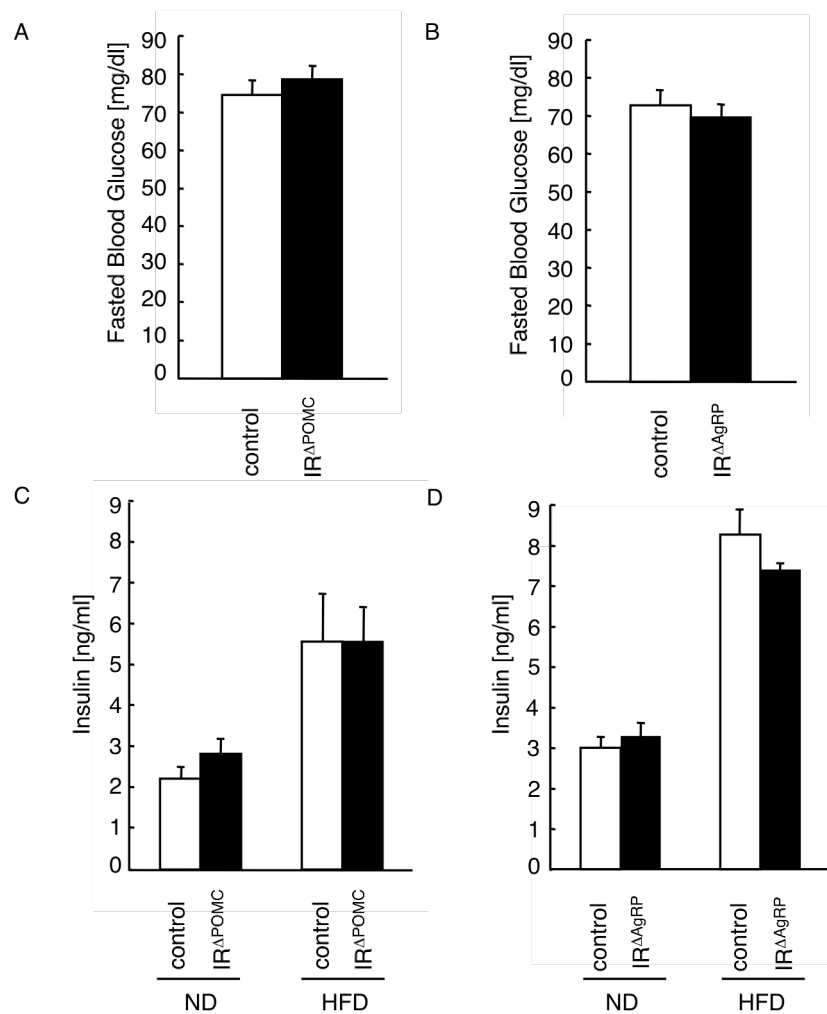


Figure 23: Fasting blood glucose levels and serum insulin concentrations in IR^{ΔPOMC} and IR^{ΔAgRP} male mice.

(A) Average fasting blood glucose levels of control (n = 18) and IR^{ΔPOMC} (n = 14) mice at the age of 10 weeks. (B) Average fasting blood glucose levels of control (n = 10) and IR^{ΔAgRP} (n = 14) mice at the age of 10 weeks. (C) Serum insulin concentrations of control (n = 10 - 12) and IR^{ΔPOMC} (n = 12 - 20) mice on normal (ND) and high fat diet (HFD) at the age of 15 weeks. (D) Serum insulin concentrations of control (n = 11 - 15) and IR^{ΔAgRP} (n = 8 - 15) mice on normal (ND) and high fat diet (HFD) at the age of 15 weeks. Displayed values are means ± S.E.M..

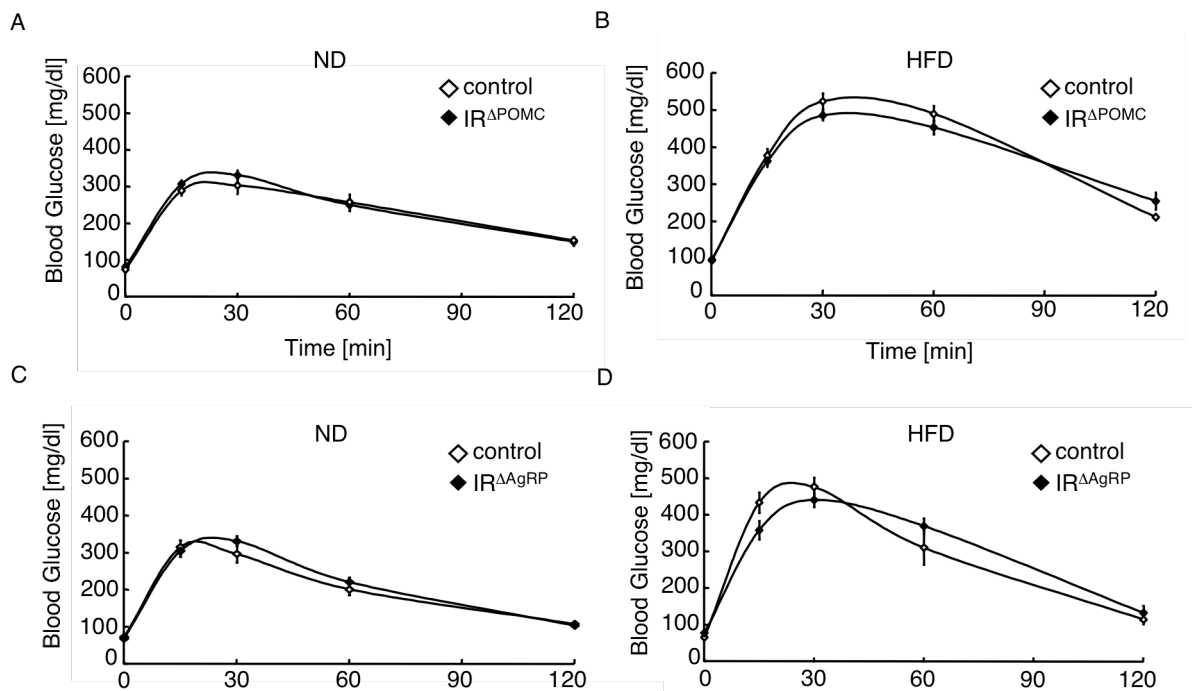


Figure 24: Glucose tolerance in IR^{ΔPOMC} and IR^{ΔAgRP} male mice.

(A) Glucose tolerance test of control (n = 13) and IR^{ΔPOMC} (n = 11) mice on normal diet (ND) at the age of 10 weeks. (B) Glucose tolerance test of control (n = 7) and IR^{ΔPOMC} (n = 17) mice on high fat diet (HFD) at the age of 10 weeks. (C) Glucose tolerance test of control (n = 10) and IR^{ΔAgRP} (n = 14) mice on normal diet (ND) at the age of 10 weeks. (D) Glucose tolerance test of control (n = 9) and IR^{ΔAgRP} (n = 14) mice on high fat diet (HFD) at the age of 10 weeks. Displayed values are means ± S.E.M..

Since the contribution of individual tissues is impossible to assess by standard glucose and insulin measurements, euglycemic-hyperinsulinemic clamps, which allow measurement of insulin sensitivity *in vivo* without causing hypoglycemia, were performed on the three different groups of mice at 15 weeks of age. After an overnight fasting period, mice received a constant infusion of insulin to produce hyperinsulinemia, and a variable infusion of glucose to maintain euglycemia over a steady state period of 30 minutes (Figure 25). Co-administration of D-[3-³H]- and 2-Deoxy-D-[1-¹⁴C] glucose enables the rate of glucose production under basal and hyperinsulinemic steady state conditions to be measured, as well as determination of the rate of insulin-stimulated tissue-specific glucose uptake.

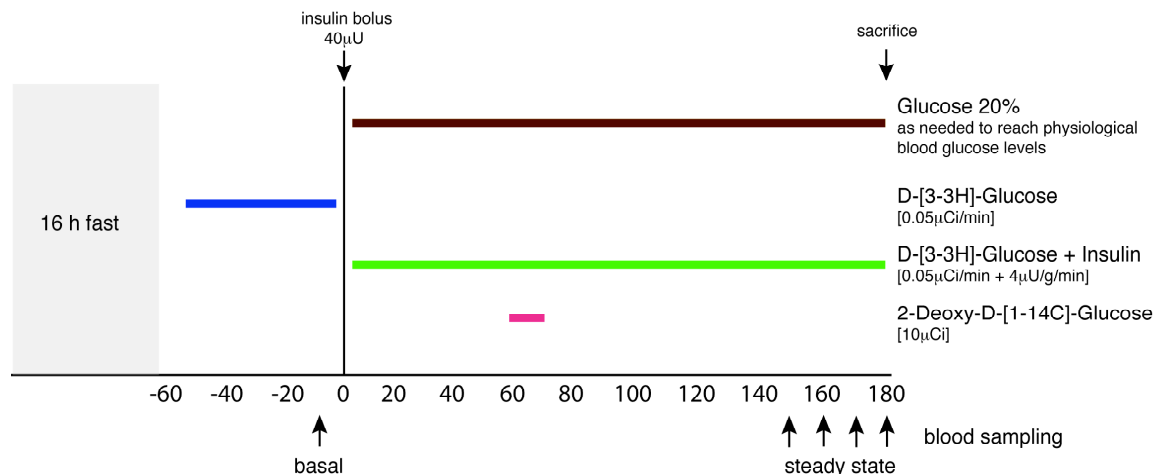


Figure 25: General scheme of a euglycemic-hyperinsulinemic clamp.

After starvation for 16 hours, mice received a continuous intravenous infusion of a D-[3-³H]-Glucose tracer solution. At the end of the basal period (50 min) a blood sample (basal) was collected for determination of basal parameters and insulin infusion was started. Blood glucose levels were determined every 10 minutes and physiological blood glucose levels (between 100 and 140 mg/dl) were maintained by adjusting a 20% glucose infusion to prevent a counterregulatory response to hypoglycemia. Approximately 120 minutes before steady state was achieved, a bolus of 2-Deoxy-D-[1-¹⁴C]-Glucose was infused. Steady state was ascertained when glucose measurements were constant for at least 30 min at a fixed glucose infusion rate. During the steady state, blood samples were collected for the measurement of steady state parameters.

The glucose infusion rate required to maintain euglycemia during steady state conditions, which indicates the balance between the rates of glucose production and glucose utilization when insulin levels are high, was comparable between the different groups (Figure 26 A, B). Hepatic glucose production was also not significantly different between the three groups of mice under basal conditions. However, whereas control and IR^{ΔPOMC} mice significantly suppressed hepatic glucose production during steady state conditions (Figure 26 C, D), insulin did not significantly reduce hepatic glucose production in IR^{ΔAgRP} mice (Figure 26 C, D). Thus, insulin action on AgRP neurons is required for the ability of peripherally applied insulin to efficiently suppress hepatic glucose production.

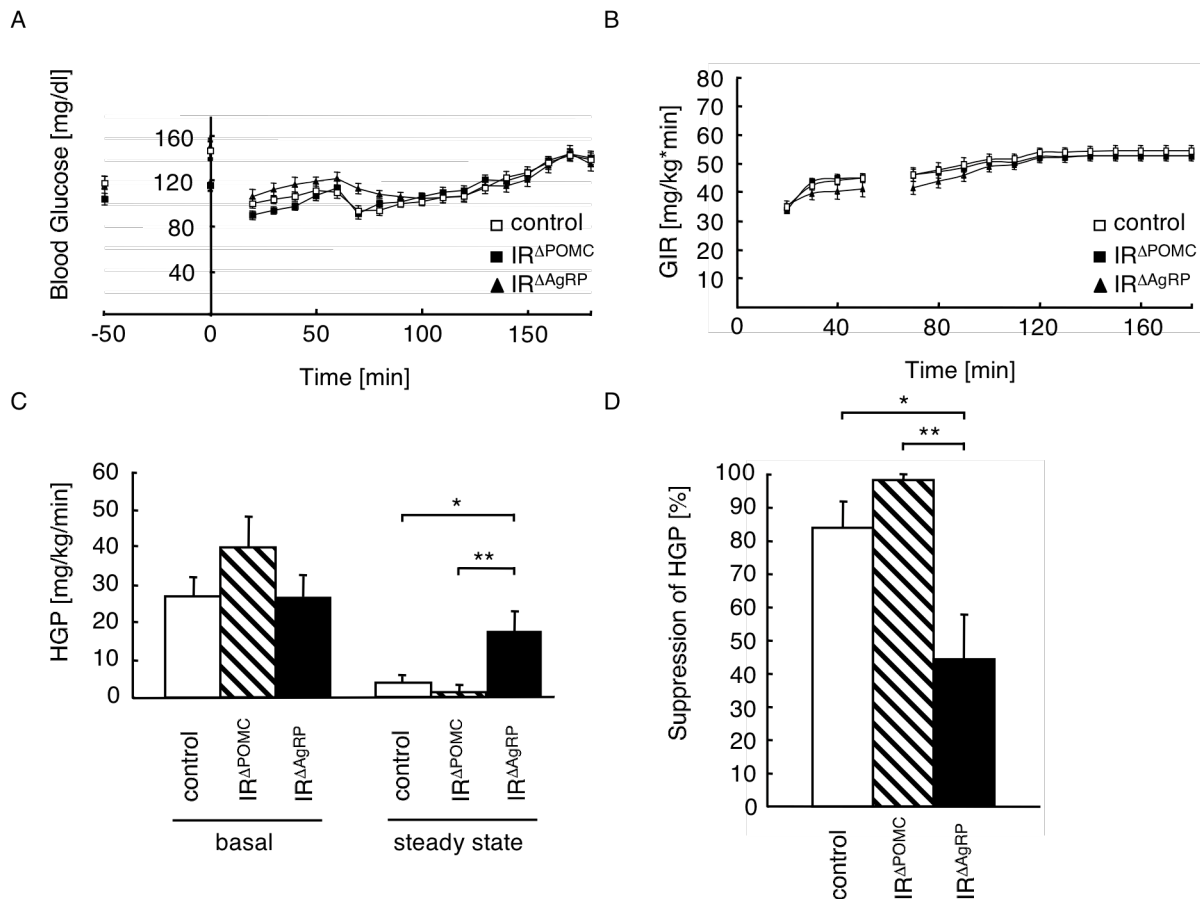


Figure 26: Regulation of glucose homeostasis in IR^{ΔPOMC} and IR^{ΔAgRP} mice.

(A) Blood glucose levels during the clamp period in control (□, n = 13), IR^{ΔPOMC} (■, n = 9) and IR^{ΔAgRP} (▲, n = 11) mice at the age of 15 weeks. (B) Glucose infusion rates during the clamp period in control (□, n = 13), IR^{ΔPOMC} (■, n = 9) and IR^{ΔAgRP} (▲, n = 11) mice at the age of 15 weeks. (C) Hepatic glucose production (HGP) measured under basal and steady state conditions during the clamp in control (n = 13), IR^{ΔPOMC} (n = 9) and IR^{ΔAgRP} (n = 11) mice. (D) Percentage suppression of hepatic glucose production (HGP) by insulin as measured under steady state conditions during the clamp in control (n = 13), IR^{ΔPOMC} (n = 9) and IR^{ΔAgRP} (n = 11) mice. Displayed values are means ± S.E.M.; *, p ≤ 0.05; **, p ≤ 0.01.

Determination of tissue-specific glucose uptake rates showed similar rates of insulin-stimulated glucose uptake in brain and skeletal muscle in the different groups of mice (Figure 27). However, insulin-stimulated glucose uptake in white adipose tissue of IR^{ΔAgRP} mice (but not IR^{ΔPOMC} mice) was significantly increased compared to control mice (Figure 27), indicating some form of compensatory response on increased hepatic glucose production or tissue cross talk.

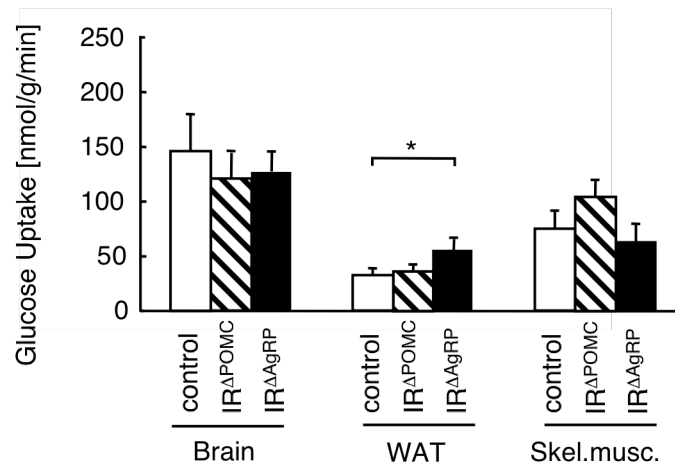


Figure 27: Insulin-stimulated tissue glucose uptake in euglycemic-hyperinsulinemic clamps.

Tissue-specific insulin-stimulated glucose uptake rates in brain, white adipose tissue (WAT) and skeletal muscle (Skel.musc.) from male control (n = 13), IR^{ΔPOMC} (n = 9) and IR^{ΔAgRP} (n = 11) mice. Displayed values are means ± S.E.M.; *, p ≤ 0.05.

3.5 Reduced hepatic IL-6 expression in IR^{ΔAgRP} mice

It has recently been shown that insulin, acting through the CNS, induces hepatic Interleukin-6 (IL-6) expression and activates STAT3 in liver parenchymal cells, thereby suppressing hepatic gluconeogenesis (48). Therefore, to further investigate the molecular mechanism underlying the failure of IR^{ΔAgRP} mice to efficiently suppress hepatic glucose production, IL-6 mRNA expression was determined in the liver of the different groups of mice under basal and clamp steady state conditions. This revealed a 30% reduction of steady state hepatic IL-6 expression in IR^{ΔAgRP} mice (Figure 28 A), whereas basal IL-6 expression levels were unaltered between the different groups (Figure 28 B).

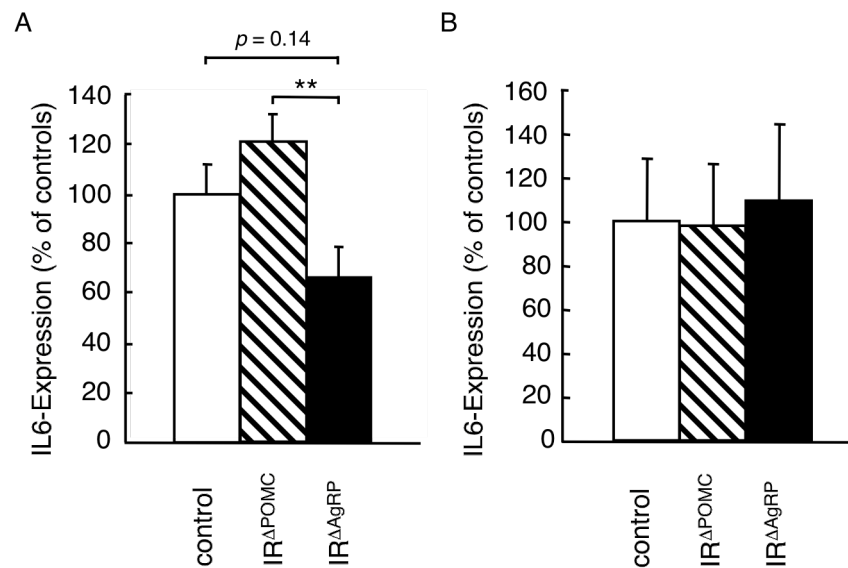


Figure 28: Hepatic interleukin-6 expression under steady state and basal conditions in euglycemic-hyperinsulinemic clamps.

(A) IL-6 mRNA expression in liver at the end of the euglycemic-hyperinsulinemic clamp of male control (n = 13), IR^{ΔPOMC} (n = 9) and IR^{ΔAgRP} (n = 11) mice. (B) IL-6 mRNA expression in liver under basal conditions of control (n = 6), IR^{ΔPOMC} (n = 5) and IR^{ΔAgRP} (n = 4) mice. Displayed values are means ± S.E.M.; **, $p \leq 0.01$.

Moreover, Western blot analysis of clamp steady state expression of the glucose-6-phosphatase protein (G6Pase), a key enzyme of gluconeogenesis, revealed a significantly upregulated expression in liver of IR^{ΔAgRP} mice compared to control and IR^{ΔPOMC} mice (Figure 29 A). On the other hand, basal expression of G6Pase was unaltered in liver of IR^{ΔAgRP} mice as compared to control and IR^{ΔPOMC} mice (Figure 29 B).

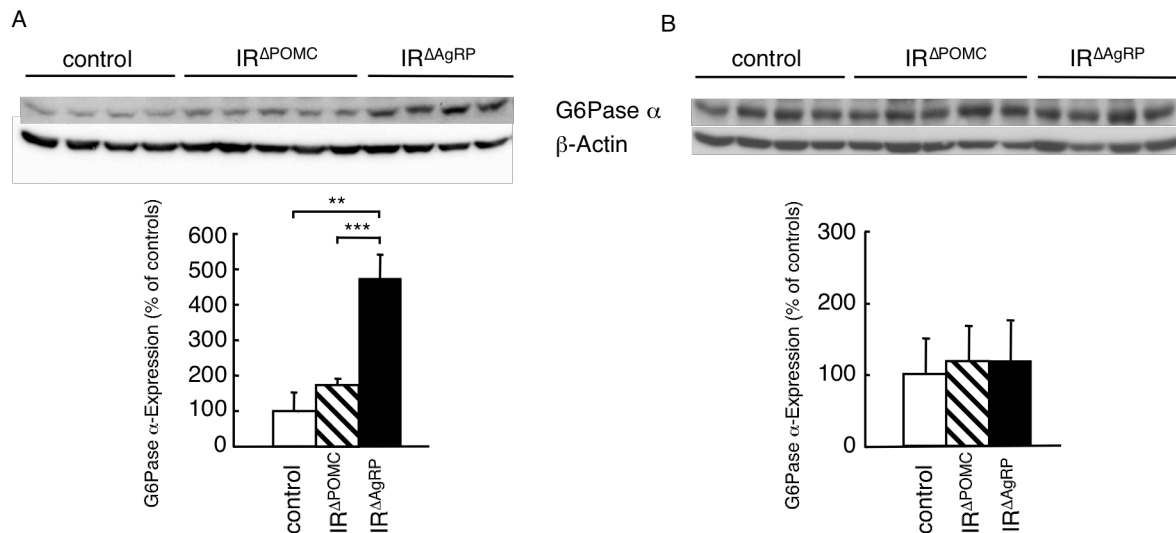


Figure 29: Hepatic G6Pase-expression under steady state and basal conditions in euglycemic-hyperinsulinemic clamps.

(A) Western blot analysis (upper panel) of the glucose-6-phosphatase (G6Pase) α subunit and β -Actin (loading control) in liver at the end of euglycemic-hyperinsulinemic clamps of control ($n = 4$), IR ^{Δ POMC} ($n = 5$) and IR ^{Δ AgRP} ($n = 4$) mice. Densitometrical analysis (lower panel) of glucose-6-phosphatase (G6Pase) α subunit expression in IR ^{Δ POMC} and IR ^{Δ AgRP} mice as compared to controls. (B) Western blot analysis (upper panel) of the glucose-6-phosphatase (G6Pase) α subunit and β -Actin (loading control) in liver under basal conditions of control ($n = 4$), IR ^{Δ POMC} ($n = 5$) and IR ^{Δ AgRP} ($n = 4$) mice. Densitometrical analysis (lower panel) of basal glucose-6-phosphatase (G6Pase) α subunit expression in IR ^{Δ POMC} and IR ^{Δ AgRP} mice as compared to controls. Displayed values are means \pm S.E.M.; **, $p \leq 0.01$; ***, $p \leq 0.001$.

Additionally, to investigate if other hepatic cytokines and chemokines are involved in the failure of IR ^{Δ AgRP} mice to efficiently suppress hepatic glucose production, mRNA expression levels of various cytokines and chemokines involved in inflammation were analyzed in liver of the different groups of mice under clamp steady state conditions. This revealed no significant differences between control, IR ^{Δ POMC} and IR ^{Δ AgRP} mice (Figure 30), further indicating that the failure of IR ^{Δ AgRP} mice to efficiently suppress hepatic glucose production is based on impaired insulin-stimulated hepatic IL-6 expression.

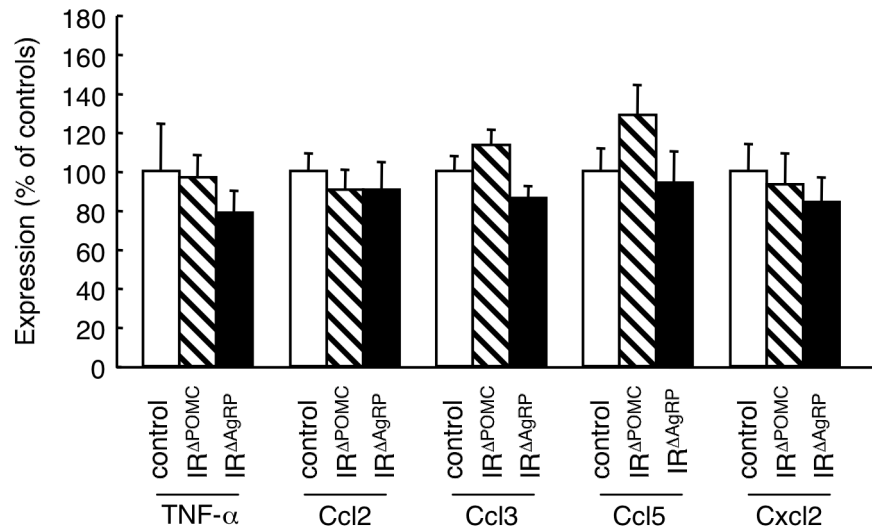


Figure 30: Hepatic cytokine and chemokine expression at the end of euglycemic-hyperinsulinemic clamps.

mRNA expression of cytokines and chemokines in liver at the end of euglycemic-hyperinsulinemic clamps of control (n = 13), IR^{ΔPOMC} (n = 9) and IR^{ΔAgRP} (n = 11) mice. TNF- α : tumor necrosis factor alpha, Ccl2: chemokine (C-C motif) ligand 2 (Mcp-1), Ccl3: chemokine (C-C motif) ligand 3 (Mip1-alpha), Ccl5: chemokine (C-C motif) ligand 5 (RANTES), Cxcl2: chemokine (C-X-C motif) ligand 2 (Mip2-alpha). Displayed values are means \pm S.E.M..

Taken together, these data indicate that IR^{ΔAgRP} mice fail to efficiently suppress hepatic glucose production in a euglycemic-hyperinsulinemic clamp, and that this is paralleled by impaired insulin-stimulated hepatic IL-6 expression and a failure to suppress expression of the glucose-6-phosphatase protein.

3.6 Inactivation of the *insulin receptor* gene in dopaminergic cells

Tyrosine hydroxylase, the rate-limiting enzyme in dopamine synthesis, is a well-established marker of dopaminergic neurons. To investigate the role of insulin signaling in tyrosine hydroxylase (Th)-expressing cells, the *insulin receptor* gene was inactivated specifically in these cells. To this end, knock-in mice expressing Cre recombinase from the 3'-untranslated region of the endogenous *tyrosine hydroxylase* gene by means of an internal ribosomal entry sequence (IRES) (261) were crossed with mice carrying a loxP-flanked *insulin receptor* gene ($IR^{lox/lox}$) (Figure 31) (58).

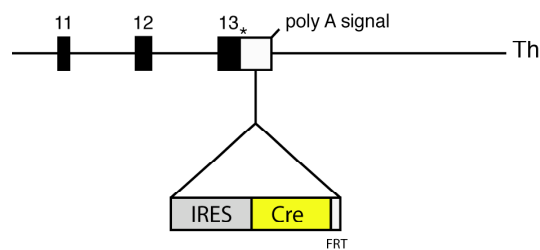


Figure 31: Restricted inactivation of the *insulin receptor* gene in tyrosine hydroxylase-expressing cells.

Map of a part of the endogenous tyrosine hydroxylase (Th) locus (exon 11-13) and the knock-in cassette. Black boxes represent translated exons of the *Th* gene and the open box stands for the 3' untranslated region. The stop codon is depicted by an asterisk (*). The knock-in cassette is located between the stop codon and poly A signal in *Th* exon 13.

In $IR^{lox/lox}$ mice, positive for expression of Cre recombinase from the 3'-untranslated region of the *tyrosine hydroxylase* gene, the loxP-flanked *insulin receptor* gene is removed upon Cre-mediated recombination, leading to the inactivation of the insulin receptor selectively in Th-expressing cells (Figure 32).

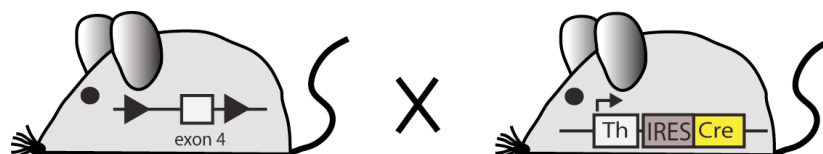


Figure 32: General scheme of mice with restricted inactivation of the *insulin receptor* gene in tyrosine hydroxylase-expressing cells (IR^{ATh}).

Mice, homozygous for a loxP-flanked exon 4 of the insulin receptor allele ($IR^{lox/lox}$) were crossed with mice expressing the Cre protein from the 3'-untranslated region of the *tyrosine hydroxylase* gene. Only one loxP-flanked allele is depicted here.

To analyze cell type-specific inactivation of the insulin receptor, Cre-mediated recombination was visualized by crossing *ThIRESCre* mice to the *Z/EG* reporter mouse strain which carries a transgene comprising a loxP-flanked *β geo* fusion gene followed by the coding sequence of a GFP protein (254). In this configuration, GFP is only expressed in cells expressing the Cre recombinase. These mice showed a pattern of GFP immunoreactivity in the ventral tegmental area (VTA) and the substantia nigra (SN) reflecting the described expression pattern of endogenously expressed tyrosine hydroxylase (Figure 33), consistent with the previously demonstrated colocalization of endogenous tyrosine hydroxylase expression and Cre recombinase activity (261).

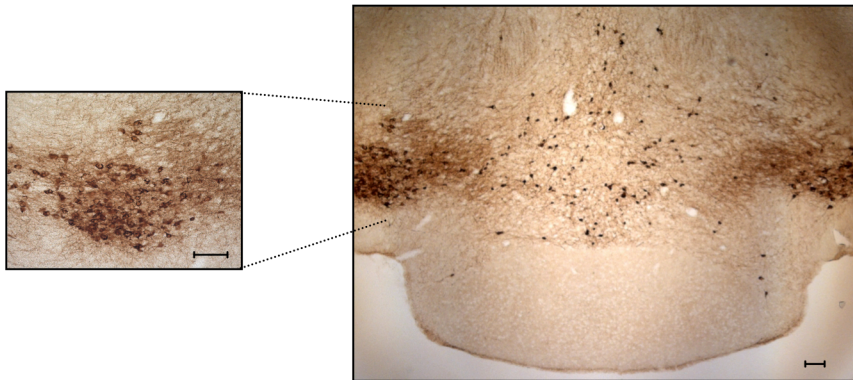


Figure 33: Verification of Cre-mediated recombination in *ThIRESCre* mice.

ThIRESCre mice were mated with *Z/EG* reporter mice and immunohistochemistry for enhanced GFP was performed on brain sections of double heterozygous reporter mice (*Z/EG^{+/-} ThIRESCre*). Cre mediated recombination removes the loxP-flanked neomycin resistance gene, thus GFP is transcribed only in tyrosine hydroxylase-expressing cells. Cre recombinase activity is present in the ventral tegmental area and the substantia nigra. GFP-positive cells, brown. Scale bar: 100 μ m.

In the VTA, insulin has been shown to activate the intracellular PI3 kinase cascade, which results in the generation of PIP3 (249). Therefore, functional effects of restricted insulin receptor deficiency in Th-expressing cells on insulin's ability to activate the PI3 kinase pathway were determined. *ThIRESCre* as well as *IR^{ΔTh}* mice were crossed to the *LacZ* reporter mouse strain in which transcription of the *β -galactosidase* gene (*LacZ*) under control of the ubiquitously expressed *Rosa26* promoter is prevented by a floxed *hygromycin resistance* gene, thus leading to a *β -galactosidase* expression only in cells expressing the Cre recombinase (253).

In the basal state, little immunoreactive PIP3 was detectable in Th-expressing neurons of control and IR^{ΔTh} reporter mice. In control mice, insulin treatment resulted in activation of PIP3 formation in Th-expressing and non-Th-expressing neurons of the VTA/SN (Figure 34 A, B). In contrast, in IR^{ΔTh} mice insulin stimulation resulted in PIP3 formation in non-Th-expressing cells, but it failed to activate PIP3 formation in Th-expressing neurons (Figure 34 A, C). These data indicate efficient and specific insulin receptor inactivation in Th-expressing cells of IR^{ΔTh} mice.

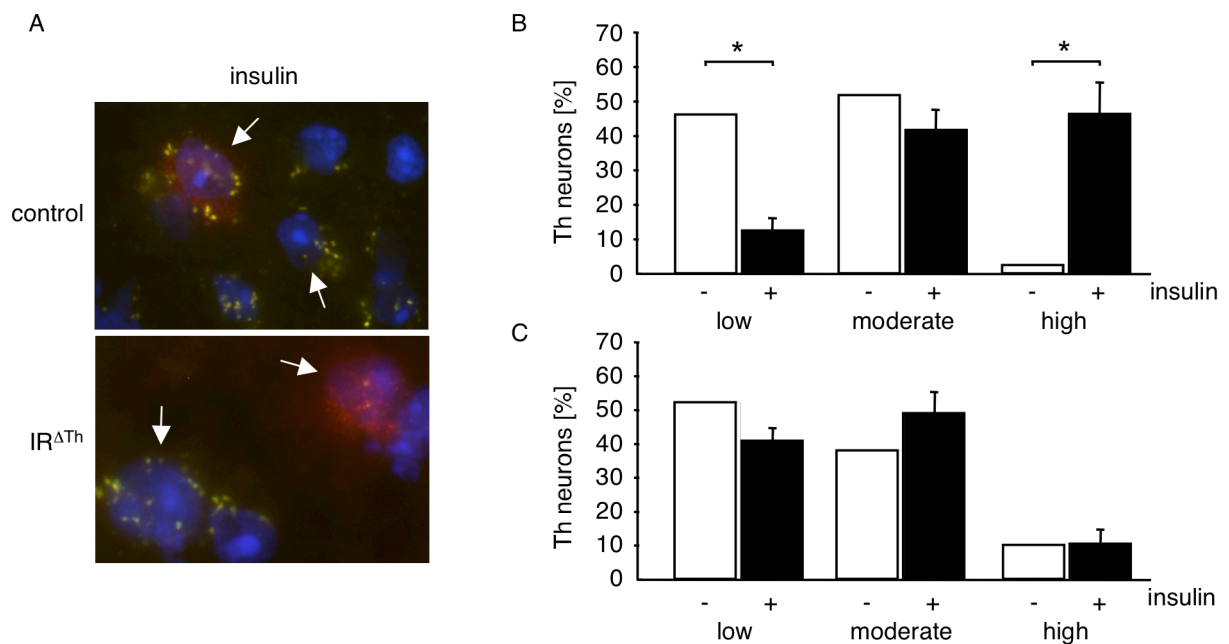


Figure 34: PIP3 formation in neurons of control and IR^{ΔTh} reporter mice.

(A) Double immunohistochemistry of ARC neurons of control and IR^{ΔTh} reporter mice was performed in overnight fasted mice, which were intravenously injected with either saline or insulin and sacrificed 10 min afterwards. Arrows indicate 1 Th-expressing neuron and 1 non-Th-expressing neuron in each panel. (B) Quantification of PIP3 levels in control reporter mice in the basal state (-) and after insulin (+) stimulation. Values are means \pm S.E.M. of sections obtained from 2 unstimulated and 3 insulin-stimulated control mice. *, $p \leq 0.05$. (C) Quantification of PIP3 levels in IR^{ΔTh} reporter mice in the basal state (-) and after insulin (+) stimulation. Values are means \pm S.E.M. of sections obtained from 2 unstimulated and 4 insulin-stimulated IR^{ΔTh} mice. Blue (DAPI), DNA; red, β -gal (Th-expressing neurons); green, PIP3.

To rule out that fertility is altered in mice with inactivation of the insulin receptor in Th-expressing cells, parameters of fertility were assessed in $IR^{\Delta Th}$ mice. This revealed no significant differences concerning litter-to-litter intervals, litter size and morphology of reproductive organs between control ($IR^{lox/lox}$) and $IR^{\Delta Th}$ mice, indicating that insulin signaling in these cells is not required for control of fertility (Figure 35).

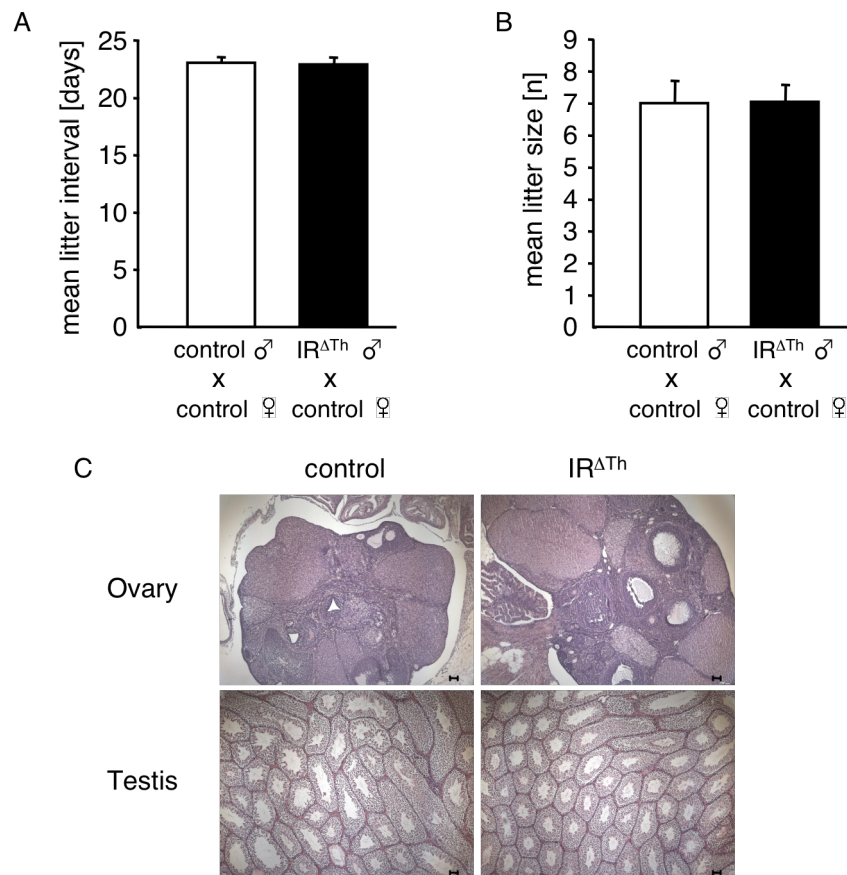


Figure 35: Fertility of $IR^{\Delta Th}$ mice.

(A) Mean litter intervals for control and $IR^{\Delta Th}$ mice assessed over a period of at least three litters ($n = 3$ breedings). (B) Mean litter size for control and $IR^{\Delta Th}$ mice assessed over a period of at least three litters ($n = 3$ breedings). (C) Representative hematoxylin/eosin staining of ovaries and testes from control and $IR^{\Delta Th}$ mice. Scale bar 100 μ m. Displayed values are means \pm S.E.M..

3.7 Increased adiposity in IR^{ΔTh} mice

To investigate the impact of insulin receptor inactivation in Th-expressing cells on the regulation of energy homeostasis, body weight of female and male control and IR^{ΔTh} mice was monitored from weaning until 20 weeks of age under normal diet conditions. Both, female and male IR^{ΔTh} mice exhibited an increased body weight from approximately 7 weeks of age on as compared to control mice (Figure 36 A, B). To investigate whether increased body weight in IR^{ΔTh} mice results from an increase in body fat mass, the amount of epigonadal fat was examined in female and male control and IR^{ΔTh} mice under normal diet conditions. Consistent with the body weight curves, female and male IR^{ΔTh} mice displayed significantly increased epigonadal fat pad mass at the age of 20 weeks compared to controls (Figure 36 C, D). Consistent with this, brown adipose tissue mass was also increased in female and male IR^{ΔTh} mice at the age of 20 weeks (Figure 36 E, F).

To further confirm increased adiposity in IR^{ΔTh} mice, body fat content of 20-week-old mice was determined by *in vivo* magnetic resonance spectrometry. Mean body fat content was increased in female and male IR^{ΔTh} mice as compared to controls (Figure 36 G, H). Consistent with these findings, adiposity was accompanied by increased concentrations of circulating leptin (Figure 36 I, J).

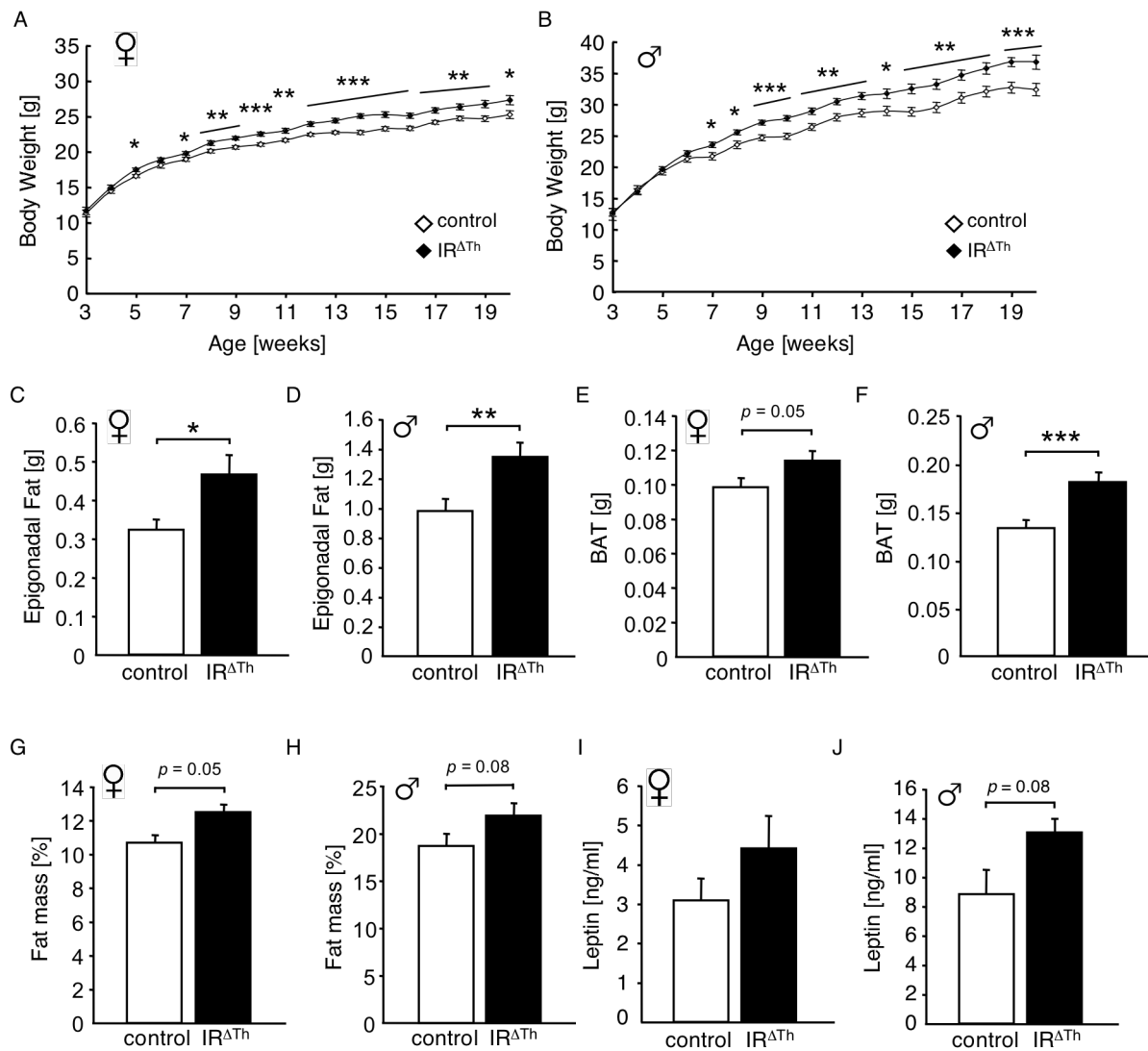


Figure 36: Body weight, fat content and leptin levels of IR^{ΔTh} mice.

(A) Average body weight of female control (◇) and IR^{ΔTh} (◆) mice under normal diet conditions (n = 27 - 30). (B) Average body weight of male control (◇) and IR^{ΔTh} (◆) mice under normal diet conditions (n = 13 - 22). (C) Parametrial fat pad weight of female control and IR^{ΔTh} mice (n = 29) at the age of 20 weeks. (D) Epididymal fat pad weight of male control and IR^{ΔTh} mice (n = 15 - 17) at the age of 20 weeks. (E) Brown adipose tissue (BAT) weight of female control and IR^{ΔTh} mice (n = 29) at the age of 20 weeks. (F) Brown adipose tissue (BAT) weight of male control and IR^{ΔTh} mice (n = 15 - 17) at the age of 20 weeks. (G) Average body fat content of female control and IR^{ΔTh} mice (n = 29) at the age of 20 weeks measured by nuclear magnetic resonance. (H) Average body fat content of male control and IR^{ΔTh} mice (n = 15 - 17) at the age of 20 weeks measured by nuclear magnetic resonance. (I) Serum leptin concentrations of female control and IR^{ΔTh} mice (n = 17 - 20) under normal diet conditions at the age of 20 weeks. (J) Serum leptin concentrations of male control and IR^{ΔTh} mice (n = 7 - 9) under normal diet conditions at the age of 20 weeks. Displayed values are means ± S.E.M.; *, p ≤ 0.05; **, p ≤ 0.01; ***, p ≤ 0.001.

Taken together, these results indicate that inactivation of the *insulin receptor* gene in Th-expressing cells results in increased body weight and adiposity.

3.8 Unaltered glucose homeostasis in IR^{ΔTh} mice

Next, glucose metabolism was compared in control and IR^{ΔTh} mice. Glucose and insulin tolerance tests revealed no alterations in glucose tolerance and insulin sensitivity in female and male IR^{ΔTh} mice compared to control mice (Figure 37). Thus, inactivation of the insulin receptor in Th-expressing cells has no effect on glucose homeostasis in these mice. Consistent with these findings, serum insulin concentrations of female and male IR^{ΔTh} mice were similar as compared to controls at an age of 9 weeks (Figure 38 A, B). However, serum insulin concentrations of female and male IR^{ΔTh} mice were significantly increased at an age of 20 weeks (Figure 38 C, D).

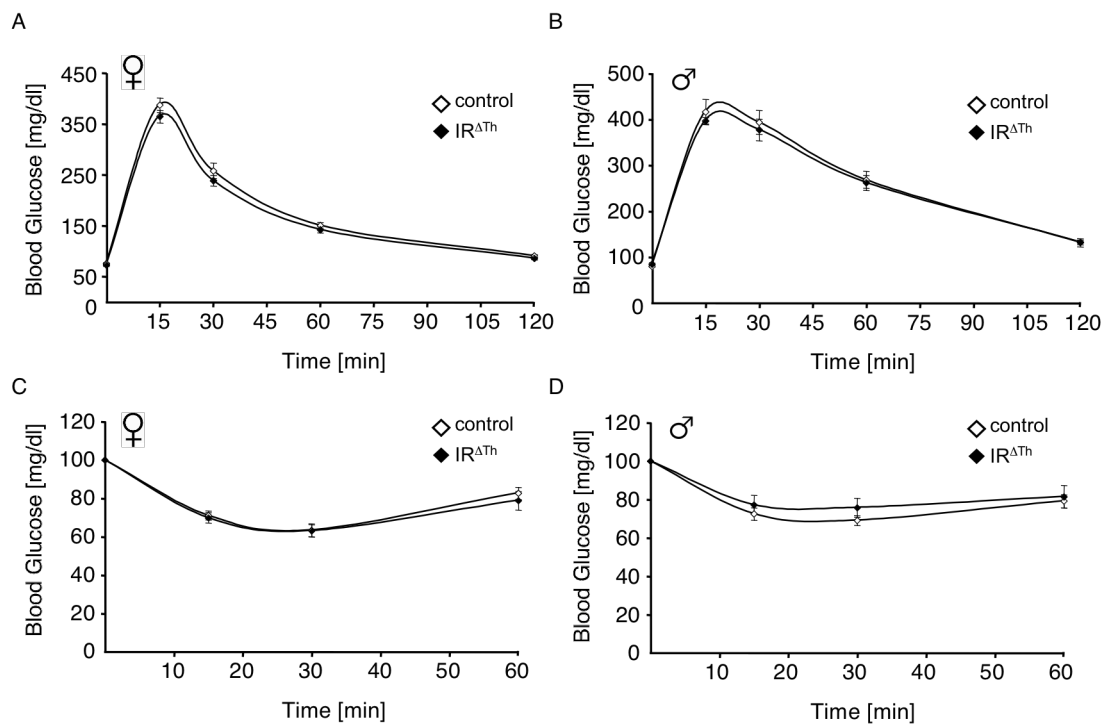


Figure 37: Glucose tolerance and insulin sensitivity in IR^{ΔTh} mice.

(A, B) Glucose tolerance tests of overnight fasted female (left panel, n = 15 - 20) and male (right panel, n = 9 - 13) control and IR^{ΔTh} mice under normal diet conditions at the age of 10 weeks. (C, D) Insulin tolerance tests of female (left panel, n = 15 - 20) and male (right panel, n = 9 - 13) control and IR^{ΔTh} mice under normal diet conditions at the age of 11 weeks. Displayed values are means ± S.E.M..

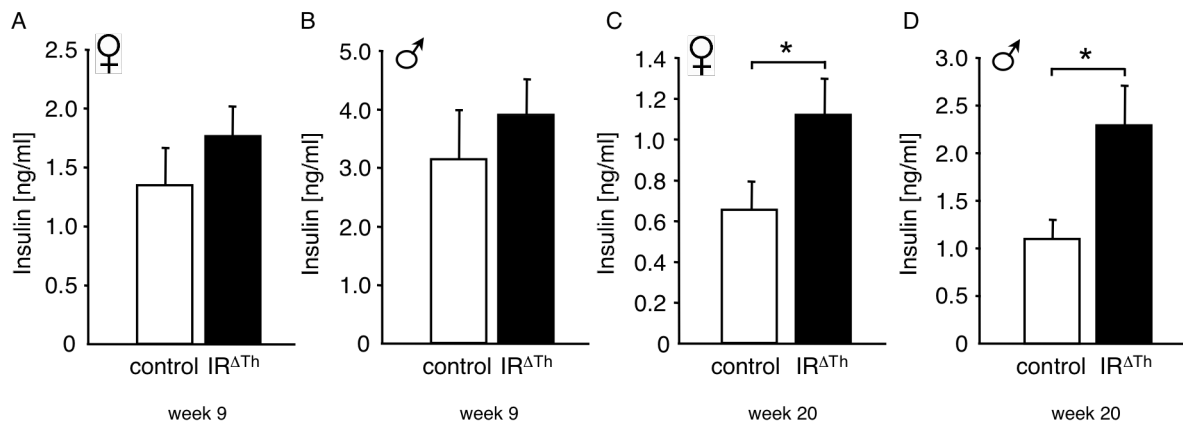


Figure 38: Serum insulin concentrations in IR^{ΔTh} mice.

(A) Serum insulin concentrations of female control (n = 27) and IR^{ΔTh} (n = 26) mice under normal diet conditions at the age of 9 weeks. (B) Serum insulin concentrations of male control (n = 14) and IR^{ΔTh} (n = 12) mice under normal diet conditions at the age of 9 weeks. (C) Serum insulin concentrations of female control (n = 20) and IR^{ΔTh} (n = 16) mice under normal diet conditions at the age of 20 weeks. (D) Serum insulin concentrations of male control (n = 8) and IR^{ΔTh} (n = 7) mice under normal diet conditions at the age of 20 weeks. Displayed values are means ± S.E.M..

3.9 Unaltered energy expenditure but increased food intake in IR^{ΔTh} mice

To further analyze the mechanism underlying the increased body weight and adiposity of IR^{ΔTh} mice, energy intake and energy expenditure were assessed in these mice. Female and male IR^{ΔTh} mice displayed an increased food intake, both at 6 and 13 weeks of age as compared to control littermates (Figure 39).

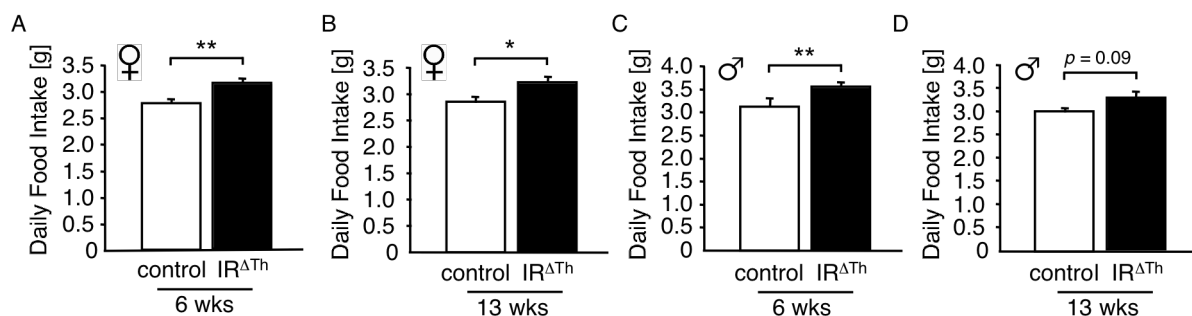


Figure 39: Food intake of IR^{ΔTh} mice.

(A) Daily food intake of female control and IR^{ΔTh} mice under normal diet conditions at the age of 6 weeks (n = 11 - 12). (B) Daily food intake of female control and IR^{ΔTh} mice under normal diet conditions at the age of 13 weeks (n = 12 - 13). (C) Daily food intake of male control and IR^{ΔTh} mice under normal diet conditions at the age of 6 weeks (n = 10 - 13). (D) Daily food intake of male control and IR^{ΔTh} mice under normal diet conditions at the age of 13 weeks (n = 11). Displayed values are means ± S.E.M.; *, p ≤ 0.05; **, p ≤ 0.01.

To investigate whether the increased adiposity in IR^{ΔTh} mice may also result from a decreased energy expenditure and/or locomotor activity, energy expenditure and basal locomotor activity of IR^{ΔTh} mice were analyzed at 20 weeks of age. This analysis revealed unaltered oxygen consumption, assessed by indirect calorimetry, in female and male IR^{ΔTh} mice as compared to control mice during both day and night phase (Figure 40 A, C). Basal locomotor activity in both female and male IR^{ΔTh} mice was also indistinguishable to control animals during both day and night phase (Figure 40 B, D).

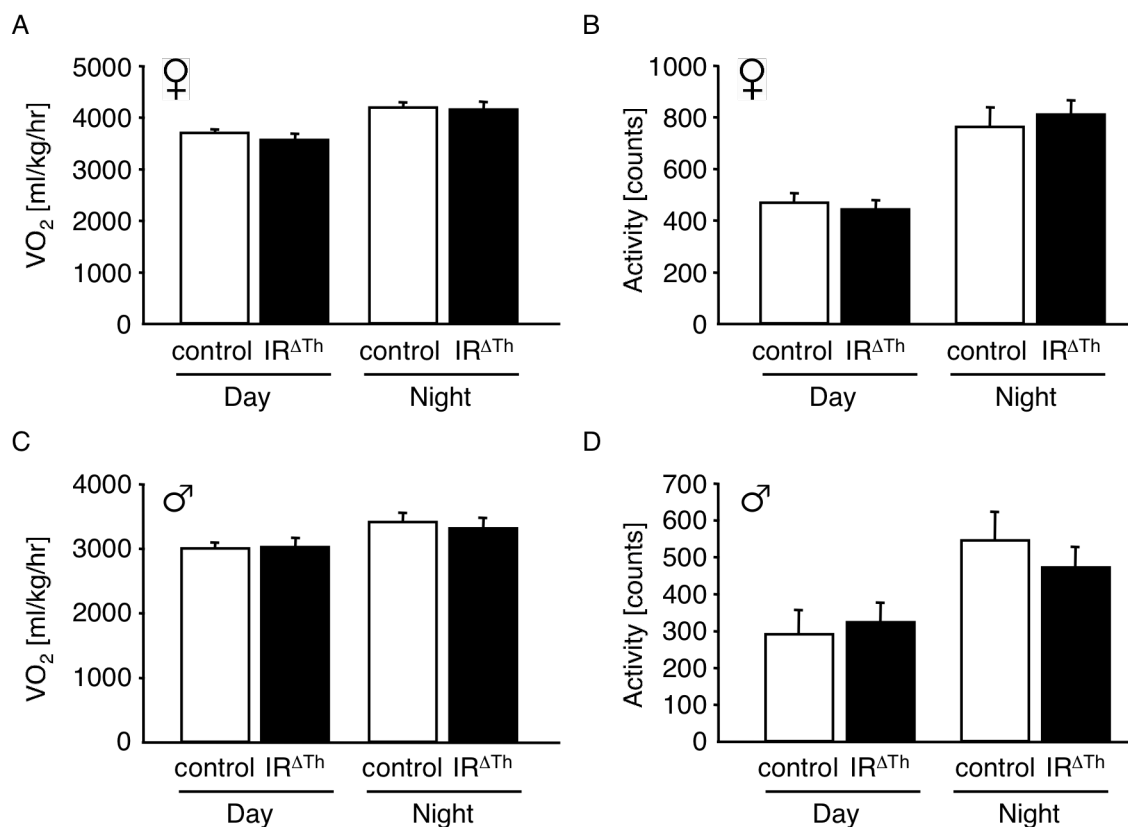


Figure 40: Basal metabolic rate and locomotor activity in IR^{ΔTh} mice.

(A) Mean oxygen consumption (VO₂) of female control (n = 11) and IR^{ΔTh} (n = 7) mice under normal diet conditions measured by indirect calorimetry at the age of 20 weeks. (B) Basal locomotor activity of female control (n = 11) and IR^{ΔTh} (n = 7) mice under normal diet conditions at the age of 20 weeks. (C) Mean oxygen consumption (VO₂) of male control (n = 7) and IR^{ΔTh} (n = 6) mice under normal diet conditions measured by indirect calorimetry at the age of 20 weeks. (D) Basal locomotor activity of male control (n = 7) and IR^{ΔTh} (n = 6) mice under normal diet conditions at the age of 20 weeks. Displayed values are means ± S.E.M..

Taken together, these data indicate that increased body weight and adiposity in IR^{ΔTh} mice is the consequence of an increased food intake but not alterations in energy expenditure and/or locomotor activity.

3.10 Increased expression of tyrosine hydroxylase and dopamine receptor 2 in the ventral tegmental area of $IR^{\Delta Th}$ mice

Next, expression levels of different genes critically involved in dopamine signaling in brain regions related to the mesolimbic and nigrostriatal dopamine system were determined in the VTA, the nucleus accumbens (NAc), and the caudate putamen (CPu) of female control and $IR^{\Delta Th}$ mice at the age of 20 weeks. This revealed significantly increased mRNA levels of Th and dopamine receptor 2 (D2R) in the VTA of $IR^{\Delta Th}$ mice as compared to controls (Figure 41 A).

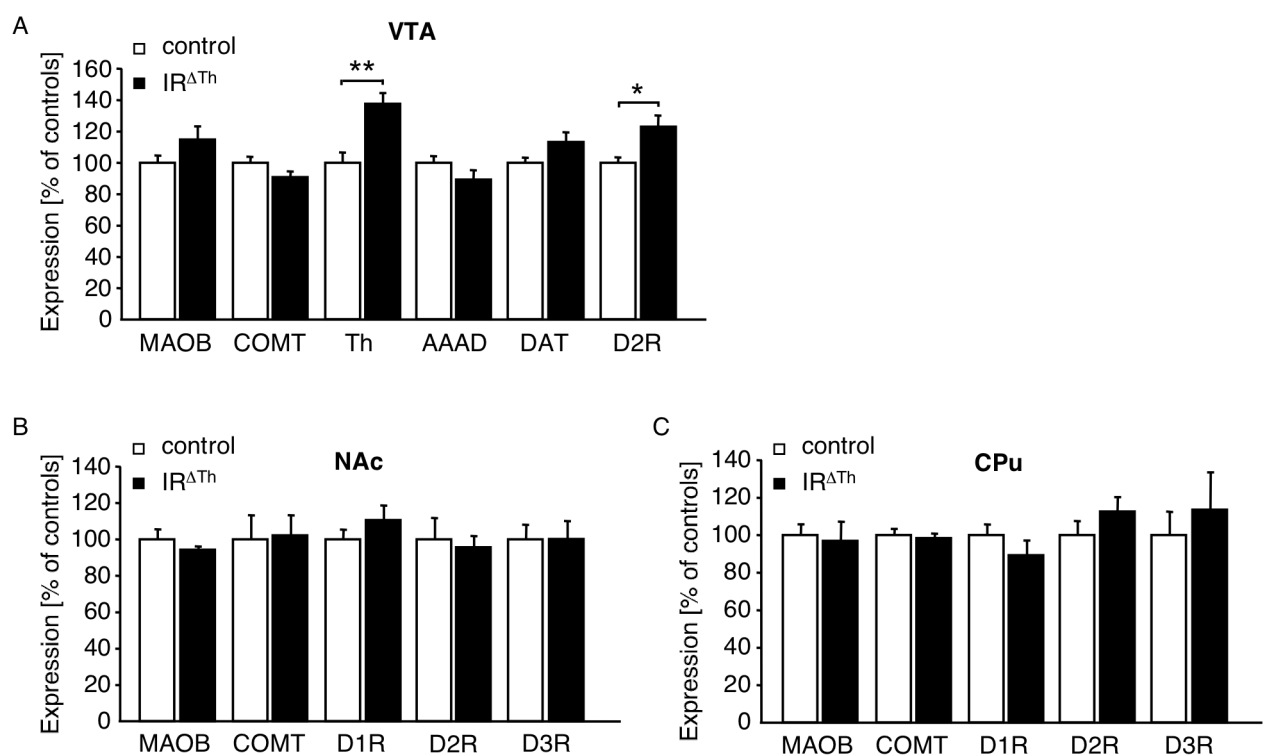


Figure 41: Expression levels of genes critically involved in dopamine signaling in the VTA, NAc, and CPu of $IR^{\Delta Th}$ mice.

(A) Expression of MAOB, COMT, TH, AAAD, DAT, and D2R in the ventral tegmental area (VTA) of female control ($n = 11$) and $IR^{\Delta Th}$ ($n = 11$) mice. (B) Expression of MAOB, COMT, D1R, D2R, and D3R in the nucleus accumbens (NAc) of female control ($n = 11$) and $IR^{\Delta Th}$ ($n = 11$) mice. (C) Expression of MAOB, COMT, D1R, D2R, and D3R in the caudate putamen (CPu) of female control ($n = 11$) and $IR^{\Delta Th}$ ($n = 11$) mice. AAAD: aromatic L-amino acid decarboxylase, COMT: catechol-O-methyl transferase, D1R: dopamine receptor 1, D2R: dopamine receptor 2, D3R: dopamine receptor 3, DAT: dopamine transporter, MAOB: monoamine oxidase B, Th: tyrosine hydroxylase. Displayed values are means \pm S.E.M.; *, $p \leq 0.05$; **, $p \leq 0.01$.

On the other hand, expression levels of monoamine oxidase B (MAOB), catechol-O-methyl transferase (COMT), aromatic L-amino acid decarboxylase (AAAD) and the dopamine transporter (DAT) were unaltered in the VTA of female IR^{ΔTh} mice as compared to controls (Figure 41 A). Moreover, expression levels of MAOB, COMT, dopamine receptor 1 (D1R), D2R, and dopamine receptor 3 (D3R) were unaltered in the NAc and CPu of these mice (Figure 41 B, C).

Thus, inactivation of the *insulin receptor* gene in Th-expressing cells leads to increased mRNA expression levels of tyrosine hydroxylase and dopamine receptor 2 in the VTA.

3.11 Insulin action decreases excitatory inputs on dopaminergic neurons in the VTA

To analyze insulin action on the dopaminergic system *in vivo*, long-term euglycemic-hyperinsulinemic clamp studies were performed in C57BL/6 male mice at 11 weeks of age. Fasted animals received continuous intravenous infusion of either somatostatin and glucose alone (control group), or insulin, somatostatin and glucose (treatment group) over a period of six hours (Figure 42 A).

Both groups received glucose infusion adapted to their blood glucose level, and thus remained in the euglycemic range of 100 to 140 mg/dl (Figure 42 B). As expected, serum insulin levels of the insulin-treated group increased steadily over the treatment period, whereas serum insulin levels remained below basal in the control group (Figure 42 C).

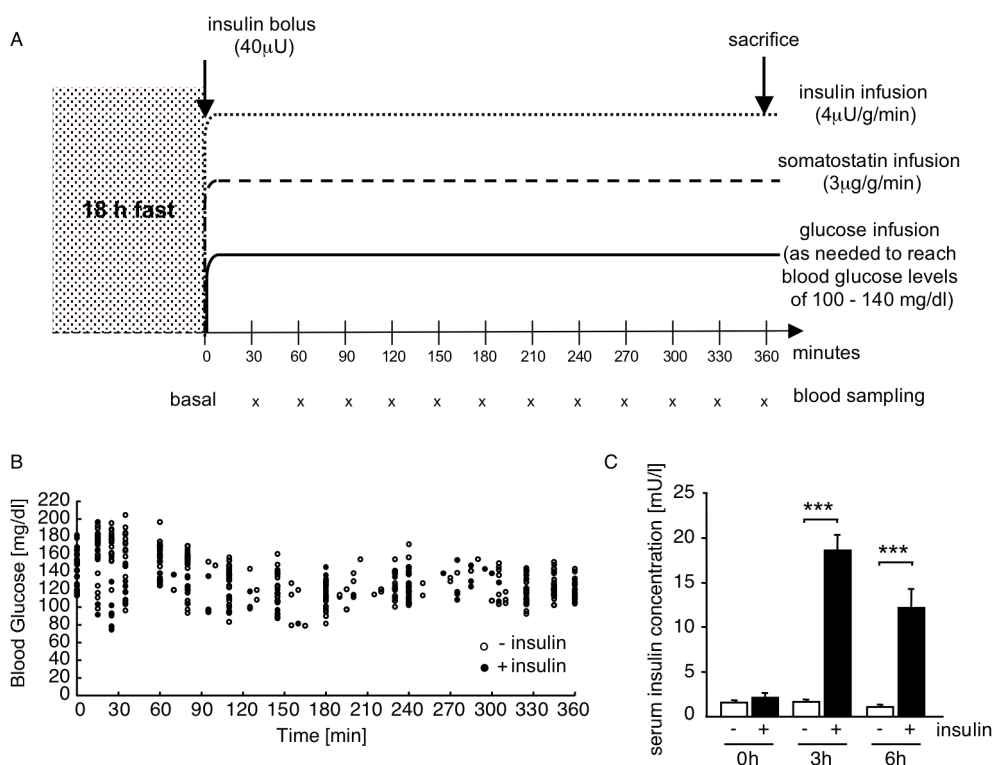


Figure 42: Long-term euglycemic-hyperinsulinemic clamps in C57BL/6 mice.

(A) Experimental design for euglycemic-hyperinsulinemic clamp studies in C57BL/6 mice. Fasted animals received continuous intravenous infusion of either somatostatin and glucose alone (control group), or, insulin, somatostatin and glucose (treatment group) over a period of six hours. At the beginning a blood sample (0h) was collected for determination of basal insulin levels and insulin infusion was started subsequently with a bolus infusion. Blood glucose levels were determined every 20-30 minutes and physiological blood glucose levels (between 100 and 140 mg/dl) were maintained by adjusting a 20% glucose infusion. During and at the end of the clamp additional blood samples were collected for determination of insulin levels (3h, 6h). (B) Blood glucose levels in control (open symbols) and treatment (filled symbols) group during a euglycemic-hyperinsulinemic clamp ($n = 13$ per group). (C) Serum insulin levels in control (open bars) and treatment (filled bars) group before (0h) and during (3h, 6h) a euglycemic-hyperinsulinemic clamp ($n = 13$ per group). Displayed values are means \pm S.E.M.; ***, $p \leq 0.001$.

After 6 hours, the mice were sacrificed and the number and type of synapses on dopaminergic neurons in the VTA were determined by electron microscopy in brains of animals from both groups. This revealed a significant decrease in the number of total synapses on dopaminergic neurons in insulin-treated animals compared to untreated animals, which could be accounted for entirely by a significant decrease in asymmetrical (excitatory) synapses (Figure 43). In contrast, inhibitory inputs (symmetrical synapses) were comparable

between insulin-treated and untreated animals (Figure 43). Thus, prolonged insulin action *in vivo* leads to a decrease of excitatory synapses on dopaminergic cells.

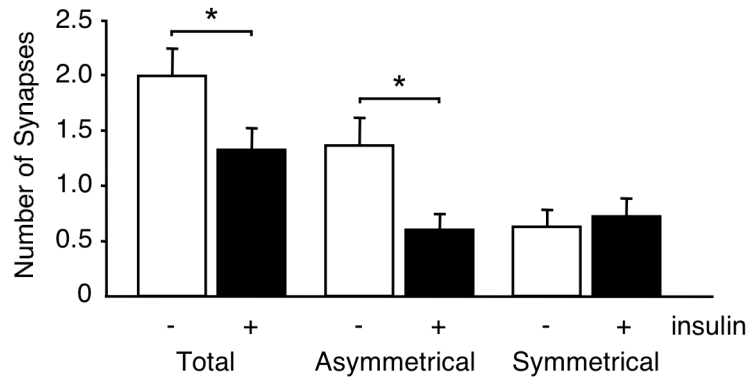


Figure 43: Synaptic input on dopaminergic neurons in C57BL/6 mice after long-term euglycemic-hyperinsulinemic clamp studies.

Quantification of total, stimulatory (asymmetrical) and inhibitory (symmetrical) synapses on dopaminergic neurons in the ventral tegmental area of wild type mice from the control (open bars) and the treatment (filled bars) group (n = 5 per group) after long-term euglycemic-hyperinsulinemic clamp studies. Displayed values are means \pm S.E.M.; *, $p \leq 0.05$.

Taken together, these data demonstrate that prolonged insulin action *in vivo* results in a decrease of excitatory inputs on dopaminergic neurons in the VTA of wildtype mice.

4 Discussion

4.1 Role of central insulin signaling in regulation of energy homeostasis and glucose metabolism

Obesity and insulin-resistant type 2 diabetes mellitus are intimately connected diseases and their incidences are steadily increasing worldwide (2). Therefore, a detailed understanding of how energy homeostasis is regulated, which signaling pathways are involved and how their activity is influenced is a prerequisite for the development of new therapeutical strategies to treat the obesity as well as the diabetes epidemic.

Already in the 1940s and 1950s, classic lesion experiments in the rodent hypothalamus could identify the brain as a critical organ in the regulation of body weight and energy homeostasis. In 1953, Kennedy first proposed that hormonal signals are released into the blood stream in proportion to the body's energy stores and are able to regulate body weight by influencing energy intake and expenditure (141). Moreover, parabiosis studies provided direct evidence that an intact hypothalamus is required for the regulating action of hormonal satiety signals produced in obesity and created the link between circulating satiety signals and their hypothalamic target regions (142).

The finding that insulin, when infused into the brain, decreases food intake and body weight led to the proposal by Woods and Porte that insulin serves as an adiposity signal in the brain, where it provides a signal related to the amount of body fat and causes a long-term, net catabolic response, decreasing food intake and increasing energy expenditure (50-53). Generation of mice in which the insulin receptor was genetically deleted in all CNS neurons and glial cells by Cre-loxP-mediated recombination (NIRKO mice) display diet-sensitive obesity, insulin resistance and impaired fertility, and thus ultimately highlight the role of central insulin action in regulation of fuel metabolism and reproduction (58). Insulin, circulating in the periphery, has access to the brain via a saturable transporter across the blood-brain barrier and insulin receptors are widely expressed in the brain, with the highest concentrations in the olfactory bulb, hypothalamus, cerebral cortex, cerebellum and the hippocampus (54-57, 269).

Besides the brain's ability to integrate peripheral hormonal signals in order to regulate energy intake and energy expenditure, it has long been suggested that the CNS plays an essential role in the control of peripheral blood glucose levels. In 1855, the French physiologist Claude Bernard demonstrated that the liver serves as a reservoir for glucose

(143). He also postulated that the CNS regulates peripheral glucose metabolism based on the observation that lesioning the floor of the fourth ventricle in rabbits results in glucosuria (143). In 2002, Obici *et al.* defined the hypothalamus as one important extrahepatic site of insulin action to regulate hepatic glucose production (47). This finding has led to the concept that besides regulating body weight, food intake and reproductive endocrinology, hypothalamic insulin signaling also controls glucose metabolism in the periphery. Along this line, insulin fails to efficiently suppress hepatic glucose production during euglycemic-hyperinsulinemic clamps in NIRKO mice (48), demonstrating that functional insulin receptor signaling in the CNS is a prerequisite for peripherally applied insulin to suppress hepatic glucose production. Additionally, recent studies demonstrated that hypothalamic insulin signaling is required for blood glucose lowering during insulin treatment of diabetes mellitus in rats (49).

Several studies indicate that the hypothalamic melanocortin system is an important target of the actions of insulin to regulate food intake and body weight (193, 194, 266, 270). Hypothalamic neurons that express the orexigenic neuropeptides NPY and AgRP, as well as those expressing the anorexigenic neuropeptide POMC co-express insulin receptors, and administration of insulin into the third cerebral ventricle of fasted rats increased expression of POMC mRNA and decreased expression of NPY mRNA (193, 266). Moreover, pharmacological studies demonstrating that MC4 receptor antagonists prevent the reduction in food intake caused by third-ventricular insulin administration suggest that the hypothalamic melanocortin system mediates the anorexigenic effects of central insulin (193).

Taken together, recent experiments have defined insulin action in the CNS as a critical determinant of energy homeostasis and of peripheral glucose metabolism in rodents.

4.2 Inactivation of the *insulin receptor* gene specifically in POMC and AgRP neurons

Our understanding about the role of insulin action in the CNS to regulate energy homeostasis and glucose metabolism has significantly improved over the last years. Nevertheless, the identity of the insulin-responsive neurons that mediate these effects remained elusive. Therefore, to precisely define the neuronal populations mediating insulin's central effects on energy and glucose homeostasis, the *insulin receptor* gene was specifically

inactivated in POMC- and AgRP-expressing neurons of mice by Cre-loxP-mediated recombination ($IR^{\Delta POMC}$ and $IR^{\Delta AgRP}$ mice). These mice display unaltered insulin receptor expression in the hypothalamus, in the rest of the brain as well as in peripheral tissues and normal insulin signaling in skeletal muscle and liver, which is consistent with restricted inactivation of the insulin receptor in defined neuronal populations of the hypothalamus. Furthermore, insulin's ability to activate the PI3 kinase pathway was blunted specifically in POMC and AgRP neurons of $IR^{\Delta POMC}$ and $IR^{\Delta AgRP}$ mice, respectively. Taken together, mice with specific inactivation of the insulin receptor in either POMC or AgRP neurons provide an adequate tool to study the role of insulin signaling in these cells *in vivo*.

Previous studies have demonstrated that AgRP neurons play a critical role in the maintenance of energy and glucose homeostasis (173, 174). Although acute ablation of AgRP neurons in adult mice results in hypoglycemia in these experiments, it is not possible to determine the role of AgRP neurons in glucose homeostasis, since these animals also exhibit severe cachexia from complete suppression of food intake. In contrast, POMC or AgRP neuron-restricted inactivation of the insulin receptor does not interfere with the regulation of food intake or energy homeostasis under normal conditions, thus allowing determination of direct effects on other tissues in a physiological setting.

4.2.1 Role of insulin action on POMC and AgRP neurons in the regulation of energy homeostasis

Strikingly, neither POMC- nor AgRP-restricted insulin receptor knockout mice exhibit alterations in energy homeostasis, indicating that insulin receptor signaling in neurons other than, or additional to, POMC or AgRP cells is required for insulin's ability to control energy homeostasis. Earlier studies have put particular emphasis on the regulation of POMC-, NPY- and AgRP-expression by insulin in insulin's ability to regulate food intake (19, 193, 266). Acute central administration of insulin in fasted animals has been shown to result in increased POMC and decreased NPY expression, without affecting AgRP expression (187, 193, 194) and a very recent study demonstrated that insulin directly regulates NPY and AgRP expression through a MAPK-dependent pathway in a hypothalamic cell line (271). Moreover, regulation of FOXO1 activity through the PI3 kinase/Akt signaling pathway has been demonstrated to promote POMC expression while inhibiting AgRP expression (192, 267).

However, expression of the anorexigenic neuropeptide POMC as well as expression of the orexigenic neuropeptides NPY/AgRP is unaltered in $IR^{\Delta POMC}$ mice. While POMC and

NPY expression are comparable to controls in IR^{ΔAgRP} mice, these mice show a slight increase in AgRP mRNA expression. Since AgRP neurons are essential for the maintenance of energy homeostasis (173, 174), these experiments reveal that lack of insulin-stimulated AgRP- and/or NPY-regulation can be physiologically compensated for when signaling by other hormonal or nutritional mediators is intact.

Furthermore, the finding that IR^{ΔPOMC} and IR^{ΔAgRP} mice show a food intake similar to control mice contrasts with the hyperphagia found in NIRKO mice, or in rats in which insulin receptor expression in the ARC and the PVN of the hypothalamus has been downregulated by antisense mRNA (58, 272). This provides direct evidence that hypothalamic neurons other than AgRP or POMC mediate insulin's ability to suppress food intake. This is consistent with the recent suggestion that leptin's effects in the VMH play an important role in controlling food intake (273), indicating that also leptin's anorexigenic effects are not exclusively mediated by neurons located in the ARC. Furthermore, expression of the leptin receptor and its functional signaling in dopaminergic neurons of the VTA provided an interesting link between the hormonal control of food intake and the reward system. Hommel *et al.* could demonstrate that direct administration of leptin to the VTA caused a decreased food intake (205). Similarly, not only leptin receptors but also insulin receptors are expressed in the VMH as well as in dopaminergic neurons of the VTA. Indeed, the present study demonstrates that insulin signaling in the dopaminergic system regulates food intake.

Another potentially contributing factor for the difference between NIRKO, IR^{ΔAgRP} and IR^{ΔPOMC} mice may be that NIRKO mice also suffer from hypogonadism (58). IR^{ΔAgRP} and IR^{ΔPOMC} mice exhibit normal fertility as assessed by litter-to-litter intervals, litter size and morphological assessment of reproductive organs. Thus, in addition to insulin receptor inactivation occurring in other neurons responsible for regulation of food intake, hypogonadism may be a confounding factor for the gender-specific obesity in NIRKO mice.

Taken together, the results of the present study support the idea that neurons other than AgRP or POMC mediate insulin's ability to suppress food intake.

4.2.2 Role of insulin action on POMC and AgRP neurons in the regulation of glucose metabolism

In 2002, Obici *et al.* demonstrated that hypothalamic insulin signaling is required for insulin's ability to suppress hepatic glucose production in euglycemic-hyperinsulinemic clamps of rats (47, 48). In these studies injection of insulin receptor antisense mRNA specifically into the third ventricle of rats, or inactivating insulin receptor expression in the

mediobasal hypothalamus, inhibited insulin's ability to suppress hepatic glucose production (47). Consistent with a role for central insulin action in regulation of hepatic glucose production, NIRKO mice show impaired suppression of hepatic glucose production in euglycemic-hyperinsulinemic clamps (48). Although in these studies inactivation of the insulin receptor co-localized with AgRP and POMC neurons, they left entirely open the question, whether insulin's central effect to regulate hepatic glucose production is mediated by POMC, AgRP, other ARC or PVN neurons.

The ARC has repeatedly been implicated as an important site for regulating peripheral glucose metabolism. Morton *et al.* demonstrated that rats lacking a functional leptin receptor presented with improved peripheral insulin sensitivity and glucose response following reconstituted expression of the leptin receptor or introduction of a constitutively active mutant of Akt in the ARC by adenoviral gene therapy (274). Importantly, this effect was not dependent on food intake and body weight. Gelling *et al.* overexpressed IRS 2 and Akt in the mediobasal hypothalamus of diabetic rats using adenoviral delivery (49). Here, the glycemic response to insulin was enhanced 2-fold, further indicating a role for PI3 kinase signaling in the mediobasal hypothalamus in regulation of peripheral glucose homeostasis. In conclusion, these results narrowed down the mediobasal hypothalamus as a critical region for regulation of peripheral glucose metabolism targeted by both insulin and leptin and controlled by the PI3 kinase signaling pathway. A previous study has addressed the role of NPY in the regulation of hepatic glucose production (275). Although cerebral application of NPY blunts insulin's ability to suppress hepatic glucose production, this type of pharmacological studies does not allow the delineation of whether the two pathways are physiologically interconnected or independently regulate hepatic glucose production.

Therefore, cell type-specific ablation of signaling components in the hypothalamus clearly provides a definitive approach to unravel the functional significance of the recently recognized action of the hypothalamus to control glucose metabolism independent of body weight. The unique feasibility of this approach has also been revealed by the new insights gained from cell type-specific ablation or restoration of leptin and melanocortin signaling (164, 273).

In the present study, insulin failed to normally suppress hepatic glucose production during euglycemic-hyperinsulinemic clamps in mice with an insulin receptor knockout specifically in AgRP neurons. The finding that AgRP neurons mediate insulin's central effect on hepatic glucose production is consistent both anatomically and mechanistically with the above-described investigations by Obici and colleagues. Moreover, Obici *et al.* showed that

insulin's ability to suppress hepatic glucose production depends on insulin-stimulated activation of the PI3 kinase pathway and can be inhibited by K_{ATP} channel blockers (47, 264). The finding of the present study that insulin stimulates POMC neuron hyperpolarization by direct interaction with insulin receptors on POMC neurons is consistent with these studies and previous reports that insulin inhibits electrical activity of POMC neurons by PIP3-dependent opening of K_{ATP} channels (202).

The present study also directly shows that insulin treatment leads to membrane hyperpolarization and a decrease in action potential frequency in identified hypothalamic AgRP neurons and that this effect involves the activation of K_{ATP} channels. Consistent with the fact that insulin activates PI3 kinase in AgRP cells (276), and that these cells express K_{ATP} channels (263), these findings directly demonstrate that the mechanism by which insulin acts in POMC cells also holds true for AgRP neurons. In 2005, Pocai *et al.* demonstrated that insulin acts on K_{ATP} channels in hypothalamic neurons to control hepatic glucose production by decreasing glucose-6-phosphatase and phosphoenolpyruvate kinase expression in the liver (264). Transection of the vagal nerve to the liver blunted this effect, indicating a role for the autonomous nervous system in transmitting insulin's central actions to the periphery. However, a recent study demonstrated that the effects of centrally applied NPY on hepatic glucose production are mediated via activation of sympathetic output to the liver (277). Thus, the exact downstream mechanism responsible for the effects of insulin action in the brain on hepatic glucose production remains to be established.

Taken together, the results of the present study propose a new model that insulin activates PI3 kinase in AgRP cells, and that subsequent PIP3 formation results in K_{ATP} channel activation and electrical silencing of these cells. This may lead to a reduced release of the inverse melanocortin receptor agonist AgRP, NPY and/or other transmitters from AgRP neurons and thereby regulates innervation of the liver, which finally leads to suppression of hepatic glucose production (Figure 44).

Recent findings implicate the cytokine IL-6 as insulin's effector in the liver; it has been shown that insulin, acting through unidentified neurons in the CNS, regulates IL-6 secretion from as-of-now uncharacterized cells in the liver (48). Furthermore, these studies demonstrated that hepatic IL-6 in turn activates STAT3 in liver parenchymal cells and inhibits glucose production, and insulin's inhibiting effect on glucose production is blunted in animals lacking STAT3 in the liver (48). The findings that both insulin-induced IL-6 mRNA expression and suppression of glucose-6-phosphatase expression are blunted in mice lacking the insulin receptor specifically in AgRP neurons provide direct evidence in support of the

idea by Inoue *et al.* that insulin, acting through the CNS, regulates hepatic IL-6 expression to control gluconeogenesis via STAT3 activation in liver parenchymal cells and clearly indicates that insulin action on AgRP neurons is responsible for regulating this signaling cascade (Figure 44).

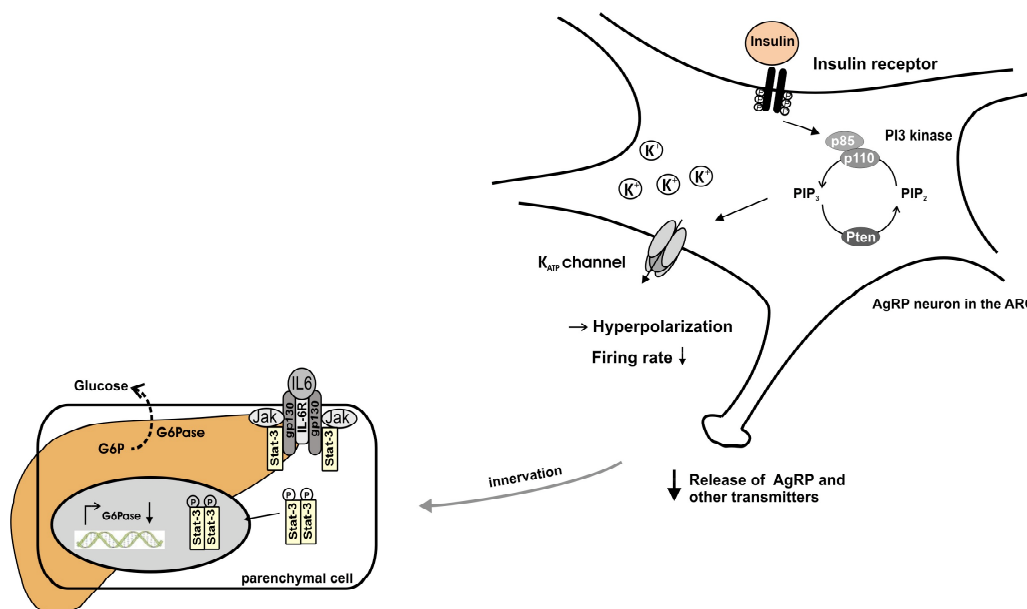


Figure 44: Model of hepatic-regulation via insulin action on AgRP neurons.

Cell autonomous action of insulin on AgRP neurons results in activation of the PI3 kinase (p85, regulatory subunit; p110, catalytic subunit) and generation of PIP₃. PIP₃ activates K_{ATP} channels, resulting in hyperpolarization and a decreased neuronal firing rate with subsequent reduced release of AgRP and/or other transmitters of AgRP neurons. This regulates innervation of the liver, leading to increased IL-6 expression. IL-6 acting on liver parenchymal cells results in STAT3 phosphorylation via activation of JAK2, thereby leading to decreased expression of glucose-6-phosphatase (G6Pase). Abbreviations: G6P, glucose-6-phosphate; gp130, glycoprotein 130; IL-6R, interleukin-6 receptor alpha; JAK2, janus kinase 2; PIP₂, phosphatidylinositol (4,5) bisphosphate; Pten, phosphatase and tensin homolog.

Although IR^{ΔAgRP} mice do not display differences in glucose levels, both fasting glucose and glucose during tolerance testing represent an integration of production and utilization. Nevertheless, the present study clearly demonstrates that insulin action in AgRP neurons is essential for insulin-induced suppression of hepatic glucose production.

Determination of tissue-specific glucose uptake rates showed similar rates of insulin-stimulated glucose uptake in brain and skeletal muscle in IR^{ΔAgRP} mice compared to controls. However, insulin-stimulated glucose uptake in white adipose tissue of IR^{ΔAgRP} mice (but not IR^{ΔPOMC} mice) was significantly increased compared to control mice. A similar increase in adipose glucose uptake has been observed in mice with selective inactivation of the insulin receptor in skeletal muscle (278). A recent study by Koch *et al.* indicated a role for central

insulin action in the neuronal control of lipogenesis in addition to the well-documented adipocyte-autonomous inhibition of lipolysis (279). Whether the increase in adipose glucose uptake in IR^{ΔAgRP} mice represents some form of compensatory response or tissue cross talk remains to be determined.

However, the relative importance of hypothalamic insulin signaling for the overall control of hepatic glucose production has lately been matter of debate, since studies in dogs demonstrated that a 4-fold rise in cranial insulin levels does not change acute hepatic glucose output (280). Thus, differences between rodents and dogs as well as humans in acute and chronic regulation of glucose homeostasis need to be carefully addressed in future studies.

4.3 Inactivation of the *insulin receptor* gene specifically in dopaminergic cells

In the last years substantial evidence has emerged, that peripheral hormonal signals such as insulin and leptin are able to modulate the reward system of the brain. Both insulin and leptin receptors are co-expressed with tyrosine hydroxylase – a marker for dopamine neurons – in the ventral tegmental area (VTA) and substantia nigra (SN) (204). Furthermore, studies demonstrated that insulin and leptin administration into the VTA results in an increased formation of PIP3, the product of the PI3 kinase, which serves as an indicator for a functional signaling pathway (249). Hommel *et al.* investigated the functional relevance of leptin receptor expression in the VTA; they could demonstrate that VTA dopamine neurons respond to leptin with activation of the intracellular JAK/STAT pathway and a reduction in firing rate (205). Direct administration of leptin to the VTA resulted in a decreased food intake, while long-term RNAi-mediated knockdown of the leptin receptor in the VTA led to increased food intake, locomotor activity, and sensitivity to high-palatable food (205). Thus, these findings support a critical role for VTA leptin receptors in regulating feeding behavior and thereby provide functional evidence for direct action of a peripheral metabolic signal on VTA dopamine neurons.

Intraventricular insulin administration prevents the expression of a place preference for high-fat food, decreases lick rates for sucrose solutions in a lickometer task, and decreases sucrose self-administration in rats that are not food deprived. Taken together, these findings support the hypothesis that insulin can blunt brain reward activity, including the rewarding attributes of food (247, 248, 281). However, the exact role of insulin signaling in dopaminergic cells has not been determined so far.

Therefore, to investigate the role of insulin signaling in dopaminergic cells in control of energy and glucose homeostasis, the *insulin receptor* gene was specifically inactivated in tyrosine hydroxylase (Th)-expressing cells by Cre-loxP-mediated recombination (IR^{ΔTh} mice). Th is the rate-limiting enzyme in dopamine synthesis and thus is a well-established marker of dopaminergic neurons. Consistent with previous studies (249), peripheral insulin administration resulted in robust PIP3 formation in identified Th-expressing cells in the VTA of control mice, supporting the notion that the insulin signaling pathway is functional and active in these cells. Importantly, insulin's ability to activate the PI3 kinase pathway was blunted specifically in identified Th-expressing cells in the VTA of IR^{ΔTh} mice, indicating a successful inactivation of the insulin receptor in these cells. Taken together, mice with specific inactivation of the insulin receptor in Th-expressing cells provide an adequate tool to study the role of insulin signaling in dopaminergic cells *in vivo*.

However, tyrosine hydroxylase is not only expressed in dopaminergic neurons of brain regions implicated in addiction and reward. Tyrosine hydroxylase is the first, rate-limiting enzyme in catecholamine synthesis and neurons of both the peripheral and central nervous system use catecholamines as neurotransmitters. In the periphery, the majority of sympathetic neurons are catecholaminergic; in the CNS the most abundant group of catecholaminergic cells are dopaminergic neurons of the mesencephalon (VTA and SN) (282). Additional groups of dopaminergic neurons reside in the medial zone incerta of the hypothalamus and the largest collection of norepinephrine-producing neurons is located in the locus coeruleus (282). Thus, Th-expression occurs not only in the VTA and the SN, but also in the sympathetic ganglia, adrenal medulla and the locus coeruleus. Therefore, additional studies are necessary to allow the delineation of insulin's effects in the VTA and SN and possible effects of insulin in other Th-expressing cells. Nevertheless, the present study demonstrates direct effects of insulin on the dopaminergic system in the VTA, thus indeed indicating a role for insulin in this system.

4.3.1 Role of insulin action on dopaminergic cells in the regulation of energy and glucose homeostasis

IR^{ΔTh} mice display increased body weight under normal diet conditions, which is accompanied by increased adiposity and leptin levels. This indicates a critical role for insulin action on Th-expressing cells in regulation of energy homeostasis. The increase in body adiposity in these mice is not a consequence of decreased energy expenditure or a decrease in locomotor activity but occurs as a consequence of increased food intake, which could be

demonstrated both at 6 weeks and 13 weeks of age. A study by Figlewicz *et al.* could show that direct acute injection of insulin into the VTA blocks VTA-initiated feeding of sucrose pellets by administration of a μ -opioid agonist, supporting a role for insulin in control of feeding via its action in the dopaminergic system (249). However, VTA insulin injection alone did not change baseline sucrose pellet intake in this study, indicating that insulin's effect on food reward may only be relevant when there is adequate stimulation or drive within the VTA (249). Nevertheless, the finding that $IR^{\Delta Th}$ mice display an increased food intake clearly demonstrates that insulin signaling in this system is important for the control of feeding behavior and thus reveals a novel role for insulin action in dopaminergic cells with respect to energy homeostasis. Further studies are necessary to investigate how these animals perform in behavioral paradigms with food as a reward.

On the other hand, glucose metabolism is unaltered in mice with an insulin receptor knockout in Th-expressing cells under normal diet conditions. $IR^{\Delta Th}$ mice exhibit unaltered fasted blood glucose levels, glucose tolerance and insulin sensitivity at 10 and 11 weeks of age. While serum insulin levels are similar to controls at an age of 9 weeks, $IR^{\Delta Th}$ mice display increased serum insulin levels at an age of 20 weeks, which is consistent with increased adiposity in these animals. Therefore, additional studies in terms of glucose homeostasis are necessary in $IR^{\Delta Th}$ mice at approximately 20 weeks of age; this may reveal alterations in glucose tolerance and insulin sensitivity in these mice as a consequence of chronically elevated adiposity.

4.3.2 Role of insulin action on dopaminergic cells in the regulation of gene expression and synaptic plasticity

Figlewicz and colleagues suggested an additional potential target for insulin action on dopaminergic neurons: the dopamine transporter (DAT), which provides the primary mechanism through which extracellular dopamine is cleared from the synapses, thereby regulating the magnitude and duration of dopaminergic signaling (214). Insulin signaling through the PI3 kinase- and Akt-pathway promotes cell-surface expression of the DAT *in vitro* (283). Chronic intracerebroventricular insulin treatment resulted in an increased DAT mRNA expression in the VTA/SN and, consistent with this, food deprivation decreased expression and activity of DAT (284, 285).

In the present study, expression analysis of different genes critically involved in dopamine signaling in brain regions related to the mesolimbic and nigrostriatal dopamine

system revealed that mRNA levels of Th and dopamine receptor 2 (D2R) are increased in the VTA of IR^{ΔTh} mice, while expression levels of DAT remained unchanged. Thus, the effect of chronic intracerebroventricular insulin treatment on DAT expression in the VTA either involves other neurons and/or synaptic transmission or the lack of insulin-stimulated DAT regulation can be physiologically compensated for when signaling by other hormonal or nutritional mediators is intact.

A recent study demonstrated that food restriction increases mRNA levels of Th, DAT and dopa decarboxylase in the VTA of rats, and DAT protein expression was also upregulated in the NAc (286). The authors suggested that chronic food restriction, in which insulin and leptin levels are low, results in a sensitization of the mesolimbic dopamine pathway characterized by increased clearance of extracellular dopamine in the NAc. Furthermore they indicate that adipostatic hormones such as insulin and leptin are potential factors mediating these effects, directly or indirectly. D2Rs are localized both on neurons targeted by dopaminergic afferences but also on presynaptic dopaminergic neurons. Here, D2 presynaptic receptors are involved in regulation of dopamine synthesis and release (287-290). Thus, increased Th and D2R mRNA expression in the VTA of IR^{ΔTh} mice points to a sensitization of the mesolimbic dopamine pathways, however, this hypothesis awaits further experimental proof in future studies.

In the present study, longterm euglycemic-hyperinsulinemic clamps in wild type mice demonstrated that prolonged insulin action *in vivo* results in a decrease of excitatory inputs on dopaminergic neurons in the VTA. The ratio of excitatory to inhibitory synaptic input on a neuron determines not only direct cell-autonomous regulation of cell electrical activity but also the set point of cell excitability (291). However, in the present study it is not clear whether the observed effects result from insulin action on postsynaptic (dopaminergic) neurons, on the presynaptic projecting neurons, or on both. Nevertheless, these results indicate that insulin exerts direct, inhibitory effects on the dopaminergic system of the brain.

4.4 Perspectives

Inactivation of the *insulin receptor* gene in AgRP-expressing neurons revealed a role for insulin action in these cells in regulation of hepatic glucose production. Further studies will be needed to identify and analyze further potential factors and neuronal circuits involved in neuronal transmission that finally results in hepatic innervation to regulate glucose production. Nevertheless, modulation of AgRP neuron-mediated regulation of hepatic glucose

production could provide an approach to support therapeutic control of insulin resistance in type 2 diabetes mellitus.

Moreover, inactivation of the *insulin receptor* gene in Th-expressing cells defined a new role for insulin signaling in these cells in control of food intake and body weight. However, further studies are necessary to assess the functional role of insulin action in the dopaminergic system and to what extent multisynaptic transmission is involved. Expanding our knowledge of how insulin regulates energy homeostasis and how its action is integrated in multiple brain circuits is pivotal for a better understanding of the pathomechanisms responsible for the growing obesity epidemic.

5 Summary

The finding that peripheral hormones, such as insulin and leptin directly can communicate to the hypothalamus to control energy homeostasis and glucose metabolism has set the ground for detailed understanding of the neuronal circuitry underlying the control of body weight homeostasis. Recent studies have implicated that insulin-stimulated activation of phosphatidylinositol 3 kinase signaling and the regulation of ATP-dependent potassium (K_{ATP}) channels in the hypothalamus is involved in the control of peripheral glucose metabolism. However, these experiments leave open the question of which specific neurons in these areas of the brain are responsible for mediating insulin's effect.

Here, mouse models with specific inactivation of the insulin receptor in either anorexigenic proopiomelanocortin (POMC)- or orexigenic agouti-related peptide (AgRP)-expressing neurons of the arcuate nucleus of the hypothalamus are described. While neither POMC- nor AgRP-restricted insulin receptor knockout mice exhibited altered energy homeostasis, insulin failed to normally suppress hepatic glucose production during euglycemic-hyperinsulinemic clamps in mice with an insulin receptor knockout specifically in AgRP neurons. These mice exhibited reduced insulin-stimulated hepatic interleukin-6 expression and increased hepatic expression of glucose-6-phosphatase. Additionally, insulin treatment resulted in membrane hyperpolarization and a decrease in action-potential frequency in identified hypothalamic AgRP neurons and this effect involved the activation of K_{ATP} channels, indicating that the same mechanism by which insulin acts in POMC cells also holds true for AgRP neurons.

Taken together, these results directly demonstrate that insulin action in POMC and AgRP cells is not required for steady state regulation of food intake and body weight. However, insulin action specifically in AgRP-expressing neurons does play a critical role in controlling hepatic glucose production, raising the possibility that dysregulation of the insulin-AgRP pathway may contribute to the development of type 2 diabetes mellitus.

Furthermore, there is much evidence that this basic homeostatic type of regulation of energy homeostasis by the hypothalamus relies on a complex intra-hypothalamic neuronal circuitry but also can be overruled by higher brain functions influenced by the addictive value of palatable food as well as its visual and gustatory aspects. Here, analysis of mice with specific inactivation of the insulin receptor in dopaminergic cells revealed an important new role for insulin signaling in these cells in regulation of food intake and energy homeostasis.

6 Zusammenfassung

Die Erkenntnis, dass periphere Signalmoleküle, wie Insulin und Leptin, dem Gehirn den Energiestatus des Körpers übermitteln können und somit die Energiehomöostase und den Glukosestoffwechsel beeinflussen, legte den Grundstein für ein detaillierteres Verständnis der an dieser Übermittlung beteiligten Neuronenpopulationen. Untersuchungen der letzten Jahre konnten zeigen, dass die Insulin-vermittelte Aktivierung der Phosphatidyl-Inositol 3 Kinase und die Stimulation ATP-sensitiver Kaliumkanäle (K_{ATP} Kanäle) im Hypothalamus an der Regulation des peripheren Glukosestoffwechsels beteiligt sind. Jedoch konnten diese Studien nicht die genaue Identität der beteiligten Neuronenpopulationen klären. Hier werden zwei Mausmodelle mit einer spezifischen Inaktivierung des Insulinrezeptors in anorexigenen Proopiomelanocortin (POMC)- und in orexigenen Agouti-Related Peptide (AgRP)-exprimierenden Neuronen beschrieben. Während weder Mäuse mit einer Inaktivierung des Insulinrezeptors in POMC- oder AgRP-Neuronen Veränderungen in der Energiehomöostase aufwiesen, war eine normale Supprimierung der hepatischen Glukoseproduktion während einer Euglykämischen-Hyperinsulinämischen Clamp-Untersuchung in Mäusen mit einer Insulinrezeptor-Inaktivierung in AgRP-Neuronen nicht mehr möglich. Weiterhin zeigte sich bei diesen Tieren eine reduzierte Insulin-stimulierte Expression von Interleukin-6 und eine erhöhte Expression des Enzyms Glukose-6-Phosphatase in der Leber. Zusätzlich wird hier gezeigt, dass Insulin zu einer Hyperpolarisierung und einer reduzierten Feuerrate in identifizierten AgRP-Neuronen führt; vermittelt durch die Aktivierung von K_{ATP} Kanälen. Somit konnten Ergebnisse aus elektrophysiologischen Studien mit POMC-Zellen auch für AgRP-Neurone bestätigt werden. Zusammenfassend zeigen diese Ergebnisse, dass die Insulinwirkung in POMC- und AgRP-Zellen nicht für eine normale Regulation von Nahrungsaufnahme und Körpergewicht von Bedeutung ist. Jedoch ist die Insulinwirkung in AgRP-Zellen von entscheidender Bedeutung in der Regulation der hepatischen Glukoseproduktion. Störungen des Insulinsignalwegs in AgRP-Neuronen könnten daher an der Entstehung des Diabetes Mellitus Typ 2 beteiligt sein.

Weiterhin gibt es vermehrt Hinweise darauf, dass die Regulation der Energiehomöostase über Neurone im Hypothalamus durch höhere Hirnfunktionen und die suchterzeugende Wirkung von wohlschmeckender Nahrung beeinflusst werden kann. Hier zeigte die Analyse von Mäusen mit einer Inaktivierung des Insulinrezeptors in dopaminergen Zellen, dass dem Insulinsignalweg in diesen Zellen eine wesentliche Bedeutung in der Regulation der Nahrungsaufnahme und Energiehomöostase zukommt.

7 References

1. Dixon, J.B. 2009. The effect of obesity on health outcomes. *Mol Cell Endocrinol*.
2. Mokdad, A.H., Ford, E.S., Bowman, B.A., Dietz, W.H., Vinicor, F., Bales, V.S., and Marks, J.S. 2003. Prevalence of obesity, diabetes, and obesity-related health risk factors, 2001. *Jama* 289:76-79.
3. WHO. 2006. Obesity and overweight. Fact sheet N° 311.
4. Mei, Z., Grummer-Strawn, L.M., Pietrobelli, A., Goulding, A., Goran, M.I., and Dietz, W.H. 2002. Validity of body mass index compared with other body-composition screening indexes for the assessment of body fatness in children and adolescents. *Am J Clin Nutr* 75:978-985.
5. Allison, D.B., Fontaine, K.R., Manson, J.E., Stevens, J., and VanItallie, T.B. 1999. Annual deaths attributable to obesity in the United States. *Jama* 282:1530-1538.
6. Colditz, G.A., Willett, W.C., Rotnitzky, A., and Manson, J.E. 1995. Weight gain as a risk factor for clinical diabetes mellitus in women. *Ann Intern Med* 122:481-486.
7. Chan, J.M., Rimm, E.B., Colditz, G.A., Stampfer, M.J., and Willett, W.C. 1994. Obesity, fat distribution, and weight gain as risk factors for clinical diabetes in men. *Diabetes Care* 17:961-969.
8. WHO. 2006. Definition and diagnosis of diabetes mellitus and intermediate hyperglycemia. *report of a WHO/IDF consultation*.
9. Wild, S., Roglic, G., Green, A., Sicree, R., and King, H. 2004. Global prevalence of diabetes: estimates for the year 2000 and projections for 2030. *Diabetes Care* 27:1047-1053.
10. Lillioja, S., Mott, D.M., Spraul, M., Ferraro, R., Foley, J.E., Ravussin, E., Knowler, W.C., Bennett, P.H., and Bogardus, C. 1993. Insulin resistance and insulin secretory dysfunction as precursors of non-insulin-dependent diabetes mellitus. Prospective studies of Pima Indians. *N Engl J Med* 329:1988-1992.
11. Martin, B.C., Warram, J.H., Krolewski, A.S., Bergman, R.N., Soeldner, J.S., and Kahn, C.R. 1992. Role of glucose and insulin resistance in development of type 2 diabetes mellitus: results of a 25-year follow-up study. *Lancet* 340:925-929.
12. Bonadonna, R.C., Groop, L., Kraemer, N., Ferrannini, E., Del Prato, S., and DeFronzo, R.A. 1990. Obesity and insulin resistance in humans: a dose-response study. *Metabolism* 39:452-459.
13. Rexrode, K.M., Manson, J.E., and Hennekens, C.H. 1996. Obesity and cardiovascular disease. *Curr Opin Cardiol* 11:490-495.
14. Frayling, T.M., Timpson, N.J., Weedon, M.N., Zeggini, E., Freathy, R.M., Lindgren, C.M., Perry, J.R., Elliott, K.S., Lango, H., Rayner, N.W., et al. 2007. A common variant in the FTO gene is associated with body mass index and predisposes to childhood and adult obesity. *Science* 316:889-894.
15. Barsh, G.S., Farooqi, I.S., and O'Rahilly, S. 2000. Genetics of body-weight regulation. *Nature* 404:644-651.
16. Hill, J.O., and Peters, J.C. 1998. Environmental contributions to the obesity epidemic. *Science* 280:1371-1374.
17. Schwartz, M.W. 2006. Central nervous system regulation of food intake. *Obesity (Silver Spring)* 14 Suppl 1:1S-8S.
18. Woods, S.C., Seeley, R.J., Porte, D., Jr., and Schwartz, M.W. 1998. Signals that regulate food intake and energy homeostasis. *Science* 280:1378-1383.
19. Schwartz, M.W., and Porte, D., Jr. 2005. Diabetes, obesity, and the brain. *Science* 307:375-379.

20. Spiegelman, B.M., and Flier, J.S. 2001. Obesity and the regulation of energy balance. *Cell* 104:531-543.
21. Schwartz, M.W., Woods, S.C., Porte, D., Jr., Seeley, R.J., and Baskin, D.G. 2000. Central nervous system control of food intake. *Nature* 404:661-671.
22. Von Mering, J., and Minkowski, O. 1890. Diabetes mellitus nach Pankreasextirpation. *Arch Exp Pathol Pharmacol* 26:371-387.
23. Benedum, J. 1999. The early history of endocrine cell transplantation. *J Mol Med* 77:30-35.
24. Banting, F.G., Best, C.H., Collip, J.B., Campbell, W.R., and Fletcher, A.A. 1922. Pancreatic extracts in the treatment of diabetes mellitus. Preliminary report. *CMAJ* 22:141-146.
25. Bliss, M. 1982. Banting's, Best's, and Collip's accounts of the discovery of insulin. *Bull Hist Med* 56:554-568.
26. Steiner, D.F., Cunningham, D., Spigelman, L., and Aten, B. 1967. Insulin biosynthesis: evidence for a precursor. *Science* 157:697-700.
27. Davidson, H.W., Rhodes, C.J., and Hutton, J.C. 1988. Intraorganellar calcium and pH control proinsulin cleavage in the pancreatic beta cell via two distinct site-specific endopeptidases. *Nature* 333:93-96.
28. Docherty, K., and Hutton, J.C. 1983. Carboxypeptidase activity in the insulin secretory granule. *FEBS Lett* 162:137-141.
29. Steiner, D.F. 1969. Proinsulin and the biosynthesis of insulin. *N Engl J Med* 280:1106-1113.
30. Duckworth, W.C., Bennett, R.G., and Hamel, F.G. 1998. Insulin degradation: progress and potential. *Endocr Rev* 19:608-624.
31. Kahn, C.R. 1994. Banting Lecture. Insulin action, diabetogenes, and the cause of type II diabetes. *Diabetes* 43:1066-1084.
32. White, M.F. 2003. Insulin signaling in health and disease. *Science* 302:1710-1711.
33. Nauck, M.A. 2009. Unraveling the science of incretin biology. *Eur J Intern Med* 20 Suppl 2:S303-308.
34. Mueller, M.K., Demol, P., Goebell, H., Fladrich, G., and Brown, J.C. 1983. Natural purified porcine gastric inhibitory polypeptide (GIP) stimulates exocrine pancreas secretion due to contamination with a cholecystokinin-like substance. *Regul Pept* 5:307-315.
35. Conaway, H.H., Griffey, M.A., and Whitney, J.E. 1975. Characterization of acetylcholine-induced insulin secretion in the isolated perfused dog pancreas. *Proc Soc Exp Biol Med* 150:308-312.
36. Bagdade, J.D., Bierman, E.L., and Porte, D., Jr. 1967. The significance of basal insulin levels in the evaluation of the insulin response to glucose in diabetic and nondiabetic subjects. *J Clin Invest* 46:1549-1557.
37. Polonsky, K.S., Given, B.D., Hirsch, L., Shapiro, E.T., Tillil, H., Beebe, C., Galloway, J.A., Frank, B.H., Karrison, T., and Van Cauter, E. 1988. Quantitative study of insulin secretion and clearance in normal and obese subjects. *J Clin Invest* 81:435-441.
38. Polonsky, K.S., Given, B.D., and Van Cauter, E. 1988. Twenty-four-hour profiles and pulsatile patterns of insulin secretion in normal and obese subjects. *J Clin Invest* 81:442-448.
39. Birnbaum, M.J. 1992. The insulin-sensitive glucose transporter. *Int Rev Cytol* 137:239-297.
40. Cushman, S.W., Wardzala, L.J., Simpson, I.A., Karnieli, E., Hissin, P.J., Wheeler, T.J., Hinkle, P.C., and Salans, L.B. 1984. Insulin-induced translocation of intracellular glucose transporters in the isolated rat adipose cell. *Fed Proc* 43:2251-2255.

41. Cushman, S.W., and Wardzala, L.J. 1980. Potential mechanism of insulin action on glucose transport in the isolated rat adipose cell. Apparent translocation of intracellular transport systems to the plasma membrane. *J Biol Chem* 255:4758-4762.
42. Pilkis, S.J., and Granner, D.K. 1992. Molecular physiology of the regulation of hepatic gluconeogenesis and glycolysis. *Annu Rev Physiol* 54:885-909.
43. Prager, R., Wallace, P., and Olefsky, J.M. 1987. Direct and indirect effects of insulin to inhibit hepatic glucose output in obese subjects. *Diabetes* 36:607-611.
44. Ader, M., and Bergman, R.N. 1990. Peripheral effects of insulin dominate suppression of fasting hepatic glucose production. *Am J Physiol* 258:E1020-1032.
45. Sindelar, D.K., Chu, C.A., Neal, D.W., and Cherrington, A.D. 1997. Interaction of equal increments in arterial and portal vein insulin on hepatic glucose production in the dog. *Am J Physiol* 273:E972-980.
46. Sindelar, D.K., Balcom, J.H., Chu, C.A., Neal, D.W., and Cherrington, A.D. 1996. A comparison of the effects of selective increases in peripheral or portal insulin on hepatic glucose production in the conscious dog. *Diabetes* 45:1594-1604.
47. Obici, S., Zhang, B.B., Karkanias, G., and Rossetti, L. 2002. Hypothalamic insulin signaling is required for inhibition of glucose production. *Nat Med* 8:1376-1382.
48. Inoue, H., Ogawa, W., Asakawa, A., Okamoto, Y., Nishizawa, A., Matsumoto, M., Teshigawara, K., Matsuki, Y., Watanabe, E., Hiramatsu, R., et al. 2006. Role of hepatic STAT3 in brain-insulin action on hepatic glucose production. *Cell Metab* 3:267-275.
49. Gelling, R.W., Morton, G.J., Morrison, C.D., Niswender, K.D., Myers, M.G., Jr., Rhodes, C.J., and Schwartz, M.W. 2006. Insulin action in the brain contributes to glucose lowering during insulin treatment of diabetes. *Cell Metab* 3:67-73.
50. Woods, S.C., Lotter, E.C., McKay, L.D., and Porte, D., Jr. 1979. Chronic intracerebroventricular infusion of insulin reduces food intake and body weight of baboons. *Nature* 282:503-505.
51. Hallschmid, M., Benedict, C., Schultes, B., Fehm, H.L., Born, J., and Kern, W. 2004. Intranasal insulin reduces body fat in men but not in women. *Diabetes* 53:3024-3029.
52. McGowan, M.K., Andrews, K.M., Fenner, D., and Grossman, S.P. 1993. Chronic intrahypothalamic insulin infusion in the rat: behavioral specificity. *Physiol Behav* 54:1031-1034.
53. Porte, D., Jr., and Woods, S.C. 1981. Regulation of food intake and body weight in insulin. *Diabetologia* 20 Suppl:274-280.
54. Margolis, R.U., and Altszuler, N. 1967. Insulin in the cerebrospinal fluid. *Nature* 215:1375-1376.
55. Woods, S.C., and Porte, D., Jr. 1977. Relationship between plasma and cerebrospinal fluid insulin levels of dogs. *Am J Physiol* 233:E331-334.
56. Havrankova, J., Roth, J., and Brownstein, M. 1978. Insulin receptors are widely distributed in the central nervous system of the rat. *Nature* 272:827-829.
57. van Houten, M., Posner, B.I., Kopriwa, B.M., and Brawer, J.R. 1979. Insulin-binding sites in the rat brain: in vivo localization to the circumventricular organs by quantitative radioautography. *Endocrinology* 105:666-673.
58. Bruning, J.C., Gautam, D., Burks, D.J., Gillette, J., Schubert, M., Orban, P.C., Klein, R., Krone, W., Muller-Wieland, D., and Kahn, C.R. 2000. Role of brain insulin receptor in control of body weight and reproduction. *Science* 289:2122-2125.
59. Braciale, V.L., Gavin, J.R., 3rd, and Braciale, T.J. 1982. Inducible expression of insulin receptors on T lymphocyte clones. *J Exp Med* 156:664-669.
60. Harbeck, M.C., Louie, D.C., Howland, J., Wolf, B.A., and Rothenberg, P.L. 1996. Expression of insulin receptor mRNA and insulin receptor substrate 1 in pancreatic islet beta-cells. *Diabetes* 45:711-717.

61. Kurokawa, K., Silverblatt, F.J., Klein, K.L., Wang, M.S., and Lerner, R.L. 1979. Binding of ¹²⁵I-insulin to the isolated glomeruli of rat kidney. *J Clin Invest* 64:1357-1364.
62. Marks, J.L., Porte, D., Jr., Stahl, W.L., and Baskin, D.G. 1990. Localization of insulin receptor mRNA in rat brain by in situ hybridization. *Endocrinology* 127:3234-3236.
63. Seino, S., Seino, M., and Bell, G.I. 1990. Human insulin-receptor gene. *Diabetes* 39:129-133.
64. Seino, S., and Bell, G.I. 1989. Alternative splicing of human insulin receptor messenger RNA. *Biochem Biophys Res Commun* 159:312-316.
65. Kasuga, M., Hedo, J.A., Yamada, K.M., and Kahn, C.R. 1982. The structure of insulin receptor and its subunits. Evidence for multiple nonreduced forms and a 210,000 possible proreceptor. *J Biol Chem* 257:10392-10399.
66. Mosthaf, L., Grako, K., Dull, T.J., Coussens, L., Ullrich, A., and McClain, D.A. 1990. Functionally distinct insulin receptors generated by tissue-specific alternative splicing. *Embo J* 9:2409-2413.
67. McClain, D.A. 1991. Different ligand affinities of the two human insulin receptor splice variants are reflected in parallel changes in sensitivity for insulin action. *Mol Endocrinol* 5:734-739.
68. Vogt, B., Carrascosa, J.M., Ermel, B., Ullrich, A., and Haring, H.U. 1991. The two isotypes of the human insulin receptor (HIR-A and HIR-B) follow different internalization kinetics. *Biochem Biophys Res Commun* 177:1013-1018.
69. Yamaguchi, Y., Flier, J.S., Benecke, H., Ransil, B.J., and Moller, D.E. 1993. Ligand-binding properties of the two isoforms of the human insulin receptor. *Endocrinology* 132:1132-1138.
70. Kellerer, M., Lammers, R., Ermel, B., Tippmer, S., Vogt, B., Obermaier-Kusser, B., Ullrich, A., and Haring, H.U. 1992. Distinct alpha-subunit structures of human insulin receptor A and B variants determine differences in tyrosine kinase activities. *Biochemistry* 31:4588-4596.
71. Leibiger, B., Leibiger, I.B., Moede, T., Kemper, S., Kulkarni, R.N., Kahn, C.R., de Vargas, L.M., and Berggren, P.O. 2001. Selective insulin signaling through A and B insulin receptors regulates transcription of insulin and glucokinase genes in pancreatic beta cells. *Mol Cell* 7:559-570.
72. Moller, D.E., Yokota, A., Caro, J.F., and Flier, J.S. 1989. Tissue-specific expression of two alternatively spliced insulin receptor mRNAs in man. *Mol Endocrinol* 3:1263-1269.
73. Ebina, Y., Ellis, L., Jarnagin, K., Edery, M., Graf, L., Clauser, E., Ou, J.H., Masiarz, F., Kan, Y.W., Goldfine, I.D., et al. 1985. The human insulin receptor cDNA: the structural basis for hormone-activated transmembrane signalling. *Cell* 40:747-758.
74. Van Obberghen, E., and Kahn, C.R. 1981. Autoantibodies to insulin receptors. *Mol Cell Endocrinol* 22:277-293.
75. Shier, P., and Watt, V.M. 1989. Primary structure of a putative receptor for a ligand of the insulin family. *J Biol Chem* 264:14605-14608.
76. Ullrich, A., Gray, A., Tam, A.W., Yang-Feng, T., Tsubokawa, M., Collins, C., Henzel, W., Le Bon, T., Kathuria, S., Chen, E., et al. 1986. Insulin-like growth factor I receptor primary structure: comparison with insulin receptor suggests structural determinants that define functional specificity. *Embo J* 5:2503-2512.
77. Rosen, O.M. 1987. After insulin binds. *Science* 237:1452-1458.
78. Ullrich, A., Bell, J.R., Chen, E.Y., Herrera, R., Petruzzelli, L.M., Dull, T.J., Gray, A., Coussens, L., Liao, Y.C., Tsubokawa, M., et al. 1985. Human insulin receptor and its relationship to the tyrosine kinase family of oncogenes. *Nature* 313:756-761.

79. Goldstein, B.J., and Dudley, A.L. 1991. Molecular heterogeneity of insulin receptors in rat tissues. *Adv Exp Med Biol* 293:187-195.
80. Kahn, C.R., Baird, K.L., Jarrett, D.B., and Flier, J.S. 1978. Direct demonstration that receptor crosslinking or aggregation is important in insulin action. *Proc Natl Acad Sci U S A* 75:4209-4213.
81. Eck, M.J., Dhe-Paganon, S., Trub, T., Nolte, R.T., and Shoelson, S.E. 1996. Structure of the IRS-1 PTB domain bound to the juxtamembrane region of the insulin receptor. *Cell* 85:695-705.
82. Miralpeix, M., Sun, X.J., Backer, J.M., Myers, M.G., Jr., Araki, E., and White, M.F. 1992. Insulin stimulates tyrosine phosphorylation of multiple high molecular weight substrates in Fao hepatoma cells. *Biochemistry* 31:9031-9039.
83. White, M.F., Shoelson, S.E., Keutmann, H., and Kahn, C.R. 1988. A cascade of tyrosine autophosphorylation in the beta-subunit activates the phosphotransferase of the insulin receptor. *J Biol Chem* 263:2969-2980.
84. Burks, D.J., Pons, S., Towery, H., Smith-Hall, J., Myers, M.G., Jr., Yenush, L., and White, M.F. 1997. Heterologous pleckstrin homology domains do not couple IRS-1 to the insulin receptor. *J Biol Chem* 272:27716-27721.
85. Burks, D.J., Wang, J., Towery, H., Ishibashi, O., Lowe, D., Riedel, H., and White, M.F. 1998. IRS pleckstrin homology domains bind to acidic motifs in proteins. *J Biol Chem* 273:31061-31067.
86. Jacobs, A.R., LeRoith, D., and Taylor, S.I. 2001. Insulin receptor substrate-1 pleckstrin homology and phosphotyrosine-binding domains are both involved in plasma membrane targeting. *J Biol Chem* 276:40795-40802.
87. Sun, X.J., Rothenberg, P., Kahn, C.R., Backer, J.M., Araki, E., Wilden, P.A., Cahill, D.A., Goldstein, B.J., and White, M.F. 1991. Structure of the insulin receptor substrate IRS-1 defines a unique signal transduction protein. *Nature* 352:73-77.
88. Sun, X.J., Wang, L.M., Zhang, Y., Yenush, L., Myers, M.G., Jr., Glasheen, E., Lane, W.S., Pierce, J.H., and White, M.F. 1995. Role of IRS-2 in insulin and cytokine signalling. *Nature* 377:173-177.
89. Lavan, B.E., Fantin, V.R., Chang, E.T., Lane, W.S., Keller, S.R., and Lienhard, G.E. 1997. A novel 160-kDa phosphotyrosine protein in insulin-treated embryonic kidney cells is a new member of the insulin receptor substrate family. *J Biol Chem* 272:21403-21407.
90. Lavan, B.E., Lane, W.S., and Lienhard, G.E. 1997. The 60-kDa phosphotyrosine protein in insulin-treated adipocytes is a new member of the insulin receptor substrate family. *J Biol Chem* 272:11439-11443.
91. Holgado-Madruga, M., Emllet, D.R., Moscatello, D.K., Godwin, A.K., and Wong, A.J. 1996. A Grb2-associated docking protein in EGF- and insulin-receptor signalling. *Nature* 379:560-564.
92. Lehr, S., Kotzka, J., Herkner, A., Sikmann, A., Meyer, H.E., Krone, W., and Muller-Wieland, D. 2000. Identification of major tyrosine phosphorylation sites in the human insulin receptor substrate Gab-1 by insulin receptor kinase in vitro. *Biochemistry* 39:10898-10907.
93. Sciacchitano, S., and Taylor, S.I. 1997. Cloning, tissue expression, and chromosomal localization of the mouse IRS-3 gene. *Endocrinology* 138:4931-4940.
94. De Fea, K., and Roth, R.A. 1997. Protein kinase C modulation of insulin receptor substrate-1 tyrosine phosphorylation requires serine 612. *Biochemistry* 36:12939-12947.
95. Myers, M.G., Jr., Backer, J.M., Sun, X.J., Shoelson, S., Hu, P., Schlessinger, J., Yoakim, M., Schaffhausen, B., and White, M.F. 1992. IRS-1 activates

- phosphatidylinositol 3'-kinase by associating with src homology 2 domains of p85. *Proc Natl Acad Sci U S A* 89:10350-10354.
96. Myers, M.G., Jr., Sun, X.J., Cheatham, B., Jachna, B.R., Glasheen, E.M., Backer, J.M., and White, M.F. 1993. IRS-1 is a common element in insulin and insulin-like growth factor-I signaling to the phosphatidylinositol 3'-kinase. *Endocrinology* 132:1421-1430.
 97. Skolnik, E.Y., Batzer, A., Li, N., Lee, C.H., Lowenstein, E., Mohammadi, M., Margolis, B., and Schlessinger, J. 1993. The function of GRB2 in linking the insulin receptor to Ras signaling pathways. *Science* 260:1953-1955.
 98. Rocchi, S., Tartare-Deckert, S., Sawka-Verhelle, D., Gamha, A., and van Obberghen, E. 1996. Interaction of SH2-containing protein tyrosine phosphatase 2 with the insulin receptor and the insulin-like growth factor-I receptor: studies of the domains involved using the yeast two-hybrid system. *Endocrinology* 137:4944-4952.
 99. Katso, R., Okkenhaug, K., Ahmadi, K., White, S., Timms, J., and Waterfield, M.D. 2001. Cellular function of phosphoinositide 3-kinases: implications for development, homeostasis, and cancer. *Annu Rev Cell Dev Biol* 17:615-675.
 100. Skolnik, E.Y., Margolis, B., Mohammadi, M., Lowenstein, E., Fischer, R., Drepps, A., Ullrich, A., and Schlessinger, J. 1991. Cloning of PI3 kinase-associated p85 utilizing a novel method for expression/cloning of target proteins for receptor tyrosine kinases. *Cell* 65:83-90.
 101. Whitman, M., Downes, C.P., Keeler, M., Keller, T., and Cantley, L. 1988. Type I phosphatidylinositol kinase makes a novel inositol phospholipid, phosphatidylinositol-3-phosphate. *Nature* 332:644-646.
 102. Vanhaesebroeck, B., and Alessi, D.R. 2000. The PI3K-PDK1 connection: more than just a road to PKB. *Biochem J* 346 Pt 3:561-576.
 103. Cheatham, B., and Kahn, C.R. 1995. Insulin action and the insulin signaling network. *Endocr Rev* 16:117-142.
 104. Zhang, Y., Proenca, R., Maffei, M., Barone, M., Leopold, L., and Friedman, J.M. 1994. Positional cloning of the mouse obese gene and its human homologue. *Nature* 372:425-432.
 105. Chen, H., Charlat, O., Tartaglia, L.A., Woolf, E.A., Weng, X., Ellis, S.J., Lakey, N.D., Culpepper, J., Moore, K.J., Breitbart, R.E., et al. 1996. Evidence that the diabetes gene encodes the leptin receptor: identification of a mutation in the leptin receptor gene in db/db mice. *Cell* 84:491-495.
 106. Bado, A., Levasseur, S., Attoub, S., Kermorgant, S., Laigneau, J.P., Bortoluzzi, M.N., Moizo, L., Lehy, T., Guerre-Millo, M., Le Marchand-Brustel, Y., et al. 1998. The stomach is a source of leptin. *Nature* 394:790-793.
 107. Masuzaki, H., Ogawa, Y., Sagawa, N., Hosoda, K., Matsumoto, T., Mise, H., Nishimura, H., Yoshimasa, Y., Tanaka, I., Mori, T., et al. 1997. Nonadipose tissue production of leptin: leptin as a novel placenta-derived hormone in humans. *Nat Med* 3:1029-1033.
 108. Moon, B.C., and Friedman, J.M. 1997. The molecular basis of the obese mutation in ob2J mice. *Genomics* 42:152-156.
 109. Halaas, J.L., Gajiwala, K.S., Maffei, M., Cohen, S.L., Chait, B.T., Rabinowitz, D., Lallone, R.L., Burley, S.K., and Friedman, J.M. 1995. Weight-reducing effects of the plasma protein encoded by the obese gene. *Science* 269:543-546.
 110. Maffei, M., Halaas, J., Ravussin, E., Pratley, R.E., Lee, G.H., Zhang, Y., Fei, H., Kim, S., Lallone, R., Ranganathan, S., et al. 1995. Leptin levels in human and rodent: measurement of plasma leptin and ob RNA in obese and weight-reduced subjects. *Nat Med* 1:1155-1161.

111. Maffei, M., Fei, H., Lee, G.H., Dani, C., Leroy, P., Zhang, Y., Proenca, R., Negrel, R., Ailhaud, G., and Friedman, J.M. 1995. Increased expression in adipocytes of ob RNA in mice with lesions of the hypothalamus and with mutations at the db locus. *Proc Natl Acad Sci U S A* 92:6957-6960.
112. Pellemounter, M.A., Cullen, M.J., Baker, M.B., Hecht, R., Winters, D., Boone, T., and Collins, F. 1995. Effects of the obese gene product on body weight regulation in ob/ob mice. *Science* 269:540-543.
113. Campfield, L.A., Smith, F.J., Guisez, Y., Devos, R., and Burn, P. 1995. Recombinant mouse OB protein: evidence for a peripheral signal linking adiposity and central neural networks. *Science* 269:546-549.
114. Cohen, P., Zhao, C., Cai, X., Montez, J.M., Rohani, S.C., Feinstein, P., Mombaerts, P., and Friedman, J.M. 2001. Selective deletion of leptin receptor in neurons leads to obesity. *J Clin Invest* 108:1113-1121.
115. Schwartz, M.W., Seeley, R.J., Campfield, L.A., Burn, P., and Baskin, D.G. 1996. Identification of targets of leptin action in rat hypothalamus. *J Clin Invest* 98:1101-1106.
116. Seeley, R.J., van Dijk, G., Campfield, L.A., Smith, F.J., Burn, P., Nelligan, J.A., Bell, S.M., Baskin, D.G., Woods, S.C., and Schwartz, M.W. 1996. Intraventricular leptin reduces food intake and body weight of lean rats but not obese Zucker rats. *Horm Metab Res* 28:664-668.
117. Banks, W.A., Kastin, A.J., Huang, W., Jaspan, J.B., and Maness, L.M. 1996. Leptin enters the brain by a saturable system independent of insulin. *Peptides* 17:305-311.
118. Montague, C.T., Farooqi, I.S., Whitehead, J.P., Soos, M.A., Rau, H., Wareham, N.J., Sewter, C.P., Digby, J.E., Mohammed, S.N., Hurst, J.A., et al. 1997. Congenital leptin deficiency is associated with severe early-onset obesity in humans. *Nature* 387:903-908.
119. Farooqi, I.S., Jebb, S.A., Langmack, G., Lawrence, E., Cheetham, C.H., Prentice, A.M., Hughes, I.A., McCamish, M.A., and O'Rahilly, S. 1999. Effects of recombinant leptin therapy in a child with congenital leptin deficiency. *N Engl J Med* 341:879-884.
120. Tulipano, G., Vergoni, A.V., Soldi, D., Muller, E.E., and Cocchi, D. 2004. Characterization of the resistance to the anorectic and endocrine effects of leptin in obesity-prone and obesity-resistant rats fed a high-fat diet. *J Endocrinol* 183:289-298.
121. Roth, J.D., Roland, B.L., Cole, R.L., Trevaskis, J.L., Weyer, C., Koda, J.E., Anderson, C.M., Parkes, D.G., and Baron, A.D. 2008. Leptin responsiveness restored by amylin agonism in diet-induced obesity: evidence from nonclinical and clinical studies. *Proc Natl Acad Sci U S A* 105:7257-7262.
122. Chua, S.C., Jr., Koutras, I.K., Han, L., Liu, S.M., Kay, J., Young, S.J., Chung, W.K., and Leibel, R.L. 1997. Fine structure of the murine leptin receptor gene: splice site suppression is required to form two alternatively spliced transcripts. *Genomics* 45:264-270.
123. Tartaglia, L.A. 1997. The leptin receptor. *J Biol Chem* 272:6093-6096.
124. Lee, G.H., Proenca, R., Montez, J.M., Carroll, K.M., Darvishzadeh, J.G., Lee, J.I., and Friedman, J.M. 1996. Abnormal splicing of the leptin receptor in diabetic mice. *Nature* 379:632-635.
125. Friedman, J.M. 1998. Leptin, leptin receptors, and the control of body weight. *Nutr Rev* 56:s38-46; discussion s54-75.
126. Elmquist, J.K., Bjorbaek, C., Ahima, R.S., Flier, J.S., and Saper, C.B. 1998. Distributions of leptin receptor mRNA isoforms in the rat brain. *J Comp Neurol* 395:535-547.

127. Banks, A.S., Davis, S.M., Bates, S.H., and Myers, M.G., Jr. 2000. Activation of downstream signals by the long form of the leptin receptor. *J Biol Chem* 275:14563-14572.
128. White, D.W., Kuropatwinski, K.K., Devos, R., Baumann, H., and Tartaglia, L.A. 1997. Leptin receptor (OB-R) signaling. Cytoplasmic domain mutational analysis and evidence for receptor homo-oligomerization. *J Biol Chem* 272:4065-4071.
129. Luttkien, C., Wegenka, U.M., Yuan, J., Buschmann, J., Schindler, C., Ziemiecki, A., Harpur, A.G., Wilks, A.F., Yasukawa, K., Taga, T., et al. 1994. Association of transcription factor APRF and protein kinase Jak1 with the interleukin-6 signal transducer gp130. *Science* 263:89-92.
130. Stahl, N., and Yancopoulos, G.D. 1994. The tripartite CNTF receptor complex: activation and signaling involves components shared with other cytokines. *J Neurobiol* 25:1454-1466.
131. Bjorbaek, C., Elmquist, J.K., Frantz, J.D., Shoelson, S.E., and Flier, J.S. 1998. Identification of SOCS-3 as a potential mediator of central leptin resistance. *Mol Cell* 1:619-625.
132. Endo, T.A., Masuhara, M., Yokouchi, M., Suzuki, R., Sakamoto, H., Mitsui, K., Matsumoto, A., Tanimura, S., Ohtsubo, M., Misawa, H., et al. 1997. A new protein containing an SH2 domain that inhibits JAK kinases. *Nature* 387:921-924.
133. Naka, T., Narazaki, M., Hirata, M., Matsumoto, T., Minamoto, S., Aono, A., Nishimoto, N., Kajita, T., Taga, T., Yoshizaki, K., et al. 1997. Structure and function of a new STAT-induced STAT inhibitor. *Nature* 387:924-929.
134. Yasukawa, H., Misawa, H., Sakamoto, H., Masuhara, M., Sasaki, A., Wakioka, T., Ohtsuka, S., Imaizumi, T., Matsuda, T., Ihle, J.N., et al. 1999. The JAK-binding protein JAB inhibits Janus tyrosine kinase activity through binding in the activation loop. *Embo J* 18:1309-1320.
135. Bjorbaek, C., El-Haschimi, K., Frantz, J.D., and Flier, J.S. 1999. The role of SOCS-3 in leptin signaling and leptin resistance. *J Biol Chem* 274:30059-30065.
136. Niswender, K.D., Morton, G.J., Stearns, W.H., Rhodes, C.J., Myers, M.G., Jr., and Schwartz, M.W. 2001. Intracellular signalling. Key enzyme in leptin-induced anorexia. *Nature* 413:794-795.
137. Mirshamsi, S., Laidlaw, H.A., Ning, K., Anderson, E., Burgess, L.A., Gray, A., Sutherland, C., and Ashford, M.L. 2004. Leptin and insulin stimulation of signalling pathways in arcuate nucleus neurones: PI3K dependent actin reorganization and KATP channel activation. *BMC Neurosci* 5:54.
138. Burks, D.J., Font de Mora, J., Schubert, M., Withers, D.J., Myers, M.G., Towery, H.H., Altamuro, S.L., Flint, C.L., and White, M.F. 2000. IRS-2 pathways integrate female reproduction and energy homeostasis. *Nature* 407:377-382.
139. Hetherington, A.W., and Ranson, S.W. 1940. Hypothalamic lesions and adiposity in the rat. *Anat. Record* 78:149.
140. Anand, B.K., and Brobeck, J.R. 1951. Localization of a "feeding center" in the hypothalamus of the rat. *Proc Soc Exp Biol Med* 77:323-324.
141. Kennedy, G.C. 1953. The role of depot fat in the hypothalamic control of food intake in the rat. *Proc R Soc Lond B Biol Sci* 140:578-596.
142. Hervey, G.R. 1959. The effects of lesions in the hypothalamus in parabiotic rats. *J Physiol* 145:336-352.
143. Bernard, C. 1855. Leçons de physiologie expérimentale appliquée à la médecine. *Baillière et Fils* Paris:296-313.
144. Simerly, R.B. 1995. *Anatomical substrates of hypothalamic integration*: Academic Press.

145. Berthoud, H.R. 2002. Multiple neural systems controlling food intake and body weight. *Neurosci Biobehav Rev* 26:393-428.
146. Broadwell, R.D., and Brightman, M.W. 1976. Entry of peroxidase into neurons of the central and peripheral nervous systems from extracerebral and cerebral blood. *J Comp Neurol* 166:257-283.
147. Faouzi, M., Leshan, R., Bjornholm, M., Hennessey, T., Jones, J., and Munzberg, H. 2007. Differential accessibility of circulating leptin to individual hypothalamic sites. *Endocrinology* 148:5414-5423.
148. Thompson, R.H., and Swanson, L.W. 1998. Organization of inputs to the dorsomedial nucleus of the hypothalamus: a reexamination with Fluorogold and PHAL in the rat. *Brain Res Brain Res Rev* 27:89-118.
149. Gao, Q., and Horvath, T.L. 2008. Neuronal control of energy homeostasis. *FEBS Lett* 582:132-141.
150. Larhammar, D. 1996. Evolution of neuropeptide Y, peptide YY and pancreatic polypeptide. *Regul Pept* 62:1-11.
151. McMinn, J.E., Wilkinson, C.W., Havel, P.J., Woods, S.C., and Schwartz, M.W. 2000. Effect of intracerebroventricular alpha-MSH on food intake, adiposity, c-Fos induction, and neuropeptide expression. *Am J Physiol Regul Integr Comp Physiol* 279:R695-703.
152. Rossi, M., Kim, M.S., Morgan, D.G., Small, C.J., Edwards, C.M., Sunter, D., Abusnana, S., Goldstone, A.P., Russell, S.H., Stanley, S.A., et al. 1998. A C-terminal fragment of Agouti-related protein increases feeding and antagonizes the effect of alpha-melanocyte stimulating hormone in vivo. *Endocrinology* 139:4428-4431.
153. Zhou, A., Bloomquist, B.T., and Mains, R.E. 1993. The prohormone convertases PC1 and PC2 mediate distinct endoproteolytic cleavages in a strict temporal order during proopiomelanocortin biosynthetic processing. *J Biol Chem* 268:1763-1769.
154. Harris, J.I. 1959. Studies on pituitary polypeptide hormones. III. The structure of alpha-melanocyte-stimulating hormone from pig pituitary glands. *Biochem J* 71:451-459.
155. Joseph, S.A., Pilcher, W.H., and Bennett-Clarke, C. 1983. Immunocytochemical localization of ACTH perikarya in nucleus tractus solitarius: evidence for a second opiocortin neuronal system. *Neurosci Lett* 38:221-225.
156. Lacaze-Masmonteil, T., de Keyser, Y., Luton, J.P., Kahn, A., and Bertagna, X. 1987. Characterization of proopiomelanocortin transcripts in human nonpituitary tissues. *Proc Natl Acad Sci U S A* 84:7261-7265.
157. Swart, I., Jahng, J.W., Overton, J.M., and Houpt, T.A. 2002. Hypothalamic NPY, AGRP, and POMC mRNA responses to leptin and refeeding in mice. *Am J Physiol Regul Integr Comp Physiol* 283:R1020-1026.
158. Fan, W., Boston, B.A., Kesterson, R.A., Hrubby, V.J., and Cone, R.D. 1997. Role of melanocortinergic neurons in feeding and the agouti obesity syndrome. *Nature* 385:165-168.
159. Biebermann, H., Castaneda, T.R., van Landeghem, F., von Deimling, A., Escher, F., Brabant, G., Hebebrand, J., Hinney, A., Tschop, M.H., Gruters, A., et al. 2006. A role for beta-melanocyte-stimulating hormone in human body-weight regulation. *Cell Metab* 3:141-146.
160. Lee, Y.S., Challis, B.G., Thompson, D.A., Yeo, G.S., Keogh, J.M., Madonna, M.E., Wraight, V., Sims, M., Vatin, V., Meyre, D., et al. 2006. A POMC variant implicates beta-melanocyte-stimulating hormone in the control of human energy balance. *Cell Metab* 3:135-140.

161. Adan, R.A., Cone, R.D., Burbach, J.P., and Gispen, W.H. 1994. Differential effects of melanocortin peptides on neural melanocortin receptors. *Mol Pharmacol* 46:1182-1190.
162. Mountjoy, K.G. 1994. The human melanocyte stimulating hormone receptor has evolved to become "super-sensitive" to melanocortin peptides. *Mol Cell Endocrinol* 102:R7-11.
163. Jegou, S., Boutelet, I., and Vaudry, H. 2000. Melanocortin-3 receptor mRNA expression in pro-opiomelanocortin neurones of the rat arcuate nucleus. *J Neuroendocrinol* 12:501-505.
164. Balthasar, N., Dalgaard, L.T., Lee, C.E., Yu, J., Funahashi, H., Williams, T., Ferreira, M., Tang, V., McGovern, R.A., Kenny, C.D., et al. 2005. Divergence of melanocortin pathways in the control of food intake and energy expenditure. *Cell* 123:493-505.
165. Minth, C.D., Bloom, S.R., Polak, J.M., and Dixon, J.E. 1984. Cloning, characterization, and DNA sequence of a human cDNA encoding neuropeptide tyrosine. *Proc Natl Acad Sci U S A* 81:4577-4581.
166. Sahu, A., Kalra, S.P., Crowley, W.R., and Kalra, P.S. 1988. Evidence that NPY-containing neurons in the brainstem project into selected hypothalamic nuclei: implication in feeding behavior. *Brain Res* 457:376-378.
167. Chronwall, B.M., Chase, T.N., and O'Donohue, T.L. 1984. Coexistence of neuropeptide Y and somatostatin in rat and human cortical and rat hypothalamic neurons. *Neurosci Lett* 52:213-217.
168. Stanley, B.G., and Leibowitz, S.F. 1984. Neuropeptide Y: stimulation of feeding and drinking by injection into the paraventricular nucleus. *Life Sci* 35:2635-2642.
169. Clark, J.T., Kalra, P.S., Crowley, W.R., and Kalra, S.P. 1984. Neuropeptide Y and human pancreatic polypeptide stimulate feeding behavior in rats. *Endocrinology* 115:427-429.
170. Stanley, B.G., Kyrkouli, S.E., Lampert, S., and Leibowitz, S.F. 1986. Neuropeptide Y chronically injected into the hypothalamus: a powerful neurochemical inducer of hyperphagia and obesity. *Peptides* 7:1189-1192.
171. Ollmann, M.M., Wilson, B.D., Yang, Y.K., Kerns, J.A., Chen, Y., Gantz, I., and Barsh, G.S. 1997. Antagonism of central melanocortin receptors in vitro and in vivo by agouti-related protein. *Science* 278:135-138.
172. Makimura, H., Mizuno, T.M., Mastaitis, J.W., Agami, R., and Mobbs, C.V. 2002. Reducing hypothalamic AGRP by RNA interference increases metabolic rate and decreases body weight without influencing food intake. *BMC Neurosci* 3:18.
173. Gropp, E., Shanabrough, M., Borok, E., Xu, A.W., Janoschek, R., Buch, T., Plum, L., Balthasar, N., Hampel, B., Waisman, A., et al. 2005. Agouti-related peptide-expressing neurons are mandatory for feeding. *Nat Neurosci* 8:1289-1291.
174. Luquet, S., Perez, F.A., Hnasko, T.S., and Palmiter, R.D. 2005. NPY/AgRP neurons are essential for feeding in adult mice but can be ablated in neonates. *Science* 310:683-685.
175. Qian, S., Chen, H., Weingarth, D., Trumbauer, M.E., Novi, D.E., Guan, X., Yu, H., Shen, Z., Feng, Y., Frazier, E., et al. 2002. Neither agouti-related protein nor neuropeptide Y is critically required for the regulation of energy homeostasis in mice. *Mol Cell Biol* 22:5027-5035.
176. Cowley, M.A., Smart, J.L., Rubinstein, M., Cerdan, M.G., Diano, S., Horvath, T.L., Cone, R.D., and Low, M.J. 2001. Leptin activates anorexigenic POMC neurons through a neural network in the arcuate nucleus. *Nature* 411:480-484.
177. Wu, Q., Howell, M.P., and Palmiter, R.D. 2008. Ablation of neurons expressing agouti-related protein activates fos and gliosis in postsynaptic target regions. *J Neurosci* 28:9218-9226.

178. Tong, Q., Ye, C.P., Jones, J.E., Elmquist, J.K., and Lowell, B.B. 2008. Synaptic release of GABA by AgRP neurons is required for normal regulation of energy balance. *Nat Neurosci*.
179. Wu, Q., Boyle, M.P., and Palmiter, R.D. 2009. Loss of GABAergic signaling by AgRP neurons to the parabrachial nucleus leads to starvation. *Cell* 137:1225-1234.
180. Gao, Q., Wolfgang, M.J., Neschen, S., Morino, K., Horvath, T.L., Shulman, G.I., and Fu, X.Y. 2004. Disruption of neural signal transducer and activator of transcription 3 causes obesity, diabetes, infertility, and thermal dysregulation. *Proc Natl Acad Sci U S A* 101:4661-4666.
181. Piper, M.L., Unger, E.K., Myers, M.G., Jr., and Xu, A.W. 2008. Specific physiological roles for signal transducer and activator of transcription 3 in leptin receptor-expressing neurons. *Mol Endocrinol* 22:751-759.
182. Balthasar, N., Coppari, R., McMinn, J., Liu, S.M., Lee, C.E., Tang, V., Kenny, C.D., McGovern, R.A., Chua, S.C., Jr., Elmquist, J.K., et al. 2004. Leptin receptor signaling in POMC neurons is required for normal body weight homeostasis. *Neuron* 42:983-991.
183. Xu, A.W., Ste-Marie, L., Kaelin, C.B., and Barsh, G.S. 2007. Inactivation of signal transducer and activator of transcription 3 in proopiomelanocortin (Pomc) neurons causes decreased pomc expression, mild obesity, and defects in compensatory refeeding. *Endocrinology* 148:72-80.
184. Kaelin, C.B., Gong, L., Xu, A.W., Yao, F., Hockman, K., Morton, G.J., Schwartz, M.W., Barsh, G.S., and MacKenzie, R.G. 2006. Signal transducer and activator of transcription (stat) binding sites but not stat3 are required for fasting-induced transcription of agouti-related protein messenger ribonucleic acid. *Mol Endocrinol* 20:2591-2602.
185. Mesaros, A., Koralov, S.B., Rother, E., Wunderlich, F.T., Ernst, M.B., Barsh, G.S., Rajewsky, K., and Bruning, J.C. 2008. Activation of Stat3 signaling in AgRP neurons promotes locomotor activity. *Cell Metab* 7:236-248.
186. Kitamura, T., Feng, Y., Ido Kitamura, Y., Chua, S.C., Xu, A.W., Barsh, G.S., Rossetti, L., and Accili, D. 2006. Forkhead protein FoxO1 mediates Agrp-dependent effects of leptin on food intake. *Nat Med*.
187. Fekete, C., Singru, P.S., Sanchez, E., Sarkar, S., Christoffolete, M.A., Riberio, R.S., Rand, W.M., Emerson, C.H., Bianco, A.C., and Lechan, R.M. 2006. Differential effects of central leptin, insulin, or glucose administration during fasting on the hypothalamic-pituitary-thyroid axis and feeding-related neurons in the arcuate nucleus. *Endocrinology* 147:520-529.
188. Morrison, C.D., Morton, G.J., Niswender, K.D., Gelling, R.W., and Schwartz, M.W. 2005. Leptin inhibits hypothalamic Npy and Agrp gene expression via a mechanism that requires phosphatidylinositol 3-OH-kinase signaling. *Am J Physiol Endocrinol Metab* 289:E1051-1057.
189. Seeley, R.J., Yagaloff, K.A., Fisher, S.L., Burn, P., Thiele, T.E., van Dijk, G., Baskin, D.G., and Schwartz, M.W. 1997. Melanocortin receptors in leptin effects. *Nature* 390:349.
190. Niswender, K.D., Gallis, B., Blevins, J.E., Corson, M.A., Schwartz, M.W., and Baskin, D.G. 2003. Immunocytochemical detection of phosphatidylinositol 3-kinase activation by insulin and leptin. *J Histochem Cytochem* 51:275-283.
191. Niswender, K.D., Morrison, C.D., Clegg, D.J., Olson, R., Baskin, D.G., Myers, M.G., Jr., Seeley, R.J., and Schwartz, M.W. 2003. Insulin activation of phosphatidylinositol 3-kinase in the hypothalamic arcuate nucleus: a key mediator of insulin-induced anorexia. *Diabetes* 52:227-231.

192. Belgardt, B.F., Husch, A., Rother, E., Ernst, M.B., Wunderlich, F.T., Hampel, B., Klockener, T., Alessi, D., Kloppenburg, P., and Bruning, J.C. 2008. PDK1 deficiency in POMC-expressing cells reveals FOXO1-dependent and -independent pathways in control of energy homeostasis and stress response. *Cell Metab* 7:291-301.
193. Benoit, S.C., Air, E.L., Coolen, L.M., Strauss, R., Jackman, A., Clegg, D.J., Seeley, R.J., and Woods, S.C. 2002. The catabolic action of insulin in the brain is mediated by melanocortins. *J Neurosci* 22:9048-9052.
194. Sipols, A.J., Baskin, D.G., and Schwartz, M.W. 1995. Effect of intracerebroventricular insulin infusion on diabetic hyperphagia and hypothalamic neuropeptide gene expression. *Diabetes* 44:147-151.
195. Shyng, S.L., and Nichols, C.G. 1998. Membrane phospholipid control of nucleotide sensitivity of KATP channels. *Science* 282:1138-1141.
196. Ashcroft, F.M. 1988. Adenosine 5'-triphosphate-sensitive potassium channels. *Annu Rev Neurosci* 11:97-118.
197. Zawar, C., Plant, T.D., Schirra, C., Konnerth, A., and Neumcke, B. 1999. Cell-type specific expression of ATP-sensitive potassium channels in the rat hippocampus. *J Physiol* 514 (Pt 2):327-341.
198. Trapp, S., and Ballanyi, K. 1995. KATP channel mediation of anoxia-induced outward current in rat dorsal vagal neurons in vitro. *J Physiol* 487 (Pt 1):37-50.
199. Fujimura, N., Tanaka, E., Yamamoto, S., Shigemori, M., and Higashi, H. 1997. Contribution of ATP-sensitive potassium channels to hypoxic hyperpolarization in rat hippocampal CA1 neurons in vitro. *J Neurophysiol* 77:378-385.
200. Baukrowitz, T., Schulte, U., Oliver, D., Herlitze, S., Krauter, T., Tucker, S.J., Ruppersberg, J.P., and Fakler, B. 1998. PIP2 and PIP as determinants for ATP inhibition of KATP channels. *Science* 282:1141-1144.
201. MacGregor, G.G., Dong, K., Vanoye, C.G., Tang, L., Giebisch, G., and Hebert, S.C. 2002. Nucleotides and phospholipids compete for binding to the C terminus of KATP channels. *Proc Natl Acad Sci U S A* 99:2726-2731.
202. Plum, L., Ma, X., Hampel, B., Balthasar, N., Coppari, R., Munzberg, H., Shanabrough, M., Burdakov, D., Rother, E., Janoschek, R., et al. 2006. Enhanced PIP3 signaling in POMC neurons causes KATP channel activation and leads to diet-sensitive obesity. *J Clin Invest* 116:1886-1901.
203. Parton, L.E., Ye, C.P., Coppari, R., Enriori, P.J., Choi, B., Zhang, C.Y., Xu, C., Vianna, C.R., Balthasar, N., Lee, C.E., et al. 2007. Glucose sensing by POMC neurons regulates glucose homeostasis and is impaired in obesity. *Nature* 449:228-232.
204. Figlewicz, D.P., Evans, S.B., Murphy, J., Hoen, M., and Baskin, D.G. 2003. Expression of receptors for insulin and leptin in the ventral tegmental area/substantia nigra (VTA/SN) of the rat. *Brain Res* 964:107-115.
205. Hommel, J.D., Trinko, R., Sears, R.M., Georgescu, D., Liu, Z.W., Gao, X.B., Thurmon, J.J., Marinelli, M., and DiLeone, R.J. 2006. Leptin receptor signaling in midbrain dopamine neurons regulates feeding. *Neuron* 51:801-810.
206. Palmiter, R.D. 2007. Is dopamine a physiologically relevant mediator of feeding behavior? *Trends Neurosci* 30:375-381.
207. Figlewicz, D.P. 2003. Adiposity signals and food reward: expanding the CNS roles of insulin and leptin. *Am J Physiol Regul Integr Comp Physiol* 284:R882-892.
208. Figlewicz, D.P., and Benoit, S.C. 2009. Insulin, leptin, and food reward: update 2008. *Am J Physiol Regul Integr Comp Physiol* 296:R9-R19.
209. Berridge, K.C. 1996. Food reward: brain substrates of wanting and liking. *Neurosci Biobehav Rev* 20:1-25.
210. Nieoullon, A., and Coquerel, A. 2003. Dopamine: a key regulator to adapt action, emotion, motivation and cognition. *Curr Opin Neurol* 16 Suppl 2:S3-9.

211. Viggiano, D., Ruocco, L.A., and Sadile, A.G. 2003. Dopamine phenotype and behaviour in animal models: in relation to attention deficit hyperactivity disorder. *Neurosci Biobehav Rev* 27:623-637.
212. Rios, M., Habecker, B., Sasaoka, T., Eisenhofer, G., Tian, H., Landis, S., Chikaraishi, D., and Roffler-Tarlov, S. 1999. Catecholamine synthesis is mediated by tyrosinase in the absence of tyrosine hydroxylase. *J Neurosci* 19:3519-3526.
213. von Bohlen und Halbach, O.a.D., R. 2002. *Neurotransmitters and Neuromodulators*.
214. Jaber, M., Jones, S., Giros, B., and Caron, M.G. 1997. The dopamine transporter: a crucial component regulating dopamine transmission. *Mov Disord* 12:629-633.
215. Kebabian, J.W., and Calne, D.B. 1979. Multiple receptors for dopamine. *Nature* 277:93-96.
216. Missale, C., Nash, S.R., Robinson, S.W., Jaber, M., and Caron, M.G. 1998. Dopamine receptors: from structure to function. *Physiol Rev* 78:189-225.
217. Zeiss, C.J. 2005. Neuroanatomical phenotyping in the mouse: the dopaminergic system. *Vet Pathol* 42:753-773.
218. Wise, R.A. 2002. Brain reward circuitry: insights from unsensed incentives. *Neuron* 36:229-240.
219. Kalivas, P.W., and Volkow, N.D. 2005. The neural basis of addiction: a pathology of motivation and choice. *Am J Psychiatry* 162:1403-1413.
220. Jankovic, J. 2008. Parkinson's disease: clinical features and diagnosis. *J Neurol Neurosurg Psychiatry* 79:368-376.
221. Grace, A.A., and Bunney, B.S. 1980. Nigral dopamine neurons: intracellular recording and identification with L-dopa injection and histofluorescence. *Science* 210:654-656.
222. Schultz, W. 1998. Predictive reward signal of dopamine neurons. *J Neurophysiol* 80:1-27.
223. Schultz, W. 2002. Getting formal with dopamine and reward. *Neuron* 36:241-263.
224. Wightman, R.M., and Zimmerman, J.B. 1990. Control of dopamine extracellular concentration in rat striatum by impulse flow and uptake. *Brain Res Brain Res Rev* 15:135-144.
225. Zhou, Q.Y., and Palmiter, R.D. 1995. Dopamine-deficient mice are severely hypoactive, adipsic, and aphagic. *Cell* 83:1197-1209.
226. Overton, P.G., and Clark, D. 1997. Burst firing in midbrain dopaminergic neurons. *Brain Res Brain Res Rev* 25:312-334.
227. Nicola, S.M., Surmeier, J., and Malenka, R.C. 2000. Dopaminergic modulation of neuronal excitability in the striatum and nucleus accumbens. *Annu Rev Neurosci* 23:185-215.
228. Hyman, S.E., Malenka, R.C., and Nestler, E.J. 2006. Neural Mechanisms of Addiction: The Role of Reward-Related Learning and Memory. *Annu Rev Neurosci*.
229. Nestler, E.J. 2005. Is there a common molecular pathway for addiction? *Nat Neurosci* 8:1445-1449.
230. Wang, G.J., Volkow, N.D., Logan, J., Pappas, N.R., Wong, C.T., Zhu, W., Netusil, N., and Fowler, J.S. 2001. Brain dopamine and obesity. *Lancet* 357:354-357.
231. Bina, K.G., and Cincotta, A.H. 2000. Dopaminergic agonists normalize elevated hypothalamic neuropeptide Y and corticotropin-releasing hormone, body weight gain, and hyperglycemia in ob/ob mice. *Neuroendocrinology* 71:68-78.
232. Deroche, V., Marinelli, M., Maccari, S., Le Moal, M., Simon, H., and Piazza, P.V. 1995. Stress-induced sensitization and glucocorticoids. I. Sensitization of dopamine-dependent locomotor effects of amphetamine and morphine depends on stress-induced corticosterone secretion. *J Neurosci* 15:7181-7188.
233. Campbell, B.A., and Fibiger, H.C. 1971. Potentiation of amphetamine-induced arousal by starvation. *Nature* 233:424-425.

234. Carroll, M.E. 1984. Food deprivation produces persistent increases in self-administration behavior during cocaine extinction. *NIDA Res Monogr* 55:125-131.
235. Carr, K.D. 2002. Augmentation of drug reward by chronic food restriction: behavioral evidence and underlying mechanisms. *Physiol Behav* 76:353-364.
236. Margules, D.L., and Olds, J. 1962. Identical "feeding" and "rewarding" systems in the lateral hypothalamus of rats. *Science* 135:374-375.
237. Jewett, D.C., Cleary, J., Levine, A.S., Schaal, D.W., and Thompson, T. 1995. Effects of neuropeptide Y, insulin, 2-deoxyglucose, and food deprivation on food-motivated behavior. *Psychopharmacology (Berl)* 120:267-271.
238. Agmo, A., Galvan, A., and Talamantes, B. 1995. Reward and reinforcement produced by drinking sucrose: two processes that may depend on different neurotransmitters. *Pharmacol Biochem Behav* 52:403-414.
239. Lepore, M., Vorel, S.R., Lowinson, J., and Gardner, E.L. 1995. Conditioned place preference induced by delta 9-tetrahydrocannabinol: comparison with cocaine, morphine, and food reward. *Life Sci* 56:2073-2080.
240. Swerdlow, N.R., van der Kooy, D., Koob, G.F., and Wenger, J.R. 1983. Cholecystokinin produces conditioned place-aversions, not place-preferences, in food-deprived rats: evidence against involvement in satiety. *Life Sci* 32:2087-2093.
241. Carr, K.D., Kim, G., and Cabeza de Vaca, S. 2000. Hypoinsulinemia may mediate the lowering of self-stimulation thresholds by food restriction and streptozotocin-induced diabetes. *Brain Res* 863:160-168.
242. Fulton, S., Pissios, P., Manchon, R.P., Stiles, L., Frank, L., Pothos, E.N., Maratos-Flier, E., and Flier, J.S. 2006. Leptin regulation of the mesoaccumbens dopamine pathway. *Neuron* 51:811-822.
243. Shalev, U., Yap, J., and Shaham, Y. 2001. Leptin attenuates acute food deprivation-induced relapse to heroin seeking. *J Neurosci* 21:RC129.
244. Figlewicz, D.P., Higgins, M.S., Ng-Evans, S.B., and Havel, P.J. 2001. Leptin reverses sucrose-conditioned place preference in food-restricted rats. *Physiol Behav* 73:229-234.
245. Russo, S.J., Bolanos, C.A., Theobald, D.E., DeCarolis, N.A., Renthal, W., Kumar, A., Winstanley, C.A., Renthal, N.E., Wiley, M.D., Self, D.W., et al. 2007. IRS2-Akt pathway in midbrain dopamine neurons regulates behavioral and cellular responses to opiates. *Nat Neurosci* 10:93-99.
246. Sipols, A.J., Stuber, G.D., Klein, S.N., Higgins, M.S., and Figlewicz, D.P. 2000. Insulin and raclopride combine to decrease short-term intake of sucrose solutions. *Peptides* 21:1361-1367.
247. Figlewicz, D.P., Bennett, J., Evans, S.B., Kaiyala, K., Sipols, A.J., and Benoit, S.C. 2004. Intraventricular insulin and leptin reverse place preference conditioned with high-fat diet in rats. *Behav Neurosci* 118:479-487.
248. Figlewicz, D.P., Bennett, J.L., Naleid, A.M., Davis, C., and Grimm, J.W. 2006. Intraventricular insulin and leptin decrease sucrose self-administration in rats. *Physiol Behav* 89:611-616.
249. Figlewicz, D.P., MacDonald Naleid, A., and Sipols, A.J. 2007. Modulation of food reward by adiposity signals. *Physiol Behav* 91:473-478.
250. Sambrook, J., and Russell, D.W. 2001. *Molecular Cloning: A Laboratory Manual*: CSHL Press. 2344 pp pp.
251. Mullis, K.B., and Faloona, F.A. 1987. Specific synthesis of DNA in vitro via a polymerase-catalyzed chain reaction. *Methods Enzymol* 155:335-350.
252. Saiki, R.K., Gelfand, D.H., Stoffel, S., Scharf, S.J., Higuchi, R., Horn, G.T., Mullis, K.B., and Erlich, H.A. 1988. Primer-directed enzymatic amplification of DNA with a thermostable DNA polymerase. *Science* 239:487-491.

253. Seibler, J., Zevnik, B., Kuter-Luks, B., Andreas, S., Kern, H., Hennek, T., Rode, A., Heimann, C., Faust, N., Kauselmann, G., et al. 2003. Rapid generation of inducible mouse mutants. *Nucleic Acids Res* 31:e12.
254. Novak, A., Guo, C., Yang, W., Nagy, A., and Lobe, C.G. 2000. Z/EG, a double reporter mouse line that expresses enhanced green fluorescent protein upon Cre-mediated excision. *Genesis* 28:147-155.
255. Janoschek, R., Plum, L., Koch, L., Munzberg, H., Diano, S., Shanabrough, M., Muller, W., Horvath, T.L., and Bruning, J.C. 2006. gp130 signaling in proopiomelanocortin neurons mediates the acute anorectic response to centrally applied ciliary neurotrophic factor. *Proc Natl Acad Sci U S A* 103:10707-10712.
256. Burdakov, D., and Ashcroft, F.M. 2002. Cholecystokinin tunes firing of an electrically distinct subset of arcuate nucleus neurons by activating A-Type potassium channels. *J Neurosci* 22:6380-6387.
257. Hogan, B., Costantini, F., and Lacey, E. 1986. *Manipulating the mouse embryo: A Laboratory Manual*: Cold Spring Harbor Laboratory Press.
258. Silver, L.M. 1995. *Mouse Genetics: Concepts and Applications*: Oxford University Press. 376 pp pp.
259. Kaelin, C.B., Xu, A.W., Lu, X.Y., and Barsh, G.S. 2004. Transcriptional regulation of agouti-related protein (*Agrp*) in transgenic mice. *Endocrinology* 145:5798-5806.
260. Xu, A.W., Kaelin, C.B., Takeda, K., Akira, S., Schwartz, M.W., and Barsh, G.S. 2005. PI3K integrates the action of insulin and leptin on hypothalamic neurons. *J Clin Invest* 115:951-958.
261. Lindeberg, J., Usoskin, D., Bengtsson, H., Gustafsson, A., Kylberg, A., Soderstrom, S., and Ebendal, T. 2004. Transgenic expression of Cre recombinase from the tyrosine hydroxylase locus. *Genesis* 40:67-73.
262. Ferre, P., Leturque, A., Burnol, A.F., Penicaud, L., and Girard, J. 1985. A method to quantify glucose utilization in vivo in skeletal muscle and white adipose tissue of the anaesthetized rat. *Biochem J* 228:103-110.
263. Spanswick, D., Smith, M.A., Mirshamsi, S., Routh, V.H., and Ashford, M.L. 2000. Insulin activates ATP-sensitive K⁺ channels in hypothalamic neurons of lean, but not obese rats. *Nat Neurosci* 3:757-758.
264. Pocai, A., Lam, T.K., Gutierrez-Juarez, R., Obici, S., Schwartz, G.J., Bryan, J., Aguilar-Bryan, L., and Rossetti, L. 2005. Hypothalamic K(ATP) channels control hepatic glucose production. *Nature* 434:1026-1031.
265. van den Top, M., Lee, K., Whyment, A.D., Blanks, A.M., and Spanswick, D. 2004. Orexigen-sensitive NPY/AgRP pacemaker neurons in the hypothalamic arcuate nucleus. *Nat Neurosci* 7:493-494.
266. Schwartz, M.W., Sipols, A.J., Marks, J.L., Sanacora, G., White, J.D., Scheurink, A., Kahn, S.E., Baskin, D.G., Woods, S.C., Figlewicz, D.P., et al. 1992. Inhibition of hypothalamic neuropeptide Y gene expression by insulin. *Endocrinology* 130:3608-3616.
267. Kim, M.S., Pak, Y.K., Jang, P.G., Namkoong, C., Choi, Y.S., Won, J.C., Kim, K.S., Kim, S.W., Kim, H.S., Park, J.Y., et al. 2006. Role of hypothalamic Foxo1 in the regulation of food intake and energy homeostasis. *Nat Neurosci* 9:901-906.
268. Huszar, D., Lynch, C.A., Fairchild-Huntress, V., Dunmore, J.H., Fang, Q., Berkemeier, L.R., Gu, W., Kesterson, R.A., Boston, B.A., Cone, R.D., et al. 1997. Targeted disruption of the melanocortin-4 receptor results in obesity in mice. *Cell* 88:131-141.
269. Banks, W.A. 2006. Blood-brain barrier and energy balance. *Obesity (Silver Spring)* 14 Suppl 5:234S-237S.

270. Choudhury, A.I., Heffron, H., Smith, M.A., Al-Qassab, H., Xu, A.W., Selman, C., Simmgren, M., Clements, M., Claret, M., Maccoll, G., et al. 2005. The role of insulin receptor substrate 2 in hypothalamic and beta cell function. *J Clin Invest* 115:940-950.
271. Mayer, C.M., and Belsham, D.D. 2009. Insulin directly regulates NPY and AgRP gene expression via the MAPK MEK/ERK signal transduction pathway in mHypoE-46 hypothalamic neurons. *Mol Cell Endocrinol* 307:99-108.
272. Obici, S., Feng, Z., Karkanas, G., Baskin, D.G., and Rossetti, L. 2002. Decreasing hypothalamic insulin receptors causes hyperphagia and insulin resistance in rats. *Nat Neurosci* 5:566-572.
273. Dhillon, H., Zigman, J.M., Ye, C., Lee, C.E., McGovern, R.A., Tang, V., Kenny, C.D., Christiansen, L.M., White, R.D., Edelman, E.A., et al. 2006. Leptin directly activates SF1 neurons in the VMH, and this action by leptin is required for normal body-weight homeostasis. *Neuron* 49:191-203.
274. Morton, G.J., Gelling, R.W., Niswender, K.D., Morrison, C.D., Rhodes, C.J., and Schwartz, M.W. 2005. Leptin regulates insulin sensitivity via phosphatidylinositol-3-OH kinase signaling in mediobasal hypothalamic neurons. *Cell Metab* 2:411-420.
275. van den Hoek, A.M., Voshol, P.J., Karnekamp, B.N., Buijs, R.M., Romijn, J.A., Havekes, L.M., and Pijl, H. 2004. Intracerebroventricular neuropeptide Y infusion precludes inhibition of glucose and VLDL production by insulin. *Diabetes* 53:2529-2534.
276. Xu, A.W., Kaelin, C.B., Takeda, K., Akira, S., Schwartz, M.W., and Barsh, G.S. 2005. PI3K integrates the action of insulin and leptin on hypothalamic neurons. *J Clin Invest* 115:951-958.
277. van den Hoek, A.M., van Heijningen, C., Schroder-van der Elst, J.P., Ouwens, D.M., Havekes, L.M., Romijn, J.A., Kalsbeek, A., and Pijl, H. 2008. Intracerebroventricular administration of neuropeptide Y induces hepatic insulin resistance via sympathetic innervation. *Diabetes* 57:2304-2310.
278. Bruning, J.C., Michael, M.D., Winnay, J.N., Hayashi, T., Horsch, D., Accili, D., Goodyear, L.J., and Kahn, C.R. 1998. A muscle-specific insulin receptor knockout exhibits features of the metabolic syndrome of NIDDM without altering glucose tolerance. *Mol Cell* 2:559-569.
279. Koch, L., Wunderlich, F.T., Seibler, J., Konner, A.C., Hampel, B., Irlenbusch, S., Brabant, G., Kahn, C.R., Schwenk, F., and Bruning, J.C. 2008. Central insulin action regulates peripheral glucose and fat metabolism in mice. *J Clin Invest* 118:2132-2147.
280. Edgerton, D.S., Lautz, M., Scott, M., Everett, C.A., Stettler, K.M., Neal, D.W., Chu, C.A., and Cherrington, A.D. 2006. Insulin's direct effects on the liver dominate the control of hepatic glucose production. *J Clin Invest* 116:521-527.
281. Sipols, A.J., Bayer, J., Bennett, R., and Figlewicz, D.P. 2002. Intraventricular insulin decreases kappa opioid-mediated sucrose intake in rats. *Peptides* 23:2181-2187.
282. Moore, R.Y., and Bloom, F.E. 1979. Central catecholamine neuron systems: anatomy and physiology of the norepinephrine and epinephrine systems. *Annu Rev Neurosci* 2:113-168.
283. Garcia, B.G., Wei, Y., Moron, J.A., Lin, R.Z., Javitch, J.A., and Galli, A. 2005. Akt is essential for insulin modulation of amphetamine-induced human dopamine transporter cell-surface redistribution. *Mol Pharmacol* 68:102-109.
284. Figlewicz, D.P., Szot, P., Chavez, M., Woods, S.C., and Veith, R.C. 1994. Intraventricular insulin increases dopamine transporter mRNA in rat VTA/substantia nigra. *Brain Res* 644:331-334.
285. Patterson, T.A., Brot, M.D., Zavosh, A., Schenk, J.O., Szot, P., and Figlewicz, D.P. 1998. Food deprivation decreases mRNA and activity of the rat dopamine transporter. *Neuroendocrinology* 68:11-20.

286. Lindblom, J., Johansson, A., Holmgren, A., Grandin, E., Nedergard, C., Fredriksson, R., and Schioth, H.B. 2006. Increased mRNA levels of tyrosine hydroxylase and dopamine transporter in the VTA of male rats after chronic food restriction. *Eur J Neurosci* 23:180-186.
287. Dickinson, S.D., Sabeti, J., Larson, G.A., Giardina, K., Rubinstein, M., Kelly, M.A., Grandy, D.K., Low, M.J., Gerhardt, G.A., and Zahniser, N.R. 1999. Dopamine D2 receptor-deficient mice exhibit decreased dopamine transporter function but no changes in dopamine release in dorsal striatum. *J Neurochem* 72:148-156.
288. Rouge-Pont, F., Usiello, A., Benoit-Marand, M., Gonon, F., Piazza, P.V., and Borrelli, E. 2002. Changes in extracellular dopamine induced by morphine and cocaine: crucial control by D2 receptors. *J Neurosci* 22:3293-3301.
289. Schmitz, Y., Schmauss, C., and Sulzer, D. 2002. Altered dopamine release and uptake kinetics in mice lacking D2 receptors. *J Neurosci* 22:8002-8009.
290. Benoit-Marand, M., Borrelli, E., and Gonon, F. 2001. Inhibition of dopamine release via presynaptic D2 receptors: time course and functional characteristics in vivo. *J Neurosci* 21:9134-9141.
291. Horvath, T.L. 2006. Synaptic plasticity in energy balance regulation. *Obesity (Silver Spring)* 14 Suppl 5:228S-233S.

8 Acknowledgements

I am sincerely grateful to Prof. Dr. Jens C. Brüning for providing me with this project, giving me the opportunity to work in his lab and his tremendous support.

I would like to thank Prof. Dr. Wilhelm Krone, Prof. Dr. Peter Kloppenburg and Dr. Ursula Lichtenberg for agreeing to form my thesis committee.

Furthermore, I would like to thank Prof. Dr. Hannsjörg Schröder for being an excellent tutor and Dr. Debora Grosskopf-Kroiher for excellent help during the Interdisciplinary Postgraduate Program Molecular Medicine.

This thesis would not have been possible without the help from my colleagues in the Department of Mouse Genetics and Metabolism. In particular, I would like to sincerely thank Brigitte Hampel and Pia Scholl for immunohistochemical stainings, Dr. Andrea Mesaros, Ruth Kuschewski and Dr. Leona Plum for all their help with the clamp studies, Sigrid Irlenbusch and Julia Goldau for help with ELISAs and Bengt Belgardt, Dr. André Kleinridders, Dr. Linda Verhagen, Dr. Andrea Mesaros, Dr. Hella Brönneke and Brigitte Hampel for proofreading the manuscript. I thank all my colleagues for stimulating discussions, help with experiments and general advice. I am especially thankful to Sabine Jordan, Dr. André Kleinridders, Dr. Andrea Mesaros, Brigitte Hampel, Ruth Kuschewski, Bengt Belgardt and Dr. Eva Rother for their support and friendship.

I remain indebted to my family, my parents Dr. Jürgen and Rita Könner, my sister Julia Könner, my brother Daniel Könner, and Philipp Hausen for their never-ending encouragement, love and ongoing support.

9 Erklärung

Ich versichere, daß ich die von mir vorgelegte Dissertation selbständig angefertigt, die benutzten Quellen und Hilfsmittel vollständig angegeben und die Stellen der Arbeit - einschließlich Tabellen, Karten und Abbildungen -, die anderen Werken im Wortlaut oder dem Sinn nach entnommen sind, in jedem Einzelfall als Entlehnung kenntlich gemacht habe; daß diese Dissertation noch keiner anderen Fakultät oder Universität zur Prüfung vorgelegen hat; daß sie - abgesehen von unten angegebenen Teilpublikationen - noch nicht veröffentlicht worden ist sowie, daß ich eine solche Veröffentlichung vor Abschluß des Promotionsverfahrens nicht vornehmen werde. Die Bestimmungen dieser Promotionsordnung sind mir bekannt. Die von mir vorgelegte Dissertation ist von Prof. Dr. Jens C. Brüning betreut worden.

Köln, August 2009

Anne Christine Könner

Teilpublikationen

Könner AC, Janoschek R, Plum L, Jordan SD, Rother E, Ma X, Xu C, Enriori P, Hampel B, Barsh GS, Kahn CR, Cowley MA, Ashcroft FM, Brüning JC. Insulin action in AgRP-expressing neurons is required for suppression of hepatic glucose production. Cell Metab. 2007 Jun; 5 (6): 438-49

10 Curriculum vitae

Persönliche Daten

Name Anne Christine Könner
 Geburt 23.06.1981 in Köln
 Adresse Berrenrather Str. 178, 50937 Köln
 Email christinekoenner@gmx.de
 Nationalität deutsch

Bildungsweg

Seit 01/2006 Promotion in der Abteilung Mausgenetik und Metabolismus des Instituts für Genetik der Universität zu Köln

2000 - 2005 Studium der Biologie an der Mathematisch-Naturwissenschaftlichen Fakultät der Universität zu Köln

Diplomarbeit in der Abteilung Mausgenetik und Metabolismus des Instituts für Genetik der Universität zu Köln zum Thema: „Bedeutung der Insulin-Signaltransduktion in AgRP-ausprägenden Neuronen für die Regulation der Energiehomöostase“

Diplomprüfungen im Hauptfach Genetik und in den Nebenfächern Biochemie und Pharmakologie

1991 - 2000 Hildegard-von-Bingen Gymnasium, Köln
 Abschluss: Allgemeine Hochschulreife

1987-1991 Katholische Grundschule Lohrbergstraße, Köln

Publikationen

2009 Wunderlich FT, Ströhle P, **Könner AC**, Gruber S, Tovar S, Ringeisen G, Brüning JC. Interleukin-6 signaling in liver parenchymal cells suppresses hepatic inflammation and improves systemic insulin action. [submitted]

2009 Kleinridders A, **Könner AC**, Brüning JC. CNS-Targets in Control of Energy and Glucose Homeostasis. [submitted]

2009 Kleinridders A, Schenten D, **Könner AC**, Belgardt BF, Mauer J, Okamura R, Wunderlich FT, Medzhitov R, Brüning JC. MyD88 signaling in the CNS is required for development of fatty acid induced leptin resistance and diet-induced obesity. [in press, Cell Metab]
 (equally contributing first author)

- 2009 Sánchez-Lasheras C, **Könner AC**, Brüning JC. Integrative neurobiology of energy homeostasis-signals, mediators and neurocircuits. [submitted]
- 2009 **Könner AC**, Klöckener T, Brüning JC. Control of energy homeostasis by insulin and leptin: targeting the arcuate nucleus and beyond. *Physiol Behav.* 2009 Jul 14; 97 (5): 632-8
- 2008 Koch L, Wunderlich FT, Seibler J, **Könner AC**, Hampel B, Irlenbusch S, Brabant G, Kahn CR, Schwenk F, Brüning JC. Central insulin action regulates peripheral glucose and fat metabolism in mice. *J Clin Invest.* 2008 Jun; 118 (6): 2132-47
- 2008 Rother E, **Könner AC**, Brüning JC. Neurocircuits integrating hormone and nutrient signaling in control of glucose metabolism. *Am J Physiol Endocrinol Metab.* 2008 May; 294 (5): E810-6
- 2007 Plum L, Rother E, Münzberg H, Wunderlich FT, Morgan DA, Hampel B, Shanabrough M, Janoschek R, **Könner AC**, Alber J, Suzuki A, Krone W, Horvath TL, Rahmouni K, Brüning JC. Enhanced leptin-stimulated Pi3k activation in the CNS promotes white adipose tissue transdifferentiation. *Cell Metab.* 2007 Dec; 6 (6): 431-45
- 2007 **Könner AC**, Janoschek R, Plum L, Jordan SD, Rother E, Ma X, Xu C, Enriori P, Hampel B, Barsh GS, Kahn CR, Cowley MA, Ashcroft FM, Brüning JC. Insulin action in AgRP-expressing neurons is required for suppression of hepatic glucose production. *Cell Metab.* 2007 Jun; 5 (6): 438-49

Vorträge

- 2008 3. Gemeinsame Tagung der AGPD und APE
7. – 9. November 2008, Bremen
Titel: Molekulare Mechanismen neuronaler Netzwerke in Diabetes und Übergewicht
- 2008 Targeting neurocircuits in obesity (NEUROTARGET)
1. Mitgliederversammlung des Kompetenznetzes Adipositas
15./16. Oktober 2008, Freiburg im Breisgau
Titel: Molecular control of reward mechanisms in feeding behavior
- 2007 DIABESITY – Novel molecular targets for obesity and type 2 diabetes
A European Union Framework Programme VI Integrated Project

Workblock C & D meetings 2007, Funchal, Madeira, Portugal
Sunday Dec 2nd – Tuesday Dec 4th 2007
Title: Genetic Analysis of Neuronal Circuits Regulating Energy and Glucose Homeostasis

General Assembly, Bologna, Italy, May 27th – 29th 2007
Title: Role of Insulin Signaling in AgRP- and POMC-expressing Neurons in Regulation of Hepatic Glucose Production